INFORMATION TO USERS

This manuscript has been reproduced from the microfilm master. UMI films the text directly from the original or copy submitted. Thus, some thesis and dissertation copies are in typewriter face, while others may be from any type of computer printer.

The quality of this reproduction is dependent upon the quality of the copy submitted. Broken or indistinct print, colored or poor quality illustrations and photographs, print bleedthrough, substandard margins, and improper alignment can adversely affect reproduction.

In the unlikely event that the author did not send UMI a complete manuscript and there are missing pages, these will be noted. Also, if unauthorized copyright material had to be removed, a note will indicate the deletion.

Oversize materials (e.g., maps, drawings, charts) are reproduced by sectioning the original, beginning at the upper left-hand corner and continuing from left to right in equal sections with small overlaps.

Photographs included in the original manuscript have been reproduced xerographically in this copy. Higher quality 6" x 9" black and white photographic prints are available for any photographs or illustrations appearing in this copy for an additional charge. Contact UMI directly to order.

ProQuest Information and Learning
300 North Zeeb Road, Ann Arbor, MI 48106-1346 USA
800-521-0600

MODELING OF EXISTING AND REHABILITATED RC BUILDINGS

BY

MAGED ALI YOUSSEF, B.Sc., M.Sc.,

A Thesis

Submitted to the school of Graduate Studies

in Partial Fulfilment of the Requirements

for the Degree of

Doctor of Philosophy

McMaster University

MODELING OF EXISTING AND REHABILITATED RC BUILDINGS

DOCTOR OF PHILOSOPHY (1999) McMaster University

(Department of Civil Engineering) Hamilton, Ontario

TITLE: Modeling of Existing and Rehabilitated RC Buildings.

AUTHOR: Maged Ali Youssef, B.Sc. Ain Shams University, M.Sc. Ain Shams University.

SUPERVISOR: Professor A. Ghobarah.

NUMBER OF PAGES: xxvi, 143

ABSTRACT

There are many existing buildings which have been designed according to earlier codes. In these codes, either design for seismic loads was not a requirement or design was for lower levels of seismic forces. One of the major challenges that faces structural engineers is to determine the seismic capacity of an existing building and to rehabilitate these buildings to upgrade their seismic capacity if needed. At present, there are no guidelines available for the rehabilitation of existing structures and for the design of different retrofitting techniques. One of the most effective ways of rehabilitation is the addition of reinforced concrete (RC) walls. Until now, there is no robust analytical model available to study the effect of adding RC walls on the building behaviour up to failure. To determine the building seismic capacity and to study the effect of adding RC walls, the analytical model used should be capable of representing all the deficiencies in existing buildings. Moreover, it should be able to represent all possible failure modes such as beam-column joint shear failure, cumulative concrete crushing and bond slip failure.

The objective of the present research is to evaluate the behaviour of buildings retrofitted by the addition of reinforced concrete structural walls. This was done by the development of a suitable analytical model that fully describes the behaviour of

existing buildings before and after rehabilitation using RC structural walls. This model was verified using test results on specimens representing existing structures and found to give results that are closely correlated to the experimental results. The model was able to detect the failure mechanisms observed in the experiments. This model was used in the analysis of an existing three-storey building to determine its seismic capacity. The effect of ignoring the beam-column joint shear deformations, bond slip and concrete crushing was studied. Ignoring any of these parameters can change the building failure mechanism which could lead to misleading results. After that, a suitable rehabilitation technique using RC walls was chosen and the building behaviour after rehabilitation was studied.

ACKNOWLEDGMENTS

The author wishes to express his sincere appreciation to his research supervisor, Dr. A. Ghobarah, for his guidance, advice and time during every stage of this research work. Sincere gratitude are due to Dr. R. Kianoush and Dr. A.D. Spence, members of his supervisory committee, for their valuable comments and suggestions.

Finally, the author dedicates the thesis to his family and his friends for their understanding and continuous encouragements. Their love is the backbone in his persistence to excel.

TABLE OF CONTENTS

LIST OF FIGURES

LIST OF TABLES

LIST OF SYMBOLS

A_c	Concrete area represented by the concrete spring.
A_{ci}	Effective area of the concrete spring of the quadrant i.
A_g	Gross cross sectional area of the concrete section.
a_o, a_1, a_2	Coefficients of σ_{st}-w curve.
A_{ps}, B_{ps}, C_{ps}	Factors defining the shape of the concrete transition curve.
A_p	The reinforcing bar area ($\pi\phi_p^2/4$).
A_s	Steel area represented by the steel spring.
A_{si}	Effective area of the steel spring of the quadrant i.
A_{st}	Cross sectional area of the transverse bar leg.
A_{sr}	The total reinforcing steel area of the section.
a_v	Area of shear reinforcement.
b	Cross section width.
B	Concrete index of confinement.
b_v	Effective width of the section.
c	Clear concrete cover.
|d1+d2|	Elongation in the diagonal spring in the beam-column joint model.

$\|d3+d4\|$	Contraction in the diagonal spring in the beam-column joint model.
D	Undistorted diagonal distance in the beam-column joint model.
d_{spx}, d_{spy}	Spacings of the corner steel springs.
d_b	Steel bar diameter (mm).
d_{cy}	Concrete compressive yield displacement.
d_p	Concrete target displacement at zero load axis.
d_r	Concrete displacement at load reversal.
d_s	Steel element displacement.
d_{s1}	The maximum displacement in preceding cycle in the steel element.
d_{shmax}	Shear displacement at point of unloading.
d_{shmin}	Shear displacement at point of reloading.
d_{su}	Displacement at which strength softening due to bond slip starts in the steel element.
d_{sy}	Yield displacement of the steel element.
d_v	Effective depth of the section.
E_p	Young's modulus of prestressing strands.
E_s	Young's modulus of transverse steel.
F	Force in the diagonal spring in the beam-column joint element.
$F(\epsilon_s)$	The steel stress as a function of strain.

f	A reduction factor to be multiplied by the maximum load reached in the preceding cycle to represent additional stiffness degradation in the steel element.
f_1	Average principal tensile stress in concrete.
f_{1max}	Maximum possible value for f_1 depending on crack width.
f_2	Average principal compressive stress in concrete.
f_{2max}	Maximum possible value for f_2 depending on f_1.
f_c	Compressive stress in concrete.
f_{cr}	Concrete cracking stress.
f_{tc}	Tensile stress of concrete.
f_{ct}	Concrete stress in the transverse direction.
f_{cto}	Strength when the crack begins to open (w=0).
f_{cx}	Concrete stress in the x direction.
f_c'	Compressive strength of concrete.
f_{iy}	The imaginary yield stress for the steel spring.
f_p	Stress in prestressing strands.
f_t	Steel stress in the transverse direction.
f_v	Yield strength of shear reinforcement.
f_x	Steel stress in the x direction.
f_y	The yield strength of the principal bars.

f_{yh}	Yield strength of transverse reinforcement.
h'	Width of the concrete core measured to outside of the ties.
k	Coefficient characterizing the shape of the theoretical hyperbolic σ_{rc}-w curve.
k_1, k_2	Coefficients of τ-σ_n curve for a constant w.
K_h	Factor determining the increase in concrete strength due to confinement.
K_s	Steel element elastic stiffness.
K_{s2}	Steel element post yielding stiffness.
K_{so}	Degraded stiffness for the steel element due to cyclic loading.
l_d	The embedded length of the bar.
M_{bx}, M_{by}	Yielding moments in the x and y directions at the balanced conditions.
N	Axial force acting on the wall in the wall element.
n_p	Number of anchored bars.
n_{st}	Number of legs of transverse reinforcement in the cross section width.
P_{cy}	Concrete yield force in compression.
P_b	The balanced axial load.
P_s	Steel element force.
P_{si} and P_{ci}	The forces in the i^{th} steel and concrete springs, respectively.

P_{siy}	The yield force for the i^{th} effective steel spring.
P_{sl}	The maximum force in the preceding cycle.
P_{so}	Residual force in the steel bars after complete slippage.
P_{su}	Maximum load attained in the steel element.
P_{sy}	Steel element yield force.
P_{ty}	Concrete cracking load.
r	Steel element hardening ratio.
R_{so}	Ratio between P_{so} and P_{su}.
S	The anchored reinforcement slip.
S(x)	The slip at some distance x away from the lead end.
S_h	Center to center spacing of the ties or hoops sets.
S_{mx}	Crack spacing in the x direction.
S_{my}	Crack spacing in the y direction.
S_x	Spacing between bars in x direction.
S_1, S_2, S_3	The characteristic slip values in the local bond slip model shown in figure 4.2.
T(S)	The anchored reinforcement bond stress at the surface between the bar and the concrete.
V	Shear force.
V_{max}	Shear force at point of unloading.

V_{min}	Shear force at point of reloading.
v	Shear stress.
v_{ci}	Limiting value for shear stress that could be transmitted across a crack.
w	crack width.
Z	Slope of the strain softening branch in the concrete model.
γ	Shear deformation.
γ_h	Horizontal shear deformation in the beam-column joint model.
γ_v	Vertical shear deformation in the beam-column joint model..
γ_{xt}	Shear strain.
ϵ_s	The strain in reinforcing bar.
θ	Angle of inclination of the diagonal compression.
λ	Factor used in tables 4.1 to 4.8 representing the degree of confinement.
λ_s	Additional stiffness deterioration parameter in the steel element.
Σo	The reinforcing bar circumference ($\pi\phi_p$).
ϕ	The angle between the diagonal and the horizontal in the beam-column joint model.
ϕ_a	Maximum aggregate size.
ϕ_p	Principal bar diameter.

α_t	Defines the residual tensile strength in concrete.
α	Shape factor characterizing transverse bar.
α_s	Softening factor which depends on the degree by which the steel loses its force.
$\beta_1, \beta_2, \gamma_1, \gamma_2$	Coefficients of τ–S curve for a constant w.
Δz	Transverse reinforcement spacing.
ε_1	Average principal tensile strain.
ε_2	Average principal compressive strain.
ε_c	Concrete strain.
ε_{cr}	Concrete cracking strain.
ε_o	Concrete strain at peak stress f_c'.
ε_p	Concrete target strain at zero load axis.
ε_{pr}	Strain in the prestressing strands.
ε_r	Concrete strain at load reversal.
ε_t	Transverse strain.
ε_x	Longitudinal strain at mid-depth of web.
ϕ_{st}	Transverse bar diameter.
λ_t	Controls the rate at which the concrete tensile strength decays.
ρ_s	The ratio of the volume of hoop reinforcement to the volume of concrete core measured to the outside of the ties.

ρ_{sl}	The steel ratio.
σ_n	Radial pressure produced by principal bar ribs on surrounding concrete.
σ_{rc}	Confining action due to residual tensile strength of cracked concrete.
$\sigma_s(x)$	The steel stress at some distance x away from the lead end.
σ_s	Steel stress.
σ_{st}	The maximum stress of transverse reinforcement close to splitting crack.
τ	The anchored reinforcement bond stress at the surface between the bar and the concrete.
τ_1, τ_3	The characteristic bond stress values in the local bond slip model shown in figure 4.2.
τ_{mo}	Maximum bond stress for uncracked concrete (w=0).
τ_{mw}	Maximum bond stress for a given crack opening w.
τ_o	The value at origin of τ–σ_n curve for a constant w.
τ_{o2}	Value at origin for second branch of ideal trilateral local bond-slip law of the transverse bars.
Ω	Tie index of confinement.
ψ_2	Slope of the τ–σ_n curve for a constant w.
Ψ_{11} and Ψ_{12}	Slopes of first and second branches of ideal trilateral local bond-slip law of the transverse bars.

CHAPTER 1

INTRODUCTION

1.1 GENERAL

The lateral resistance of multistory reinforced concrete frame structures, designed before the availability of current seismic design codes, may not be adequate. In addition, buildings designed to low levels of seismic loads according to older codes that have since been upgraded, may also be deficient. The use of nonductile detailing in these codes results in low seismic capacity. One of the major challenges that faces structural engineers is how to determine the seismic capacity of these buildings and how to decide whether rehabilitation is required and which rehabilitation techniques need to be used. One of the most common rehabilitation techniques is to provide additional reinforced concrete structural walls. The resisting mechanism of reinforced concrete shear panel is derived mainly from the diagonal compression of the infilled concrete. Therefore, the initial stiffness and ultimate resistance are high. However, deformability is small because of brittle nature of the system.

In the past decade, a number of experimental and analytical studies were conducted to gain better understanding of the behaviour of existing reinforced concrete (RC) buildings. However, on the analytical side, models to represent existing structures are still in the process

of development and improvement.

To determine the seismic capacity of existing buildings and analyze the structure after rehabilitation using structural walls, accurate, simple and practical models are needed. The availability of such models will allow the assessment of the seismic performance of existing structures which is necessary information for the design of cost effective rehabilitation systems.

1.2 REVIEW OF PREVIOUS WORK

Seismic strengthening by adding structural walls is widely practiced. The location of these structural walls is determined considering the configuration of the structural system, the architectural design and the use of the building.

1.2.1 Evaluation of the seismic capacity of existing reinforced concrete buildings

Numerous methodologies and approaches have been proposed for conducting seismic evaluation of existing buildings. These methods range from rapid visual inspection which requires only a few man-hours to sophisticated analyses which require hundreds of man-hours, (Miranda, 1991). An example of the screening methods is the comprehensive handbook prepared by the Applied Technology Council under the sponsorship of the Federal Emergency Management Agency, FEMA (Applied Technology Council, 1988).

The three-level procedure for seismic capacity evaluation of existing reinforced concrete buildings, (Aoyama, 1981 and 1986; Hirosawa, 1981) is one of the first multi-level

methods. The procedure is based on the calculation of a seismic index which is mainly a function of strength and ductility. Then a seismic protection index is calculated and compared with the seismic index. On the basis of this comparison, a decision could be made on the condition of the building.

Other screening methodologies are available (Applied Technology Council, 1978, 1987; Allen and Rainer, 1995). These methodologies are inadequate for estimating the actual response of an individual building to severe earthquakes. More refined methodologies are needed to determine the most suitable and effective rehabilitation technique to be used for a specific building.

1.2.2 Framed wall panels

In a framed wall, the wall panel is an element to stiffen the shear resistance of a plane frame. The predominant action in a framed wall is shear. The Japan Concrete Institute collected data on repair and/or strengthening of 157 existing reinforced concrete building between 1933 and 1975. The most common method of strengthening is to add structural walls (85% of the cases), (Endo et al., 1984).

Aoyama (1986) proposed the method shown in figure 1.1 for installation of postcast concrete shear walls. The following steps are proposed:

- Mechanical or chemical anchors are driven into concrete or peripheral frame members.
- Wall reinforcement is placed and the peripheral portion is further reinforced by anti-splitting reinforcement, consisting of either spirals or welded wire fabric (called ladder

bars).

- Installation of form work and pouring of concrete.

Higashi et al. (1981) tested a total of 22 specimens. Three moment frames, two monolithic wall with frames, two frames strengthened by cast in place infilled reinforced concrete walls. The details of one of the specimens are shown in figure 1.2. The behaviour of these specimens was analyzed using simplified inelastic frame models. In these models, the beams and columns are considered as rigidly jointed elements. The wall elements were idealized as compressive bracing or compressive bracing plus tensile bracing. The moment-rotation relationship at the end of frame members and the stress-strain relationship of the additional walls were assumed to be multilinear. The behaviour of frames strengthened by cast in place infilled reinforced concrete walls was nearly the same as that of frames with monolithic wall.

1.2.3 Available models

Most available analysis procedures were developed for buildings with ductile detailing. These methods and computer programs are not applicable to existing nonductile structures as they are unable to detect the failure mechanism and hence, the lateral load resistance capacity of the structure.

Most of the available programs, such as PC-ANSR (Maison, 1992); DRAIN-2DX (Prakash and Powell, 1992), use bilinear force-displacement relationship for modeling the concrete in compression and normally ignore concrete tensile strength. Most importantly, these models ignore failure and represent the concrete as a plastic material. The effect of bond

slip and how it results in a drop in the steel forces which decrease the shear forces on the joints is a behaviour that is normally not represented in most of the available models. Attempts were made to capture the response of concrete elements by using complicated concrete and steel models. However, these models are applicable to single components and are impractical to apply to an actual structure. Most analysis procedures consider beam-column joints to be rigid when analyzing RC structures (Pessiki et al., 1990), this leads to an incorrect prediction of the structural behaviour, particularly in the case of existing structures.

All of the above assumptions will lead to a crude representation of nonductile RC structures. Models that can represent the behaviour of RC elements up to failure are needed. These models should be simple, sufficiently accurate and should be capable of modeling all the deficiencies in existing structures to detect the failure mechanism.

1.3 OBJECTIVE AND SCOPE

The main objective of this study is to develop analytical models to predict the response of beams, columns, beam-column joints and structural walls subjected to monotonic, cyclic or earthquake loading. The model should be able to describe the shear, flexural and bond slip deformations in the critical regions. Moreover, the model should be able to distinguish and detect different failure mechanisms such as bond slip failure, concrete crushing, beam-column joint shear failure and structural wall shear failure. The models are incorporated into a structural analysis computer program that can be used in the analysis of complete structures. In order to achieve the objectives, the scope of research is as follows:

1. Develop material models to represent the behaviour of concrete and steel under

monotonic, reversed cyclic or earthquake loading.

2. Develop a bond slip model that can be used in analysing RC structures.
3. Develop kinematic models to represent shear, bond slip and flexural deformations in beams, columns, beam-column joints and structural walls.
4. Incorporate the kinematic models into a structural analysis computer program and examine the validity of the model by comparing its predictions with the available experimental data.
5. Study the behaviour of a reinforced concrete building before and after rehabilitation by conducting pushover and time history analyses.

1.4 ORGANIZATION

This thesis is organized into eight chapters. Chapter 2 describes the concrete and steel models developed in this study. Detailed description of the newly developed hysteretic models is outlined. The shear model is described in Chapter 3 which starts with describing compatibility, equilibrium and constitutive equations governing the shear response. Then, the solution procedure for these equation is outlined. Finally, the shear hysteretic model is presented.

Chapter 4 describes a new approach for considering the bond slip and how to implement it in the steel element behaviour. The local bond slip problem is described. The solution of the problem of a bar embedded in a concrete section is carried out. Finally, tables were developed to calculate the steel element parameters that will fully define the bond slip problem.

Review of the available models for beams, columns, beam-column joints and structural

walls is presented in Chapter 5. Kinematic models for beams, columns, beam-column joints and structural walls are developed.

Applications of the models are discussed in Chapter 6. Verification examples are given to examine the validity of the reinforced concrete model in describing the behaviour of simple structures to detect their failure mechanism. In Chapter 7, a three-storey building is analyzed before and after rehabilitation. First the building is analyzed using pushover analysis to determine the effect of accounting for different failure mechanisms on the predicted building behaviour. The capacity of the building to resist earthquake loading is determined using time-history analysis. The building is rehabilitated using RC structural walls and the rehabilitated building behaviour was assessed.

In Chapter 8, conclusions of the study and recommendations for future research are presented.

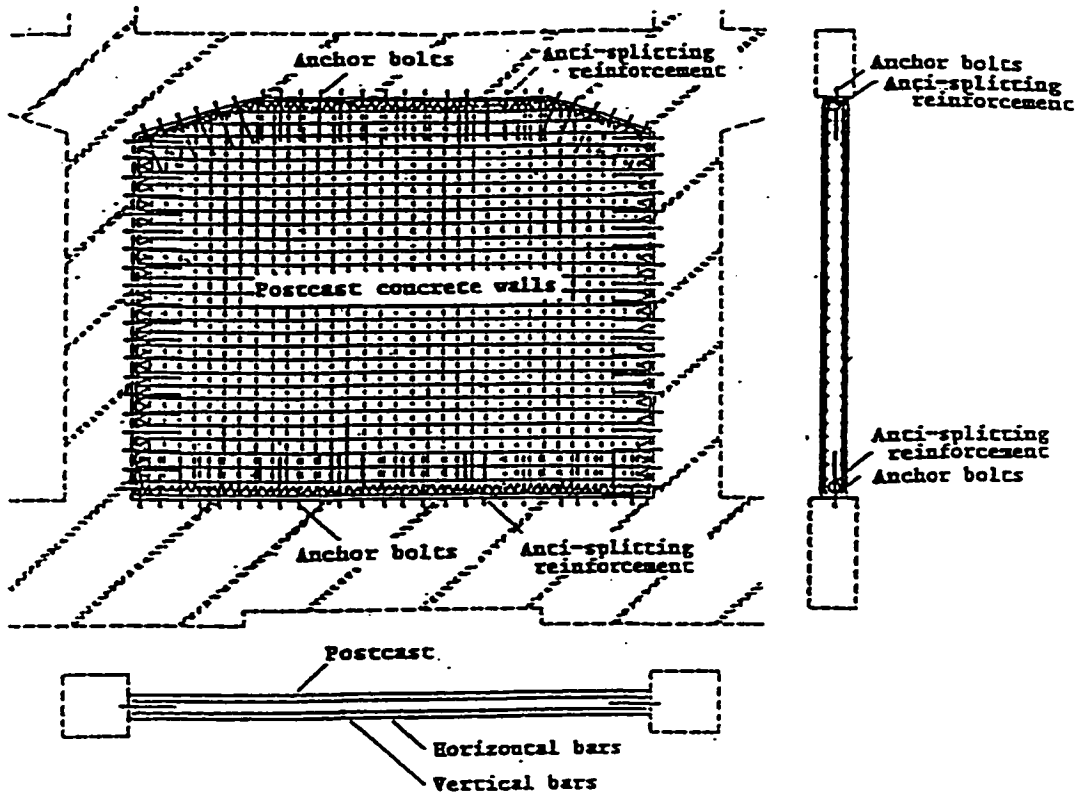

Figure 1.1 Method of erection of postcast concrete shear wall (Aoyama, 1986).

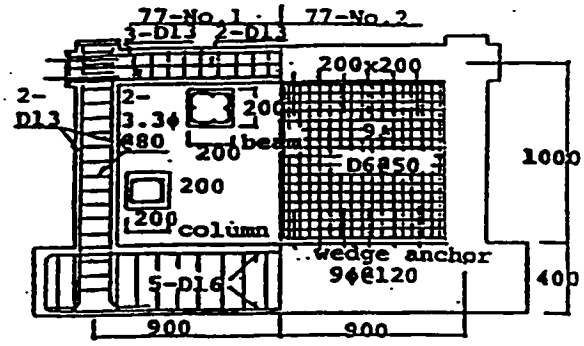

Figure 1.2 Moment frame specimen strengthened by infilled reinforced concrete wall (Higashi et al., 1981).

CHAPTER 2

MATERIAL MODELS

2.1 INTRODUCTION

The development of constitutive models for RC has received a lot of attention by researchers but yet still needs much work especially under cyclic loading. A limited number of models for reinforced concrete under cyclic loading is available. This is due to the complexity of the problem and the numerical difficulties associated with the rules describing the behaviour.

To be able to simulate the hysteretic behaviour of RC elements, the adopted material model should feature the main characteristics that describe completely the hysteretic behaviour of the structural components. These characteristics include stiffness degradation, strength deterioration and pinching behaviour. In addition, the model should be as simple as possible so that the analysis can be performed with reasonable computational effort.

In this Chapter a constitutive model for predicting the response of RC under cyclic loading is introduced. The force-displacement relationship for both concrete and steel are defined. The proposed model is simple enough to be introduced in any macro-model and can be used to analyze prototype structures.

The proposed model is based on the findings of previous experimental and analytical studies. Simplified hysteretic rules defining the cyclic force-displacement curves of concrete and steel are used. Representation of strength degradation and thus representation of failure is introduced. In the concrete model, strength softening is a direct result from concrete crushing while in the steel model, strength softening results from bond slip failure.

2.2 CONCRETE MODEL

Due to the nature of the developed elements, as will be shown in Chapter 4, the concrete model refers to the relationship between the force in a concrete element and the corresponding elongation or shortening. The same idea was used by few researchers (Lai et al., 1984; Ghusn and Saiidi, 1986; Li et al., 1988; Jiang and Saiidi, 1990) but their concrete models included few simplifications. These simplifications include:

- The use of a bilinear curve for concrete in compression.
- Ignoring concrete tensile strength.
- Ignoring confinement effect on the shape of the concrete stress-strain curve.
- Ignoring failure and representing concrete as an elastic-plastic material.
- Determining the initial stiffness by assuming the concrete yield displacement equal to the steel yield displacement.

The above assumptions will lead to a crude representation of concrete behaviour. Moreover, a suitable mapping technique should be used to transfer stresses and strains to forces and displacements.

2.2.1 Concrete tension envelope

The monotonic force-displacement relationship in tension includes a linear branch until the cracking load, P_{ty}, is reached and a softening branch which describes the post cracking stage. The tension stiffening relationship developed by Stevens et al. (1987) is adopted. It describes the uniaxial concrete tensile response after cracking. The relationship is shown in figure 2.1 and is expressed as follows:

$$f_{ct} = f_{cr}\left[(1-\alpha_t)\times e^{-\lambda_t\times(\varepsilon_c-\varepsilon_{cr})}+\alpha_t\right] \qquad (2.1)$$

where ε_c is the concrete strain, ε_{cr} is the concrete cracking strain and f_{cr} is the concrete cracking stress and is equal to:

$$f_{cr} = 0.33\sqrt{f_c'} \qquad (2.2)$$

where f_c' is the concrete compressive cylinder strength in MPa, α_t defines the residual tensile strength in concrete and its value could be taken equal to 75 ρ_{sl} / d_b as suggested by Elmorsi (1998), where, ρ_{sl} is the steel ratio and d_b is the bar diameter (mm).

The parameter λ_t controls the rate at which the response decays and is equal to:

$$\lambda_t = \frac{270}{\sqrt{\alpha_t}} \qquad \lambda_t \le 1000 \qquad (2.3)$$

2.2.2 Concrete compression envelope

The monotonic compression curve follows the model of Kent and Park (1971) that was later extended by Scott et al.(1982). Even though more accurate and complete models

have been published since (Stevens et al., 1987; Sittipunt and Wood, 1993), the so-called modified Kent and Park model offers a good balance between simplicity and accuracy. In this model, the monotonic concrete stress-strain relation in compression is described by two regions:

$$f_c = K_h f_c' \left[2.0 \left(\frac{\varepsilon_c}{\varepsilon_o} \right) - \left(\frac{\varepsilon_c}{\varepsilon_o} \right)^2 \right] \qquad \varepsilon_c \le \varepsilon_o \qquad (2.4)$$

$$f_c = K_h f_c' \left[1 - Z(\epsilon_c - \epsilon_o) \right] \qquad \ge 0.2 K_h f_c' \qquad \epsilon_c \ge \epsilon_o \qquad (2.5)$$

where the concrete strain ε_o at maximum stress is

$$\varepsilon_o = 0.002\ K_h \qquad (2.6)$$

and the strength increase due to confinement is determined by the factor K_h:

$$K_h = 1 + \frac{\rho_s f_{yh}}{f_c'} \qquad (2.7)$$

The slope of the strain softening branch Z is calculated as:

$$Z = \frac{0.5}{\dfrac{3 + 0.29 f_c'}{145 f_c' - 1000} + 0.75 \rho_s \sqrt{\dfrac{h'}{S_h}} - 0.002 K_h} \qquad (2.8)$$

where f_c' is the concrete compressive cylinder strength in MPa, f_{yh} is the yield strength of

transverse reinforcement in MPa, ρ_s is the ratio of the volume of hoop reinforcement to the volume of concrete core measured to the outside of the ties, h' is the width of the concrete core measured to outside of the ties and S_h is the center to center spacing of the ties or hoops sets. Figure 2.2 shows the stress-strain relation for confined and unconfined concrete of 30 MPa compressive strength.

2.2.3 Mapping

To apply the set of equations 2.1 to 2.8, transformation from stress to force and from strain to displacement should be made. The force transformation factor is taken equal to the concrete area represented A_c, multiplied by 0.85. The factor 0.85 is taken to average the concrete stress over the area A_c. For example, the yield force in compression, P_{cy}, is:

$$P_{cy} = 0.85\ A_c\ K_h\ f_c' \qquad (2.9)$$

The plastic deformation of the effective concrete element is postulated to represent the accumulated crushing behaviour of the concrete over the plastic hinge length. The methodology used for the determination of the concrete compressive yield displacement d_{cy} that corresponds to the compressive yield force P_{cy} depends on the fact that the displacement is the integration of the strain over a certain length. The displacement transformation factor is taken as d_{cy} / ε_o.

2.2.4 Cyclic force-displacement relationship

The main function of the concrete element is to represent the opening and closing of

cracks. Some of the available hysteretic models were found to be inadequate for the idealization of the concrete elements (Lai et al., 1984; Ghusn and Saiidi, 1986; Li et al., 1988; Jiang and Saiidi, 1990). This is mainly because their models neglect the concrete resistance in tension and the convergence difficulties that appear due to the abrupt change in stiffness from a low value to a high value. A typical hysteretic cycle for the concrete element is shown in figure 2.3. In this cycle, loading starts in the positive direction until the cracking load, P_{cy}, is reached and the post cracking curve is followed. When the load direction is reversed, loading proceeds in the negative direction until the open cracks are closed. Crack closing is characterized by an abrupt change in the stiffness from very low stiffness to the initial stiffness which may cause convergence difficulties. To overcome this problem a smooth transition curve that represents gradual change in stiffness is used. This curve is actually closer to what happens in reality as can be seen from figure 2.4 which shows the results of a cyclic tensile test. Mattock (1979) represented the stress-strain response of prestressing strand by two straight lines joined by a curve given by the following equation:

$$f_p = E_p \, \varepsilon_{pr} \left[A_{ps} + \frac{(1 - A_{ps})}{[1 + (B_{ps} \varepsilon_{pr})^{C_{ps}}]^{\frac{1}{C_{ps}}}} \right] \qquad (2.10)$$

where f_p is the stress in the prestressing strands, ε_{pr} is the strain in the prestressing strands, E_p is Young's modulus of prestressing strands. The constants A_{ps} and B_{ps} can be determined as shown in figure 2.5 and C_{ps} is a constant that controls the shape of the transition curve. The same curve was adopted as a transition curve. The C_{ps} value was taken equal to 10. This transition curve is followed until the envelope curve is reached. If loading continues in the

same direction, the yield force P_{cy}, is reached and the post yield branch is followed. If the load direction is reversed at displacement d_r corresponding to strain ε_r, unloading takes place aiming at displacement d_p corresponding to strain ε_p on the zero load axis. The strain ε_p is calculated using the equations given by Taucer et al. (1991) as:

$$\frac{\varepsilon_p}{\varepsilon_o} = 0.145\left(\frac{\varepsilon_r}{\varepsilon_o}\right)^2 + 0.13\left(\frac{\varepsilon_r}{\varepsilon_o}\right) \qquad \left(\frac{\varepsilon_r}{\varepsilon_o}\right) < 2 \qquad (2.11a)$$

$$\frac{\varepsilon_p}{\varepsilon_o} = 0.707\left(\frac{\varepsilon_r}{\varepsilon_o} - 2\right) + 0.834 \qquad \left(\frac{\varepsilon_r}{\varepsilon_o}\right) \geq 2 \qquad (2.11b)$$

Loading then proceeds with zero stiffness until the displacement changes from negative (compression) to positive (tension). The loading line then aims at the point on the post crack branch where unloading started in the previous cycle. If unloading occurs again, the transition curve is again followed until the monotonic envelope curve is reached and then the loading line aims at the previous unloading point on the post yield branch of the previous cycle. The remaining part of the cycle follows the same route previously described.

2.3 STEEL MODEL

The steel model refers to the relationship between the force in a steel element and the slippage of the bar. The same idea was used by several researchers (Lai et al., 1984; Ghusn and Saiidi, 1986; Li et al., 1988; Jiang and Saiidi, 1990) however, their model was based on several restrictively simplifying assumptions. The simplifications involved in the model

include:

- The given equation to calculate the elastic stiffness K_s describes only one case of bond slip which is not defined.
- The yield force of the steel model is based on the steel yield stress.
- Bond slip failure was not represented.

All of the above assumptions will lead to a crude representation of steel. Moreover, the steel element should include the effects of the inelastic behaviour of the steel and its bond-slip behaviour with the concrete.

2.3.1 Steel monotonic envelope

The steel model includes a bilinear monotonic envelope in tension and the same envelope in compression as shown in figure 2.6. The relevant parameters (the elastic stiffness K_s, the post yielding stiffness $K_{s2} = r K_s$, the steel yield force P_{sy}), can be defined as discussed in Chapter 4.

To define the post slip failure ($d_s > d_{su}$) behaviour of the steel element, it is suggested that the force P_s corresponding to a displacement d_s is given by:

$$P_s = P_{sy}\left(R_{so} + \frac{1 - R_{so}}{1 + \alpha_s (d_s - d_{su})^2} \right) \qquad (2.12)$$

where R_{so} is the ratio between the residual force P_{so} in the steel bars after complete slippage and the maximum load attained P_{su}, α_s is a softening factor which depends on the degree by which the steel loses its force, d_{su} is the displacement at which strength softening due to bond

slip starts. All these factors can be determined as explained later in Chapter 4.

2.3.2 Cyclic force-displacement relationship

The criteria for developing the hysteretic model for the steel element is that when this element is combined with the concrete element, it will describe the main behavioural characteristics of RC elements. Figure 2.7 illustrates a typical hysteretic cycle for the steel element. In this cycle, loading starts in the positive direction with stiffness K_s until the yield load P_{sy} is reached and then the post yielding curve is followed at stiffness K_{s2}. As the load direction is reversed, unloading proceeds with the same initial stiffness K_s. When the force reaches zero, the stiffness changes and aims at the yield point in the first cycle or at the previous unloading point on the negative envelope. Unloading from the negative envelope will be parallel to the initial stiffness K_s, until zero force. Loading in tension will begin aiming at the previous unloading point or if the additional stiffness degradation starts (after reaching yield), loading will be with degraded stiffness K_{s0} until reaching the envelope curve. As the load direction is reversed, unloading will proceed in the same manner described above. The difference between the hysteretic model for the steel element and that of an ideal elastic-plastic rule was implemented to represent the pinching effect due to the bond-slip.

The additional stiffness deterioration is taken into account in cycles following the cycle when the yield load is exceeded. A formula similar to that presented by (Park et al., 1987), is adopted.

$$f = 1.0 - \lambda_s \frac{d_{s1}}{d_{sy}} \qquad (2.13)$$

where f is a reduction factor to be multiplied by the maximum load reached in the preceding cycle as shown in Figure 2.7, λ_s is the strength deterioration parameter, the maximum achieved displacement in the preceding cycle d_{s1} corresponds to load P_{s1}, and d_{sy} is the yield displacement corresponding to yield load P_{sy}. In the absence of test data, typical values for λ_s to be used are: 0.0 for no degradation, 0.0001 for slight degradation, 0.01 for moderate degradation and 0.1 for substantially increased degradation, (Youssef and Ghobarah, 1999). Once the deteriorated strength ($f P_{s1}$) is determined, the stiffness for the next cycle can be defined.

2.4 SUMMARY

Concrete and steel constitutive models are presented in this Chapter. The models when combined by a suitable macro element are expected to reproduce most of the characteristic features of RC behaviour under reversed cyclic loading.

The concrete model includes representation of tension stiffening and strength degradation. Transition curves were used to overcome the numerical instability. Simple hysteretic models were developed.

The steel model includes the relaxation of the bars due to bond slip. A formula was suggested to describe the post peak stress response. The developed hysteretic model includes the pinching effect resulting from bond slip.

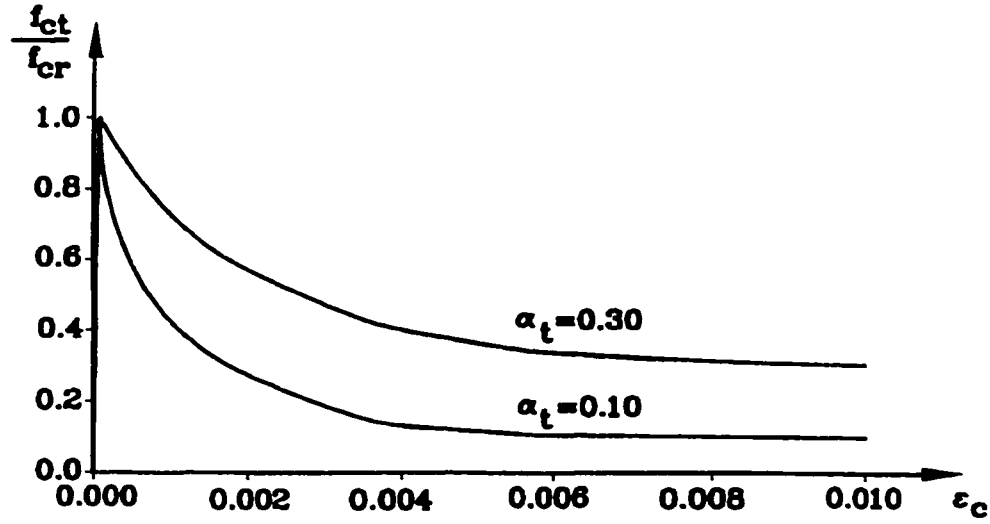

Figure 2.1 Uniaxial concrete tensile response for various values of α_t(Stevens et al., 1987)

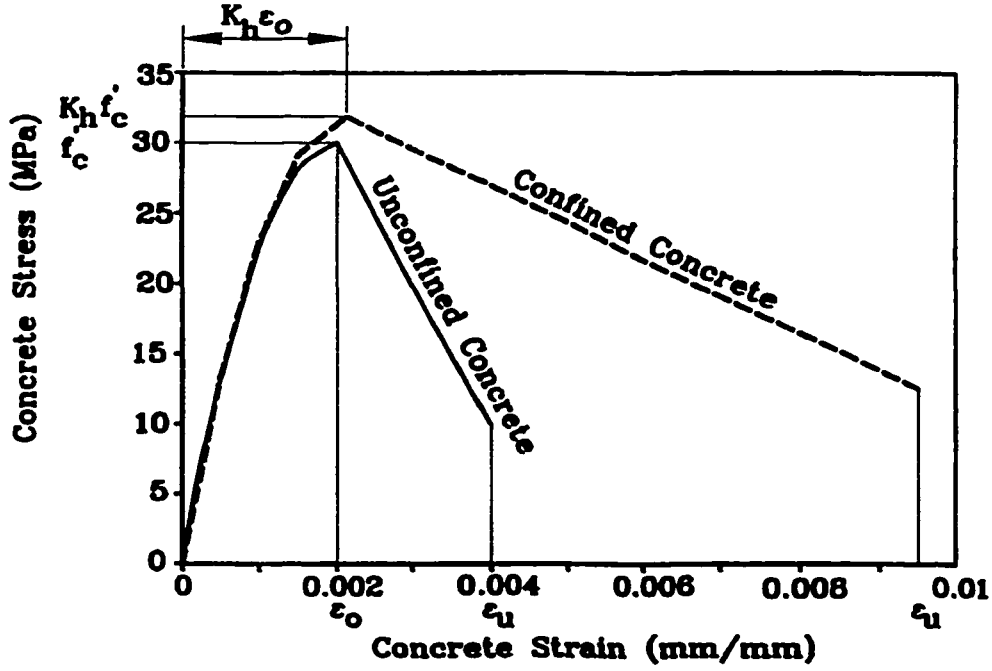

Figure 2.2 Stress–strain relation for confined and unconfined concrete with f_c' = 30 MPa

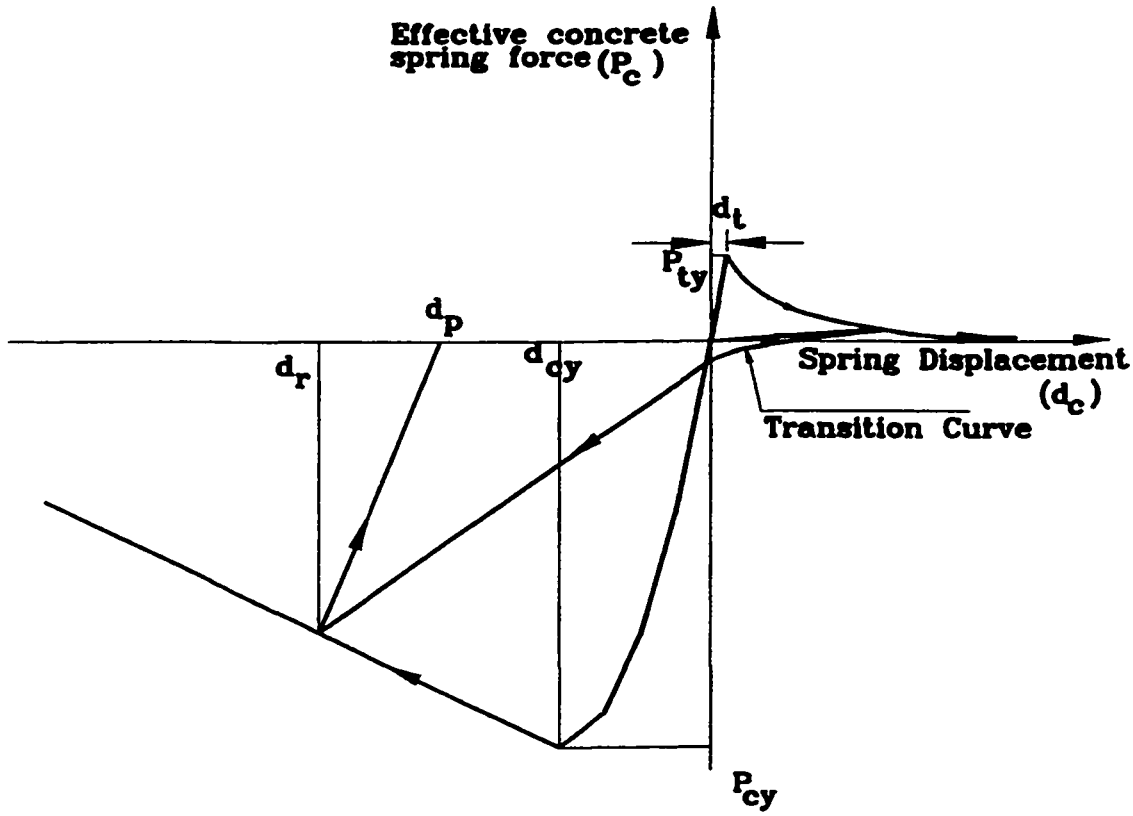

Figure 2.3 Cyclic force–displacement relationship for concrete.

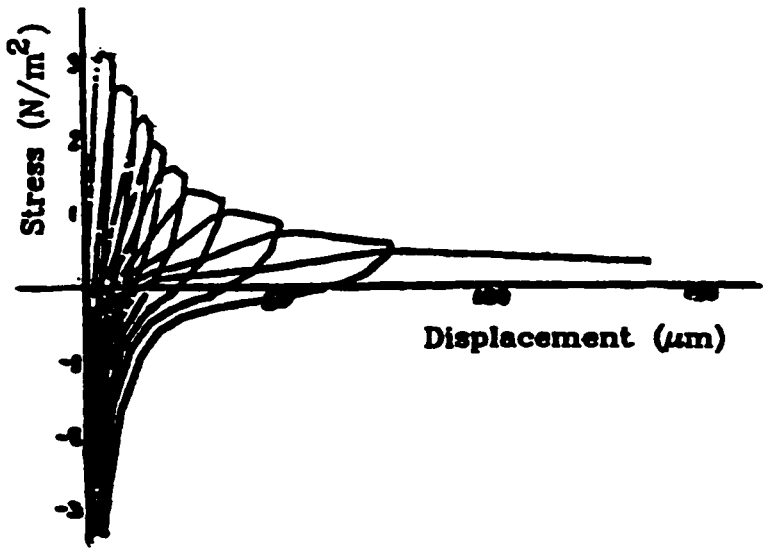

Figure 2.4 Uniaxial tensile cyclic test (Yankelevsky and Reinhardt, 1989)

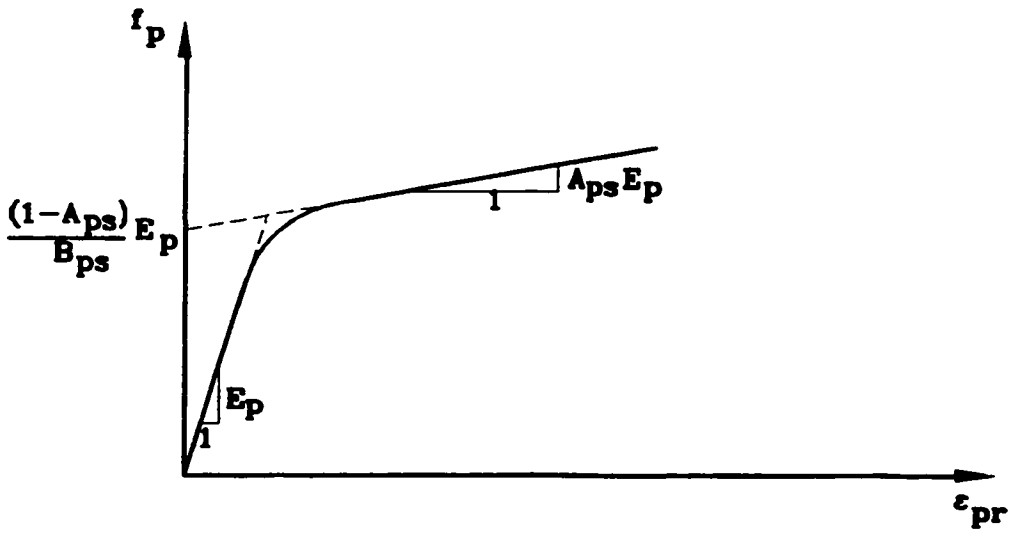

Figure 2.5 Stress–strain response of a prestressing strand (Mattock, 1979)

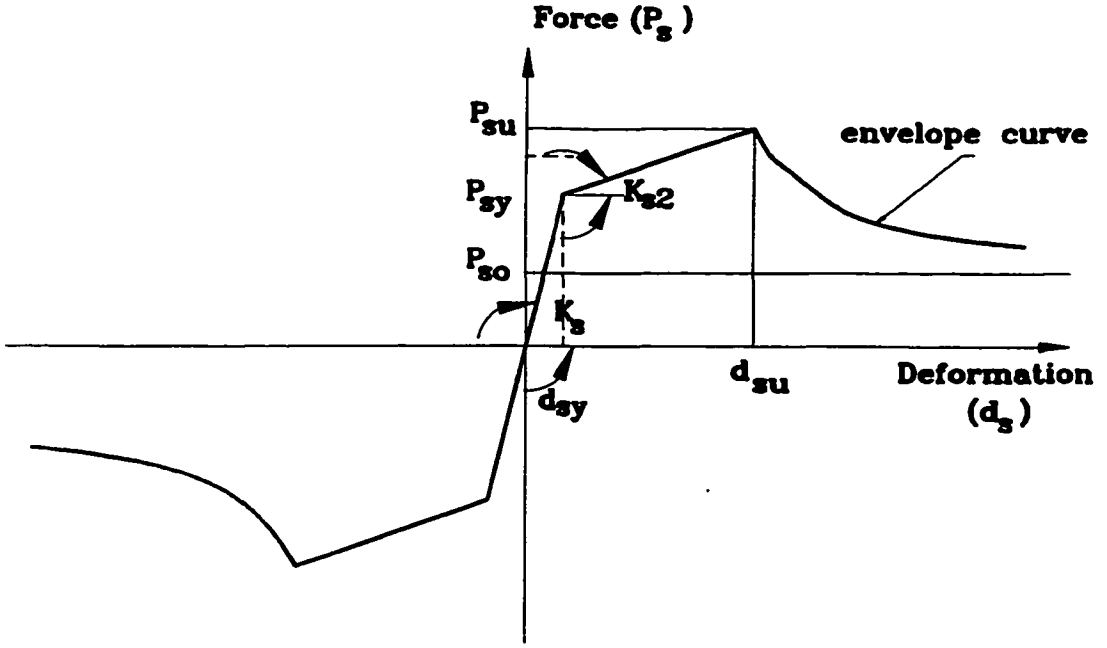

Figure 2.6 Envelope for steel response in tension and compression

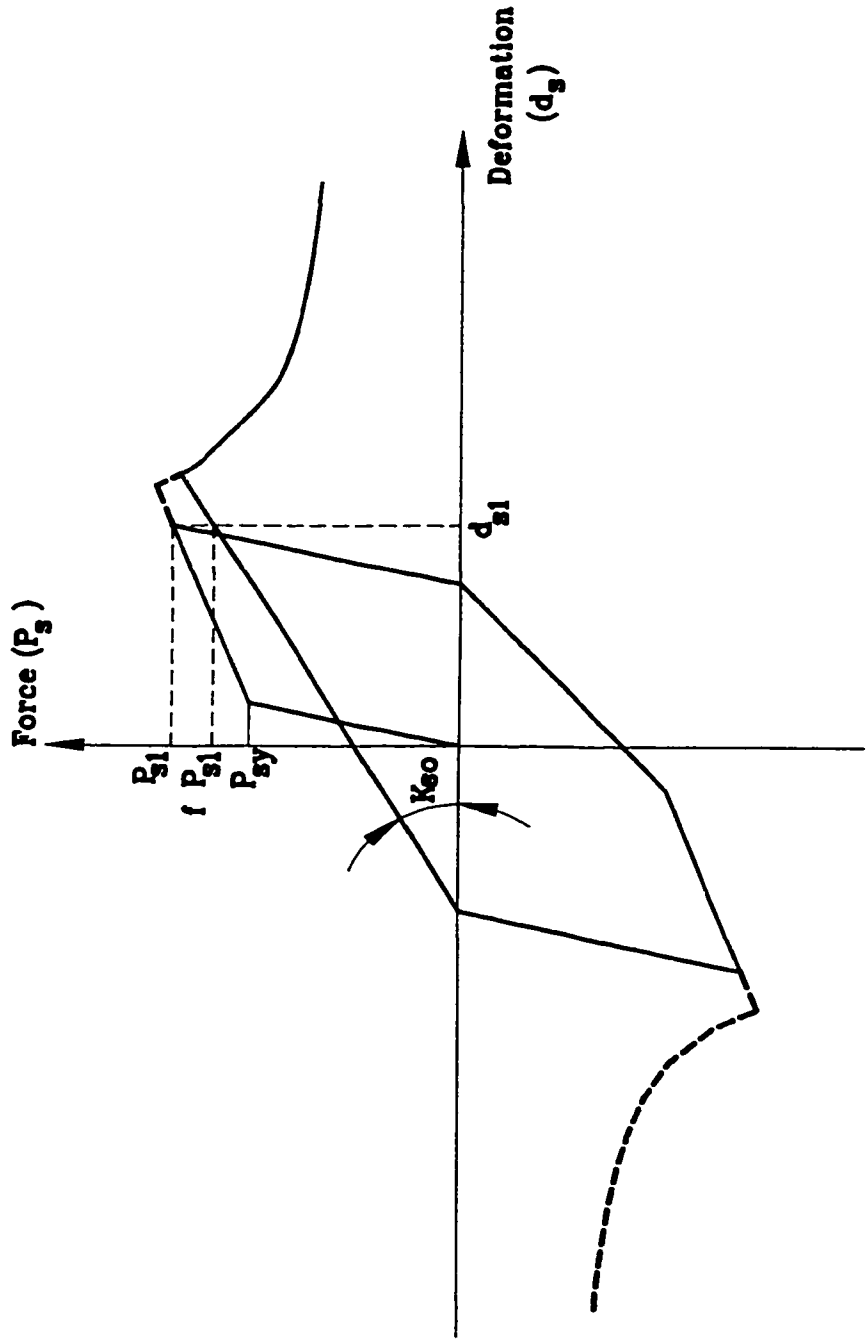

Figure 2.7 Hysteretic model for the steel element

CHAPTER 3

SHEAR MODEL

3.1 INTRODUCTION

The modeling of the shear response of concrete structures is an important and a difficult task due to the interaction between the shear and the axial force acting on the section. There are several models available. One of the more complex models is that of Ozcebe and Saatcioglu (1989). These models also describe the cyclic shear response of RC members but require a great computational effort and are more time consuming. A new hysteretic model for the shear behaviour of reinforced concrete members subjected to shear force reversals is proposed. The modified compression field theory is used to define the envelope curve. The effect of the normal force on the shear behaviour of the shear element is taken into account using sectional analysis.

3.2 COMPATIBILITY EQUATIONS

From Mohr's circle of strains shown in figure 3.1 (Collins and Mitchell, 1987), the following equations can be written:

$$\epsilon_2 = \epsilon_1 - \frac{\gamma_{xt}}{\sin(2\theta)}$$
$$\epsilon_x = \epsilon_1 - \frac{\gamma_{xt}}{2}\left(\frac{1}{\sin(2\theta)} + \frac{1}{\tan(2\theta)}\right) \qquad (3.1)$$
$$\epsilon_1 = \epsilon_x + \epsilon_t - \epsilon_2$$

where ε_x is the longitudinal strain at mid-depth of web, ε_t is the transverse strain, ε_1 is the principal tensile strain, ε_2 is the principal compressive strain, γ_{xt} is the shear strain and θ is the angle of inclination of the diagonal compression given by the formula:

$$\tan^2\theta = \frac{(\epsilon_x - \epsilon_2)}{(\epsilon_t - \epsilon_2)} \qquad (3.2)$$

3.3 CONSTITUTIVE EQUATIONS

In shear problems, stresses are in two directions and thus strain conditions to which the concrete is subjected differ from those in a cylinder test. Tensile stresses f_1 will weaken the principal compressive stress in concrete f_2 as given by Vecchio and Collins (1986) as:

$$f_{2max} = \frac{K_h f_c'}{(0.8 - 0.34\frac{\epsilon_1}{\epsilon_o})} \qquad \leq K_h f_c' \qquad (3.3c)$$

Applying this equation and using the same concrete model defined by equations (2.4), (2.5), (2.6) , (2.7) and (2.8) in Chapter 2:

$$f_2 = f_{2max}\left[2\left(\frac{\epsilon_2}{\epsilon_o}\right) - \left(\frac{\epsilon_2}{\epsilon_o}\right)^2\right] \qquad \epsilon_2 \le \epsilon_o \qquad (3.3a)$$

$$f_2 = f_{2max}\left[1 - Z(\epsilon_2 - \epsilon_o)\right] \qquad \ge 0.2K_h f_c' \qquad \epsilon_2 \ge \epsilon_o \qquad (3.3b)$$

where f_c' is the compressive strength of concrete and ε_o is the concrete strain at peak stress f_c'.

The relationship between the average tensile stress f_1, and the average tensile strain ε_1 used is the same as that explained in Section 2.2.1.

The ability of the crack interface to transmit shear stresses depends on the crack width w which can be calculated from the equation:

$$w = \frac{\epsilon_1}{\frac{\sin\theta}{S_{mx}} + \frac{\cos\theta}{S_{my}}} \qquad (3.4)$$

where S_{mx} and S_{my} are the crack spacing in the x and y directions, respectively. Bhide and Collins (1989) used the CEBFIP (Comité Euro-International du Béton-Fédération Internationale de la Précontrainte) code formula, given by equation 3.5, for calculating the crack spacing:

$$S_{mx} = 2(c + \frac{S_x}{10}) + 0.1\frac{d_b}{\rho_{sl}} \qquad (3.5)$$

where c is the clear concrete cover, S_x is the spacing between bars in x direction, d_b is the bar diameter and ρ_{sl} is the ratio of the reinforcement area to the concrete area.

Collins and Mitchell (1987) suggested that the limiting value for the shear stresses v_{ci}, that could be transmitted across a crack is:

$$v_{ci} = \frac{0.17\sqrt{f_c'}}{0.3 + 0.6w} \tag{3.6}$$

where the limiting value for the shear stresses v_{ci} and the crushing strength f_c' are in MPa and the crack width w is in mm.

Hence, f_l is limited to (Collins et al., 1996):

$$f_{lmax} = v_{ci} \tan \theta \tag{3.7}$$

3.4 ELEMENT EQUILIBRIUM

The shear force V, can be calculated from the following equation:

$$V = \frac{\frac{a_v f_v d_v}{S_h} + f_l b_v d_v}{\tan \theta} \tag{3.8}$$

where a_v and f_v are the area and yield strength of the shear reinforcement, respectively, b_v is the effective width of the section, d_v is the effective depth of the section, and S_h is the spacing between the stirrups, or the spacing between the web reinforcement in the case of structural walls.

Mohr's circle of stresses is shown in figure 3.2. Here, f_{cx} is the concrete stress in the x direction, f_{ct} is the concrete stress in the transverse direction, v is the shear stress, f_x is the steel stress in the x direction and f_t is the steel stress in the transverse direction. For

equilibrium, the following equation should be satisfied:

$$\text{error} = f_2 + f_1 - \left(\tan\theta + \frac{1}{\tan\theta}\right)\frac{V}{b_v\, d_v} = 0$$

$$v = \frac{V}{b_v\, d_v} \qquad (3.9)$$

3.5 SOLUTION STRATEGY

The approach to the solution is shown in figure 3.3. During each cycle of the iteration process, the shear force corresponding to a specified shear deformation calculated by the structural model based on wall deformation is determined using the modified compression field theory. The solution strategy to determine the shear force corresponding to a specified shear strain at which equilibrium is satisfied is shown in figure 3.4. Iterations are carried out over an incrementally increasing average principal tensile strain, ε_1. For each iteration, ε_x is calculated from equation 3.1 then the axial force corresponding to this ε_x is calculated using sectional analysis. This procedure is repeated until for a certain ε_1, the axial force on the section is equal to the acting axial force.

3.6 CYCLIC FORCE-DISPLACEMENT RELATIONSHIP FOR SHEAR

The above solution strategy establishes the primary curve for the shear element. Every point on this curve will be evaluated for the corresponding axial force acting on the section represented by the shear element. The modified compression field theory has the ability of determining the point at which degradation in shear strength will start and thus modelling of failure is included in the shear element. To account for the continually varying stiffness and

energy absorption characteristics under cyclic loading, a suitable hysteretic model is needed. The hysteretic model developed is shown in figure 3.5, which describes a typical reversed shear cycle. The loading cycle starts in the positive direction and follows the monotonic curve described in the previous section. At point 1, the load direction is reversed. The unloading from point 1 is assumed to aim at point 2 which is 85% of the shear displacement of the unloading point. As loading is increased in the negative direction, a significant reduction in the tangent stiffness occurs which represents the pinching effect experienced by RC structures under cyclic loading. The reduced tangent stiffness is calculated based on the V_{max} and d_{shmax} as shown in figure 3.5. If loading proceeds in this direction, the envelope curve in the negative direction is reached (point 3). This is also calculated using the shear constitutive equations. As the loading is reversed at point 4, the unloading stiffness is calculated in the same manner described in the positive direction. After point 5, positive loading continues with a reduced stiffness, calculated based on V_{min} and d_{shmin}, until the positive unloading branch is reached at point 6. Loading then follows that positive unloading branch until the positive envelope curve is reached.

3.7 SUMMARY

The proposed model is characterized by its simplicity and its ability to describe the pinching experienced as a result of shear deformations under cyclic loading by using simple loading and unloading rules.

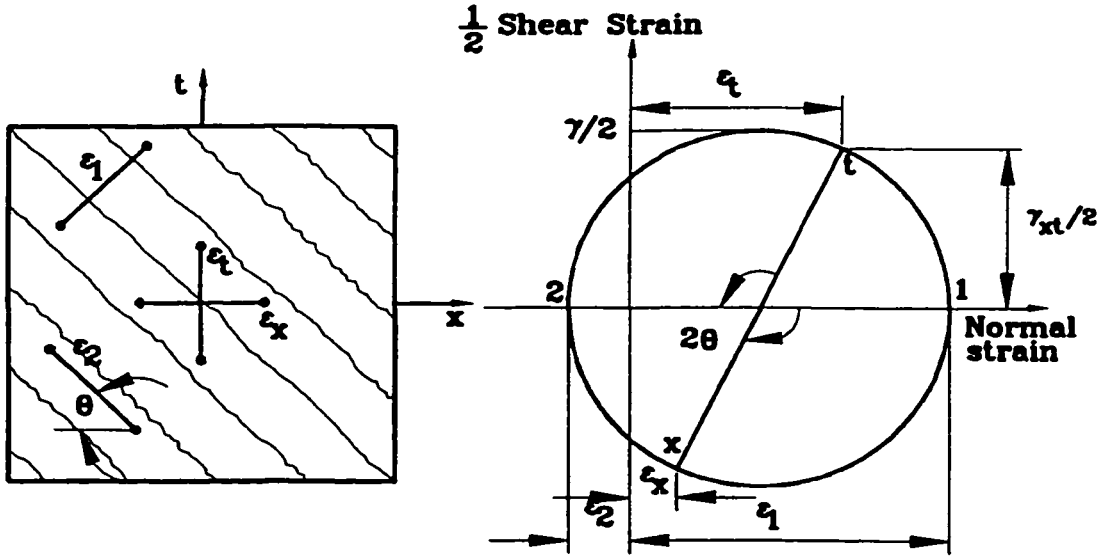

Average strains in cracked element

Mohr's circle for average strains

Figure 3.1 Compatibility conditions for cracked web element (Collins and Mitchell, 1987)

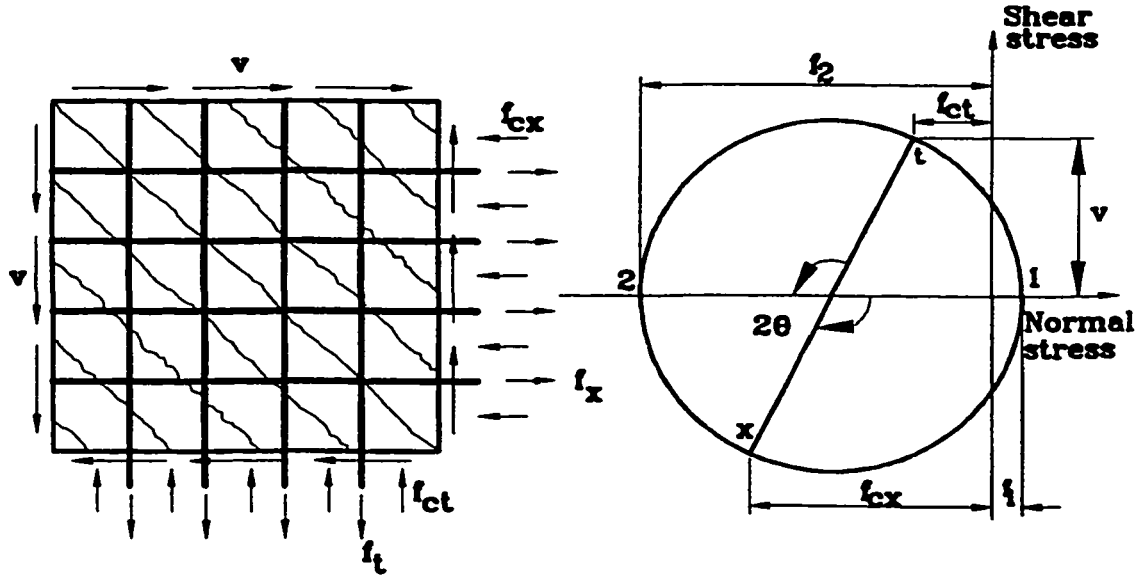

Average stresses in cracked element

Mohr's circle for average concrete stresses

Figure 3.2 Equilibrium conditions for cracked web element (Collins and Mitchell, 1987)

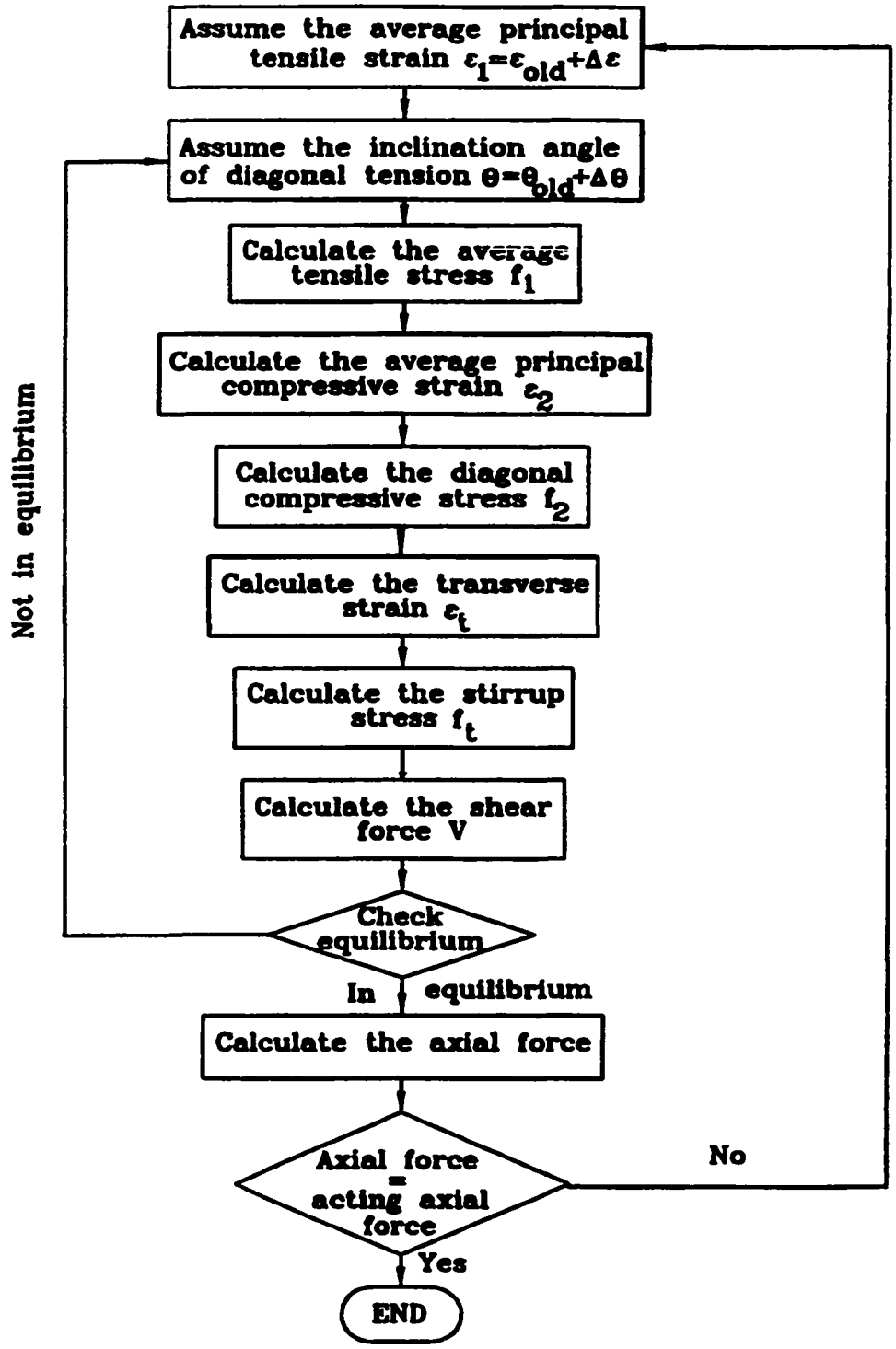

Figure 3.3 Solution strategy for determining the shear force corresponding to a given shear strain.

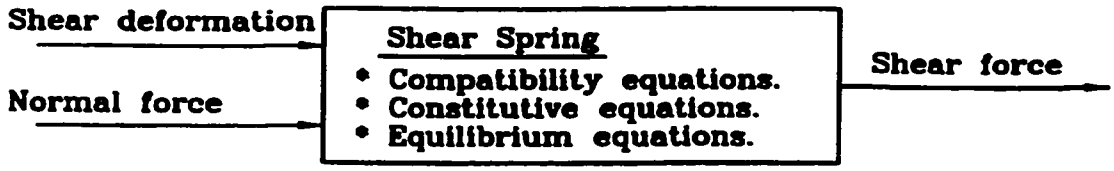

Figure 3.4 Shear spring model

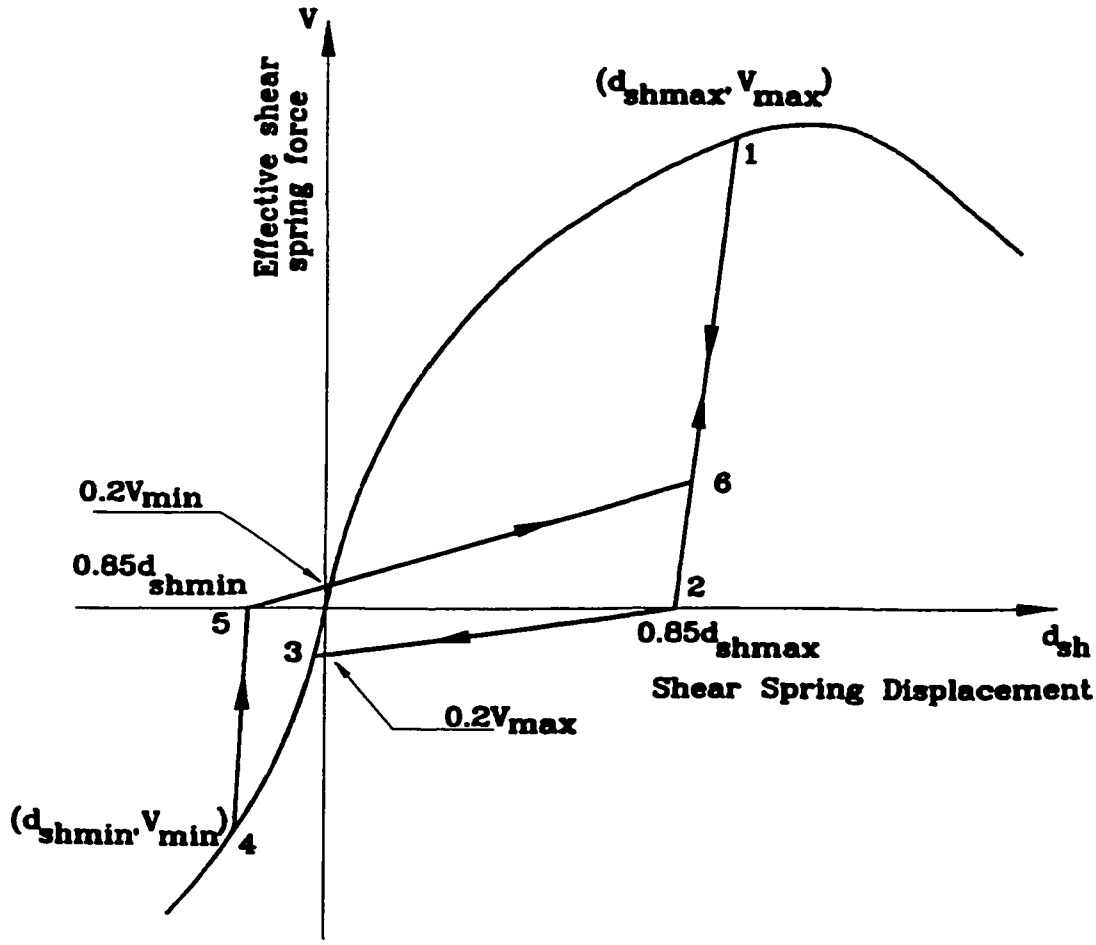

Figure 3.5 Shear hysteretic model

CHAPTER 4

BOND SLIP MODEL

4.1 INTRODUCTION

Most of the analytical studies on the hysteretic behaviour of reinforced concrete elements are based on the assumption of perfect bond between steel and concrete. In some cases, bond slip deformations could constitute a major part of the overall deformations of the structure. One such a case is existing reinforced concrete frame structures built before the 1970's. Ignoring bond slip may lead to the wrong failure mechanism prediction.

In Lai et al. (1984) model, the calculation of the elastic stiffness K_s of the steel element was assumed to be based on the cumulative slip of the steel bar as shown in figure 4.1. The given equation to calculate K_s describes only one case of bond slip which is not defined. Moreover, Lai et al. (1984) assumed that the yield force of the steel elements is based on the steel yield stress which is not the case for poor bond conditions (short splice or insufficient confinement). In such case, bond slip will occur before steel yielding (curve A in the strain diagram in figure 4.1) and this will result in further lowering of the steel stress. On the other hand, for good bond conditions (adequate splice and confinement), bond slip will occur after yield is reached. This does not mean that the steel force will yield at the same time when steel reaches its yield stress. Due to favourable bond conditions, accumulative yielding of

successive sections in the steel bar will occur (the steel strain will change from curve B to C to D as shown in figure 4.1. The yield force will depend on the degree of confinement and the anchorage length. Therefore, the steel element should include the effects of the inelastic behaviour of the steel and its bond-slip behaviour with the concrete. As such, yield stress of the element in this context could refer to the yielding of the steel bar, inelastic bond response or a combination thereof.

Some researchers (Ghusn and Saiidi, 1986; Li et al., 1988; Jiang and Saiidi, 1990) introduced modifications to the macroscopic element developed by Lai et al. (1984), however, most of the deficiencies remain and the modified elements do not account for strength deterioration due to bond slip failure or concrete crushing.

In this chapter, an accurate and efficient bond slip model is described. This model is used to determine the characteristics of different bars embedded in RC and tables are introduced to calculate the force-displacement relationship of any bar embedded in RC. The model could be easily implemented in steel element to represent the static and dynamic behaviour of RC members.

4.2 LOCAL BOND SLIP

4.2.1 Introduction

The local bond slip law of an anchored bar after the splitting of its surrounding concrete needs to be defined. Figure 4.2 shows the overall shape of the local bond stress-slip constitutive model used in this study (Ustuner, 1992). It consists of a monotonic envelope and reduced bond resistance curve corresponding to pullout failure. The characteristic bond stress

and slip values in this local bond slip model (τ_1, τ_3, S_1, S_2, S_3) depend on the bar diameter, the concrete strength, the clear distance between the lugs of the reinforcing bars, the concrete cover and the local confining action. The local confining action varies depending on both concrete mechanical properties and geometrical characteristics of the specimen. Concrete cover effect can be ignored as it cracks and falls off at low load levels.

4.2.2 Confining action due to transverse reinforcement

Based on numerous statistical evaluations of experimental data, Orangun et al. (1977) proposed an equation to evaluate the ultimate bond strength (τ_1) taking into account its dependence on the confining action provided by the transverse reinforcement by adding a term which includes the yield strength of transverse reinforcement. Darwin et al. (1996) analyzed the test results for 299 specimens and arrived at an opposite conclusion. They found that the yield strength of transverse reinforcement plays no significant role in its effectiveness in preventing bond failure. The local mechanical properties of concrete and the interaction phenomenon between the principal and transverse reinforcement were included in an analytical model developed by Giuriani et al. (1991). This model was found to give good correlation with the experimental results. It was used in the present model to determine the values of ultimate bond strength (τ_1) and the corresponding slip (S_1). The solution strategy used is as follows:

First, assume a value for the splitting crack opening width w. The maximum stress in the transverse reinforcement before the splitting crack, σ_{st} can be determined using the equation:

$$\sigma_{st} = E_{st}\sqrt{\frac{a_2}{(\alpha\phi_{st})^2}w^2 + \frac{a_1}{(\alpha\phi_{st})}w + a_o} \qquad (4.1a)$$

where

$$a_o = \frac{a_1^2\,\frac{\psi_{12}}{\psi_{11}}}{4a_2\left(\frac{\psi_{12}}{\psi_{11}} - 1\right)} \qquad (4.1b)$$

$$a_1 = 8\frac{\tau_{o2}}{E_s} \qquad (4.1c)$$

$$a_2 = \frac{4\psi_{12}\phi_{st}}{E_s} \qquad (4.1d)$$

The shape factor characterizing the transverse bar is α, ϕ_{st} is the transverse-bar diameter, E_{st} is the modulus of elasticity of the transverse steel, a_o, a_1, a_2 are coefficients of σ_{st}-w curve, τ_{o2} is the value at origin for second branch of ideal trilateral local bond-slip law of the transverse bars shown in figure 4.3, ψ_{11} and ψ_{12} are the slopes of first and second branches of the same curve.

4.2.3 Confining action due to residual strength of cracked concrete

The second confining action σ_{rc} which is due to residual tensile strength of the cracked

concrete is determined as:

$$\sigma_{rc} = \frac{f_{cto}}{\left(k\frac{w}{\phi_a} + 1 \right)} \tag{4.2}$$

where f_{cto} is the concrete strength when the crack begins to open (w=0), k is a coefficient characterizing the shape of the hyperbolic σ_{rc}-w curve and ϕ_a is the maximum aggregate size.

4.2.4 Global confining action

Knowing σ_{st} and σ_{rc}, the global confining action which is equal to the global radial force produced by the anchored longitudinal bars is given by:

$$\sigma_n = \Omega\sigma_{st} + B\sigma_{rc} \tag{4.3a}$$

where

$$\Omega = \frac{n_{st}A_{st}}{n_p\phi_p\Delta z} \tag{4.3b}$$

$$B = \frac{(b - n_p\phi_p)}{n_p\phi_p} \tag{4.3c}$$

The radial pressure produced by the ribs of the principal bar on the surrounding concrete is σ_n, Ω is the hoop steel index of confinement and B the concrete index of confinement, n_{st} is the number of tie legs in the cross section width, n_p is the number of anchored bars, A_{st} is the cross sectional area of the transverse bar leg, Δz is the transverse

reinforcement spacing, ϕ_p is the principal-bar diameter and b is the cross section width.

4.2.5 Anchored reinforcement bond stress and slip

The anchored reinforcement bond stress τ can now be determined as:

$$\tau = \tau_o \left(\frac{1}{1 + k_1 \frac{w}{\phi_p}} \right) + \psi_2 \left(\frac{1}{1 + k_2 \frac{w}{\phi_p}} \right) (\Omega \sigma_{st} + B \sigma_{rc}) \tag{4.4}$$

where k_1 and k_2 are coefficients of the τ-σ_n curve for a constant crack width, τ_o and ψ_2 are the values at the origin and the slope of the τ-σ_n curve for a constant crack width w.

The anchored-reinforcement slip S, is determined as:

$$S = \gamma_2 w - \frac{\phi_p \ln\left(1 - \frac{\tau}{\tau_{mw}} \right)}{\beta_2 \frac{w}{\phi_p} + \beta_1} \tag{4.5a}$$

with

$$\tau_{mw} = \tau_{mo} \left(1 - \gamma_1 \frac{w}{\phi_p} \right) \tag{4.5b}$$

where β_1, β_2 and γ_2 are coefficients of the τ-S curve for a constant crack width as explained by Giuriani et al. (1991), τ_{mw} is the maximum bond stress for a given crack opening w, τ_{mo} is the maximum bond stress for uncracked concrete (w=0) and γ_1 is the coefficient of the τ–σ curve for a constant crack width.

The above procedure is repeated for an incrementally increasing crack width until the τ-S relation reaches a peak at which τ_1 and S_1 are defined.

4.3 GOVERNING EQUATIONS OF A BAR EMBEDDED IN CONCRETE

The boundary value problem of a reinforcing bar embedded in concrete can be idealized in terms of four unknown fields; the steel stress σ_s, the bond stress τ at the surface between the bar and the concrete, the strain in the reinforcing bar ε_s, and the relative slip S which is the difference between steel and concrete displacements. Since this study is concerned with the behaviour of a bar subjected to large inelastic deformation; the concrete contribution to relative slip is negligible (Filippou et al., 1983). All unknown fields are defined in the one dimensional domain of the embedded length l_d of the bar by the following equilibrium, compatibility and constitutive relations:

$$A_p \frac{d\sigma_s}{dx} = \tau \sum o \qquad \text{(Equilibrium)} \qquad (4.6a)$$

$$\frac{dS}{dx} = \varepsilon_s - \varepsilon_c \approx \varepsilon_s \qquad \text{(Compatability)} \qquad (4.6b)$$

$$\sigma_s = F(\varepsilon_s) \qquad \text{(Steel constituitive relationship)} \qquad (4.6c)$$

$$\tau = T(S) \qquad \text{(Bond slip constituitive relationship)} \qquad (4.6d)$$

where σ_s is the steel stress as a function of the steel strain $F(\varepsilon_s)$, τ is the bond stress as a function of the bond slip T(S), A_p is the reinforcing bar area, and Σo is the perimeter of the reinforcing bar.

4.4 SOLUTION FOR THE BOND SLIP EQUATIONS

A number of approaches has been proposed for the solution of the above equations of bond slip. Filippou et al. (1983) used the weighted residual method to solve the differential equations of equilibrium and compatibility of an anchored reinforcing bar. However, this formulation was used to permit the implementation of a general purpose finite element analysis program. Monti et al. (1997) developed a model for reinforcing bars anchored in concrete. Their model uses force interpolation function instead of displacement interpolation function, and is derived from the variational statement of the bond slip problem. This element was implemented and used in a general purpose finite element analysis program.

A more direct approach to solve these equations outside the finite element analysis context, is to divide the reinforcing bar into small elements of length, Δx, and use the one dimensional incremental stiffness analyses to satisfy a given set of boundary conditions. The numerical model is similar in principle to that adopted by different authors (Harajli, 1994; Filippou, 1986; Mukaddam and Kasti, 1986). The bond stress and slip at some distance x away from the lead end of the bar can be estimated by approximating equations 4.6a and 4.6b in the form:

$$\sigma_s(x) = \sigma_s(x_o) - \frac{\sum \tau\ \pi\ \phi_p\ \Delta x}{\frac{\pi\ \phi_p^2}{4}} \qquad \text{(Equilibrium)} \qquad (4.7a)$$

$$S(x) = S(x_o) - \sum \varepsilon_{sx}\ \Delta x \qquad \text{(Compatability)} \qquad (4.7b)$$

in which the summation is over the number of elements from the lead end to the point under consideration, S(x) and $\sigma_s(x)$ are the slip and the steel stress at some distance x away from the lead end, and $S(x_o)$ and $\sigma_s(x_o)$ are the slip and the steel stress at the lead end. The approximation is a direct result from the numerical integration of equations 4.6a and 4.6b using the mid-point rule.

The boundary conditions of this problem are the slip value at the lead end and the steel stress at the tail end. The stress at the tail end $\sigma_s(x=l_d)$, is always equal to zero. To draw the relation between the steel stress at the lead end (x=0) and the slip at (x=0), equations 4.7a and 4.7b can be solved using the incremental stiffness analysis as follows:

1. A small value is given for slip at the lead end $S(x_o)$.
2. Assume a small value for the steel stress at the lead end, $\sigma_s(x_o)$.
3. Calculate $\sigma_s(x=l_d)$ using equations 4.6 and 4.7. These equations are applied simultaneously to each node at the beginning and the end of each Δx, until finally reaching the last node $(x=l_d)$.
4. If $\sigma_s(x=l_d)$ equals to zero, this means that the assumption of $\sigma_s(x_o)$, in step 2, satisfies the boundary conditions. Otherwise, another iteration is made by increasing $\sigma_s(x_o)$, assumed in step 2, until $\sigma_s(x=l_d)$ changes its sign. Then, more iterations are performed to determine the exact value of $\sigma_s(x_o)$ that will lead to zero value of $\sigma_s(x=l_d)$.
5. The slip assumed in step 1 is increased and the above procedure is followed to calculate the stress at the lead end at this new slip value. This process is repeated again until the curve between the slip and the steel stress at the lead end is achieved.

An example of the steel stress-bond slip relationship is shown in figure 4.4.

4.5 DETERMINATION OF THE STEEL ELEMENT PARAMETERS

The above methodology was used to establish design tables from which the different parameters used in the steel element could be determined. To define the local bond stress-slip relationship (figure 4.2), τ_1 and S_1 are to be determined using equations 4.1 to 4.5. The constants to be used are taken equal to those used by Giuriani et al. (1991), assuming the concrete compressive strength to be equal to 30 MPa:

$$\alpha = 2.0;\ \beta_1 = 60;\ \beta_2 = 0;\ \gamma_1 = 70;\ \gamma_2 = 0.8;\ E_{st} = 206{,}000 \text{ MPa};\ f_{cto} = 1.2 \text{ MPa};$$

$$\phi_s = 20 \text{ mm};\ k = 100;\ k_1 = 115;\ k_2 = 35;\ \tau_{o2} = 2.4 \text{ MPa};\ \psi_{11} = \psi_{12} / 0.3;$$

$$\psi_{12}\, \phi_{st} = 550 \text{ MPa};\ \tau_o = 1.8 \text{ MPa};\ \tau_2 = 0.8; \text{ and } \tau_{mo} = 15 \text{ MPa}. \qquad (4.8)$$

To fully define the envelope curve, the values of τ_3, S_2 and S_3 are estimated by taking ($\tau_3 = \tau_1 / 3.0$, $S_2 = 3 \times S_1$, $S_3 = 10 \times S_1$). After defining the local bond stress-slip relationship, the steel stress-bond slip curve is determined using equations 4.6 and 4.7. From this curve, the steel element parameters K_s, f_{iy}, r, R_{so}, α_s and d_{su} are defined.

For the purpose of developing design tables from which the parameters used in the steel element can be obtained, a parametric analysis was conducted. The parametric study included different bar diameters (ϕ_p = 11.3, 16.0, 19.5 and 25.2 mm), transverse steel ratio ($\lambda = (n_{st}\, \phi_{st}) / (n_p\, \Delta z) = 0.005$, 0.201 and 1.300), principal bar yield stress (f_y = 300 and 500 MPa), effective width ratio (b / n_p = 50 and 150 mm) and development length (l_d / ϕ_p = 5, 20 and 40). The steel stress-strain curve was assumed to be bilinear with a strain hardening ratio of 2%. Discussion of the case of ϕ_p = 16.0 mm, $\lambda = 0.201$, f_y = 500 MPa, b / n_p = 50 mm and

$l_d / \phi_p = 20$ is presented to illustrate the procedure used.

Given the longitudinal bar diameter $\phi_p = 16.0$ mm, $\lambda = 0.201$ and $b / n_p = 50$ mm, the values of τ_1 and S_1 (using equations 4.1 to 4.5) are calculated as 11.08 MPa and 0.961 mm respectively. Given $f_y = 500$ MPa and $l_d / \phi_p = 20$, the calculated bond slip-steel stress can be drawn as shown in figure 4.4. From this relationship, the following parameters are determined: $d_{su} = 8.17$ mm, $f_{iy} = 598.1$ MPa, $K_s / A_s = 650.0$ N/mm^3, $r = 0.052$ and $R_{so} = 0.368$. The value of α_s is calculated at points along the degrading slope (using equation 2.12 in Chapter 2) with a slip increment of 0.005 mm and then by averaging these values after rejecting the values that are three times greater than the mean. The parameter α_s is found to be 0.094 mm^{-2}. The adopted curve that will be used in the steel elements for the steel stress-bond slip relationship shown in figure 4.4 is a close representation of the calculated curve. The above procedure was repeated for all the selected ranges of parameters which resulted in tables 4.1 to 4.8.

From tables 4.1 to 4.8, it is observed that the imaginary yield steel stress, f_{iy}, ranges from 0.07 to 2.63 times the original yield stress. This will cause substantial change in the element parameters. The imaginary yield stress, f_{iy}, and the displacement at which softening starts in the steel element, d_{su}, are found to increase with increasing the confinement either by the transverse steel or by increasing the concrete confining width. In addition, f_{iy} and d_{su}, increase with the increase of l_d / ϕ_p ratio. Therefore, the element will exhibit less strength deterioration.

Tables 4.1 to 4.8 are developed for concrete compressive strength of 30 MPa and steel strain hardening ratio of 0.02. In addition, the constants used to determine τ_1 and S_1 are

those given by equation 4.8. Any change in the concrete compressive strength, steel strain hardening ratio or values of equation 4.8 should be accompanied by suitable adjustment of the values obtained from tables 4.1 to 4.8. In developing the tables, the possibility of steel reaching its ultimate strain (failure) before reaching the displacement at which softening starts, was not taken into consideration.

For different values of f_c', it is suggested to take the values of the factors used in equations 4.1 to 4.7 to be the same as those given by equation 4.8 except for f_{cto}, τ_{o2}, τ_o and τ_{mo} which need to be modified by a factor of $\sqrt{\frac{f_c'}{30}}$ to account for the difference in the concrete strength. The element parameters may also be taken from tables 4.1 to 4.8 after making corrections to account for the different concrete compressive strength and the different strain hardening ratios for the steel bars. From equations (4.1) to (4.6), approximate values are determined after modifying b by multiplying it by $\frac{f_c'}{30}$ and λ by multiplying it by $\sqrt{\frac{f_c'}{30}}$. The effect of the strain hardening on d_{su} is determined approximately by assuming that the ultimate stress will remain constant and by determining the corresponding ultimate displacement.

4.6 SUMMARY

In this Chapter, a bond slip model is introduced. The model is based on idealizing bond slip effect as part of the steel element. The local confining action due to transverse reinforcement and residual strength of cracked concrete is used to calculate the local bond stress-slip curve. This curve was used to calculate bar force-cumulative slip relationship which is suggested to be used as an envelope for the steel element. Tables containing the parameters

that define the shape of the curve are introduced. The main advantage of this model is its simplicity in idealizing bond slip in the steel element.

Table 4.1 Model parameters for $f_c' = 30$ MPa, $f_y = 300$ MPa and $\phi_p = 11.3$ mm (nominal 10 mm diameter bar)

b/n_p mm	l_e/ϕ_p	λ	d_{ss} mm	f_{ty} MPa	α_s mm^{-2}	K_s/A_s N/mm^3	R_{so}	r
50	5	0.005	0.500	80.82	93.30	900.0	0.600	0.020
		0.201	2.414	227.8	0.333	300.0	0.394	0.050
		1.300	2.509	280.3	0.284	300.0	0.384	0.048
	20	0.005	1.125	339.0	47.85	1900.0	0.406	0.026
		0.201	12.20	428.5	0.160	790.0	0.441	0.037
		1.300	15.73	582.1	0.185	790.0	0.466	0.025
	40	0.005	9.521	344.0	56.99	1900.0	0.559	0.010
		0.201	46.92	633.1	0.219	900.0	0.606	0.011
		1.300	57.57	776.6	0.215	900.0	0.630	0.009
150	5	0.005	1.119	210.9	3.191	650.0	0.428	0.020
		0.201	2.939	272.8	0.179	300.0	0.378	0.045
		1.300	2.987	272.8	0.171	300.0	0.376	0.065
	20	0.005	8.755	434.7	4.248	1900.0	0.494	0.013
		0.201	16.24	661.5	0.120	790.0	0.447	0.019
		1.300	16.96	668.3	0.116	790.0	0.450	0.019
	40	0.005	36.53	495.3	2.192	1900.0	0.663	0.007
		0.201	59.22	711.4	0.141	920.0	0.612	0.010
		1.300	61.40	790.0	0.133	900.0	0.615	0.009

Table 4.2 Model parameters for $f_c' = 30$ MPa, $f_y = 500$ MPa and $\phi_p = 11.3$ mm (nominal 10 mm diameter bar)

b/n_p mm	l_e/ϕ_p	λ	d_{ss} mm	f_{sy} MPa	α_s mm^{-2}	K_t/A_s N/mm^3	R_{ss}	r
50	5	0.005	0.500	80.82	93.30	900.0	0.600	0.020
		0.201	2.414	227.8	0.333	300.0	0.394	0.050
		1.300	2.509	280.3	0.284	300.0	0.384	0.048
	20	0.005	0.461	354.8	73.47	1900.0	0.401	0.049
		0.201	7.344	660.7	0.178	790.0	0.378	0.046
		1.300	10.78	748.2	0.167	790.0	0.406	0.032
	40	0.005	3.640	542.8	412.0	1900.0	0.464	0.012
		0.201	38.37	823.3	0.218	900.0	0.542	0.010
		1.300	48.94	902.0	0.202	900.0	0.572	0.011
150	5	0.005	1.119	210.9	3.191	650.0	0.428	0.020
		0.201	2.939	272.8	0.179	300.0	0.378	0.045
		1.300	2.987	272.8	0.171	300.0	0.376	0.065
	20	0.005	4.994	592.2	1.388	1900.0	0.414	0.020
		0.201	11.00	685.2	0.107	900.0	0.391	0.036
		1.300	11.71	699.6	0.103	790.0	0.395	0.040
	40	0.005	28.56	696.4	11.77	1900.0	0.578	0.007
		0.201	50.30	897.0	0.128	920.0	0.556	0.011
		1.300	52.47	1010.7	0.123	900.0	0.560	0.009

Table 4.3 Model parameters for $f_c' = 30$ MPa, $f_y = 300$ MPa and $\phi_p = 16.0$ mm (nominal 15 mm diameter bar)

b/n_p mm	l_e/ϕ_p	λ	d_{ss} mm	f_{sy} MPa	α_s mm^{-2}	K_s/A_s N/mm^3	R_{so}	r
50	5	0.005	0.575	56.10	154.4	750.0	0.686	0.025
		0.201	2.954	201.8	0.177	200.0	0.390	0.009
		1.300	3.192	264.8	0.140	250.0	0.376	0.080
	20	0.005	0.491	279.1	72.06	1900.0	0.421	0.010
		0.201	14.87	498.0	0.110	790.0	0.431	0.020
		1.300	21.89	547.3	0.097	790.0	0.468	0.018
	40	0.005	6.996	337.6	241.6	1900.0	0.515	0.007
		0.201	59.15	606.0	0.130	900.0	0.594	0.008
		1.300	80.37	685.9	0.115	900.0	0.632	0.008
150	5	0.005	1.214	176.6	2.993	600.0	0.440	0.030
		0.201	3.724	250.8	0.102	200.0	0.379	0.075
		1.300	3.836	277.8	0.098	200.0	0.376	0.070
	20	0.005	9.259	405.9	1.290	1250.0	0.483	0.015
		0.201	20.78	503.2	0.070	600.0	0.445	0.029
		1.300	23.39	599.4	0.068	620.0	0.457	0.021
	40	0.005	41.81	516.1	2.070	1300.0	0.658	0.006
		0.201	77.16	674.2	0.081	700.0	0.609	0.009
		1.300	84.96	706.0	0.079	750.0	0.621	0.009

Table 4.4 Model parameters for $f_c' = 30$ MPa, $f_y = 500$ MPa and $\phi_p = 16.0$ mm (nominal 15 mm diameter bar)

b/n_p mm	l_d/ϕ_p	λ	d_m mm	f_{fy} MPa	α_s mm^{-2}	K_s/A_s N/mm^3	R_{so}	r
50	5	0.005	0.575	56.10	154.4	750.0	0.686	0.025
		0.201	2.954	201.8	0.177	200.0	0.390	0.009
		1.300	3.192	264.8	0.140	250.0	0.376	0.080
	20	0.005	0.491	279.1	72.06	1900.0	0.421	0.010
		0.201	8.170	598.1	0.094	650.0	0.368	0.052
		1.300	14.95	662.6	0.086	750.0	0.407	0.030
	40	0.005	1.000	399.4	1150.8	1400.0	0.469	0.080
		0.201	47.18	764.3	0.120	650.0	0.528	0.012
		1.300	68.21	785.3	0.107	750.0	0.573	0.012
150	5	0.005	1.214	176.6	2.993	600.0	0.440	0.030
		0.201	3.724	250.8	0.102	200.0	0.379	0.075
		1.300	3.836	277.8	0.098	200.0	0.376	0.070
	20	0.005	4.480	577.6	1.327	1250.0	0.398	0.025
		0.201	13.55	713.1	0.167	600.0	0.386	0.035
		1.300	16.12	731.5	0.060	650.0	0.400	0.030
	40	0.005	30.71	660.9	2.564	1250.0	0.560	0.008
		0.201	64.71	846.1	0.074	720.0	0.551	0.010
		1.300	72.49	875.9	0.072	750.0	0.565	0.010

Table 4.5 Model parameters for $f_c' = 30$ MPa, $f_y = 300$ MPa and $\phi_p = 19.5$ mm (nominal 20 mm diameter bar)

b/n_p mm	l_d/ϕ_p	λ	d_m mm	f_{iy} MPa	α_s mm^{-2}	K_s/A_s N/mm^3	R_{so}	r
50	5	0.005	0.630	44.90	213.1	500.0	0.741	0.040
		0.201	3.409	189.5	0.120	160.0	0.391	0.106
		1.300	3.822	273.7	0.095	200.0	0.377	0.060
	20	0.005	0.520	241.4	77.00	1200.0	0.435	0.009
		0.201	16.68	493.9	0.078	500.0	0.425	0.026
		1.300	26.45	596.0	0.067	600.0	0.468	0.017
	40	0.005	5.219	324.4	408.5	1200.0	0.495	0.011
		0.201	67.73	582.2	0.091	600.0	0.588	0.010
		1.300	97.24	604.9	0.079	650.0	0.632	0.010
150	5	0.005	1.169	142.2	7.794	500.0	0.462	0.042
		0.201	4.109	223.3	0.082	150.0	0.383	0.120
		1.300	4.400	276.8	0.074	200.0	0.376	0.060
	20	0.005	7.721	375.9	1.599	1100.0	0.465	0.016
		0.201	22.24	501.2	0.056	500.0	0.439	0.028
		1.300	27.93	637.3	0.051	550.0	0.461	0.015
	40	0.005	38.61	463.8	2.704	1100.0	0.636	0.006
		0.201	84.70	645.4	0.065	600.0	0.603	0.009
		1.300	101.8	660.4	0.060	620.0	0.625	0.010

Table 4.6 Model parameters for $f_c' = 30$ MPa, $f_y = 500$ MPa and $\phi_p = 19.5$ mm (nominal 20 mm diameter bar)

b/n_p mm	l_e/ϕ_p	λ	d_{ss} mm	f_{ty} MPa	α_s mm^{-2}	K_s/A_s N/mm^3	R_{so}	r
50	5	0.005	0.630	44.90	213.1	500.0	0.741	0.040
		0.201	3.409	189.5	0.120	160.0	0.391	0.106
		1.300	3.822	273.7	0.095	200.0	0.377	0.060
	20	0.005	0.520	241.4	77.00	1200.0	0.435	0.009
		0.201	8.615	607.5	0.063	500.0	0.363	0.055
		1.300	18.02	674.4	0.059	600.0	0.407	0.030
	40	0.005	1.055	324.4	1880.4	1000.0	0.479	0.105
		0.201	53.25	750.4	0.085	600.0	0.520	0.011
		1.300	82.45	793.3	0.204	650.0	0.573	0.011
150	5	0.005	1.169	142.2	7.794	500.0	0.462	0.042
		0.201	4.109	223.3	0.082	150.0	0.383	0.120
		1.300	4.400	276.8	0.074	200.0	0.376	0.060
	20	0.005	2.746	556.3	1.820	1100.0	0.375	0.029
		0.201	13.66	667.5	0.049	500.0	0.378	0.041
		1.300	19.20	701.9	0.045	550.0	0.402	0.031
	40	0.005	26.09	575.1	4.739	1100.0	0.534	0.010
		0.201	69.75	798.8	0.060	600.0	0.541	0.011
		1.300	86.69	829.9	0.055	630.0	0.568	0.011

Table 4.7 Model parameters for f_c' = 30 MPa, f_y = 300 MPa and ϕ_p = 25.2 mm (nominal 25 mm diameter bar)

b/n_p mm	l_d/ϕ_p	λ	d_{ss} mm	f_{sy} MPa	α_s mm^{-2}	K_s/A_s N/mm^3	R_{so}	r
50	5	0.005	0.715	34.93	354.7	350.0	0.810	0.055
		0.201	4.259	184.9	0.079	125.0	0.395	0.088
		1.300	4.841	280.5	0.059	160.0	0.377	0.047
	20	0.005	0.575	176.4	80.04	1000.0	0.456	0.065
		0.201	19.51	474.8	0.048	375.0	0.418	0.028
		1.300	33.76	531.2	0.040	450.0	0.468	0.022
	40	0.005	2.593	274.9	639.5	1000.0	0.479	0.029
		0.201	81.35	554.7	0.057	450.0	0.581	0.011
		1.300	124.4	605.8	0.048	530.0	0.632	0.010
150	5	0.005	1.174	109.3	5.022	430.0	0.493	0.045
		0.201	4.809	208.0	0.060	120.0	0.388	0.090
		1.300	5.360	272.0	0.048	150.0	0.376	0.080
	20	0.005	5.700	349.2	1.848	900.0	0.437	0.019
		0.201	24.33	451.8	0.039	370.0	0.430	0.033
		1.300	35.28	592.9	0.033	420.0	0.464	0.020
	40	0.005	34.65	380.1	4.164	900.0	0.609	0.008
		0.201	96.07	601.3	0.045	450.0	0.593	0.010
		1.300	129.0	648.0	0.039	500.0	0.628	0.010

Table 4.8 Model parameters for $f_c' = 30$ MPa, $f_y = 500$ MPa and $\phi_p = 25.2$ mm (nominal 25 mm diameter bar)

b/n_p mm	l_d/ϕ_p	λ	d_{ss} mm	f_{fy} MPa	α_s mm^{-2}	K_c/A_s N/mm^3	R_{so}	r
50	5	0.005	0.715	34.93	354.7	350.0	0.810	0.055
		0.201	4.259	184.9	0.079	125.0	0.395	0.088
		1.300	4.841	280.5	0.059	160.0	0.377	0.047
	20	0.005	0.575	176.4	80.04	1000.0	0.456	0.065
		0.201	9.376	602.2	0.038	400.0	0.359	0.057
		1.300	22.91	703.6	0.036	465.0	0.407	0.028
	40	0.005	1.139	283.6	1649.8	750.0	0.492	0.087
		0.201	62.78	728.2	0.052	465.0	0.511	0.011
		1.300	105.3	833.1	0.045	520.0	0.527	0.010
150	5	0.005	1.174	109.3	5.022	430.0	0.493	0.045
		0.201	4.809	208.0	0.060	120.0	0.388	0.090
		1.300	5.360	272.0	0.048	150.0	0.376	0.080
	20	0.005	1.285	459.4	5.403	900.0	0.379	0.068
		0.201	13.60	576.2	0.033	400.0	0.368	0.058
		1.300	24.16	763.5	0.029	430.0	0.404	0.025
	40	0.005	19.66	564.3	12.79	900.0	0.499	0.009
		0.201	77.04	756.4	0.041	460.0	0.528	0.012
		1.300	109.7	818.4	0.036	500.0	0.570	0.011

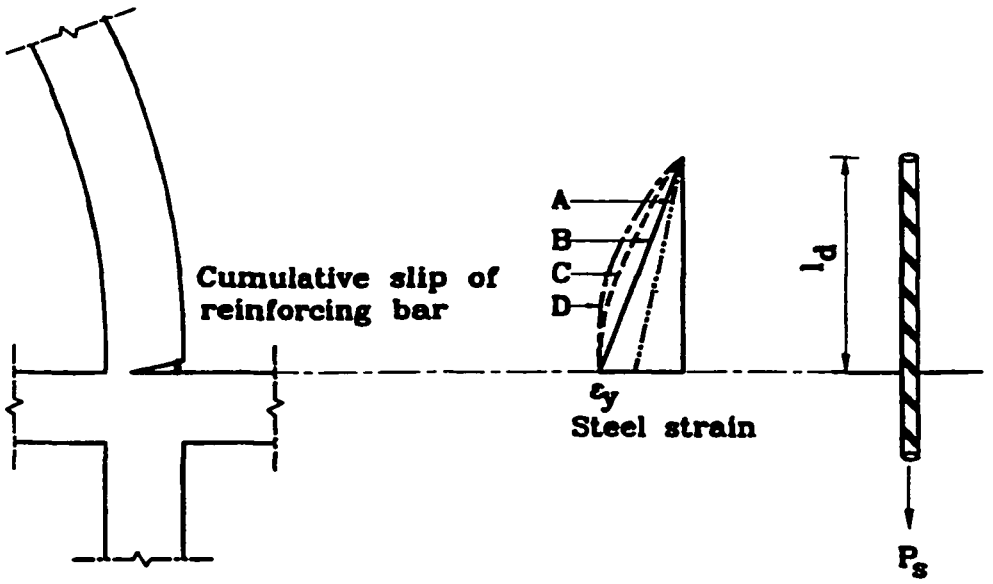

Figure 4.1 Cumulative slip of reinforcing bar

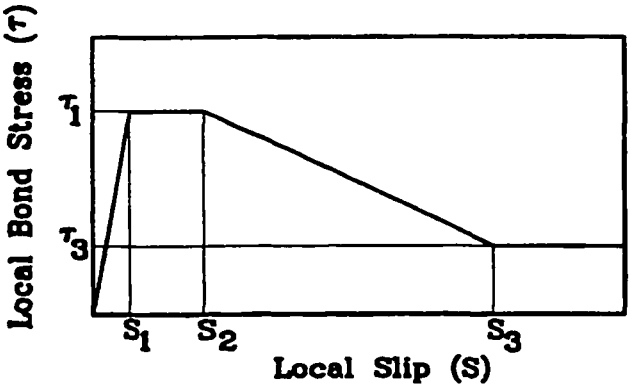

Figure 4.2 Local bond stress–slip constitutive model. (Ustuner, 1992)

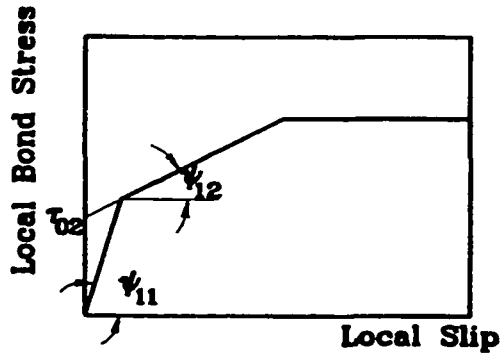

Figure 4.3 Ideal trilateral local bond–slip law of the transverse bars (Giuriani et al., 1991)

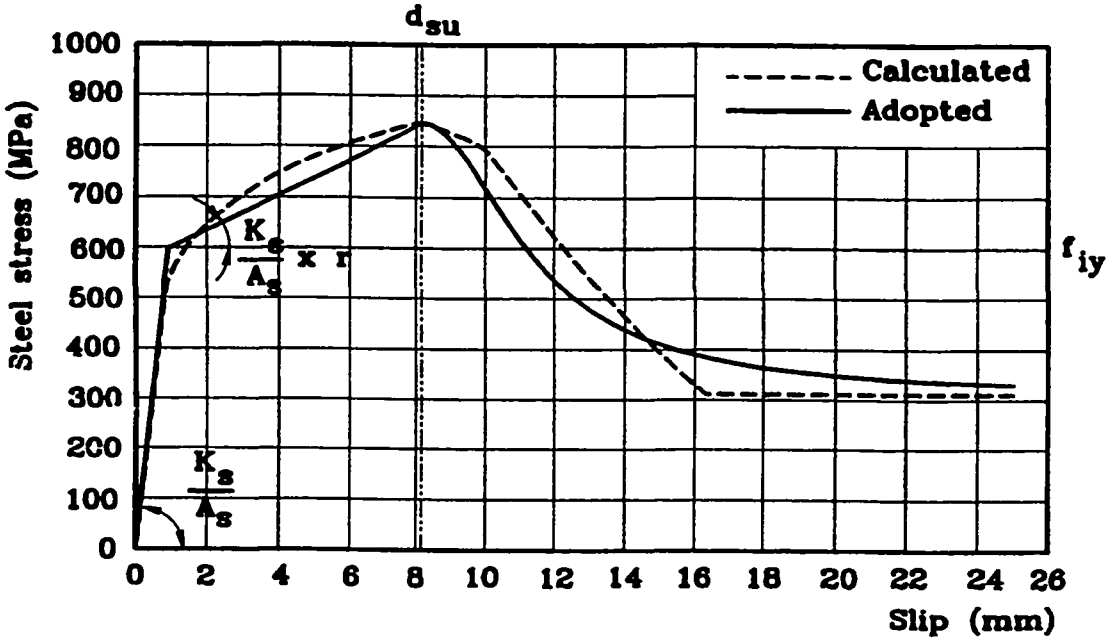

Figure 4.4 Steel stress–bond slip relationship

CHAPTER 5

KINEMATIC MODELS

5.1 INTRODUCTION

A representative model should contain the main characteristics that describe completely the hysteretic behaviour of reinforced concrete structural components when subjected to reversed cyclic loads. These characteristics include stiffness degradation, strength softening and pinching behaviour. In addition, the model used should be as simple as possible so that the analysis can be performed with a reasonable computational effort, especially in the case of multistorey structural systems.

There are two types of models; microscopic models and macroscopic models. Microscopic models, like the finite element method, have the disadvantage of the large amount of computation required even for simple structures (Lai, 1984). The finite element method is used for the analysis of individual elements to establish their behaviour. It is also used with the available experimental results for the verification of the macroscopic elements that require relatively limited storage and lower computational effort than microscopic models. Extensive research has been conducted to simulate the hysteretic behaviour of RC elements, (Takeda et al., 1970; Ozcebe and Saatcioglu, 1989; Roufaiel and Meyer, 1987). The results from this research provided helpful information for the development of suitable

analytical models that are capable of closely describing the hysteretic behaviour of each structural element of the building.

Available models for representing RC structures are concerned only with the maximum load carrying capacity. To the best of the author knowledge, none of the available models was able to predict the post peak strength response and most importantly the failure mechanism. Some researchers (Abouelfath, 1998; park et al., 1987) predicted the post peak response by using parameters that were calibrated using the available experimental results. Other researchers (Miramontes et al., 1996; Chung et al., 1989) used damage indices to define the degrading slope. These methods are doubtful as it might be correct for certain cases but they cannot be generalized. The model adopted for the analysis of reinforced concrete elements should be capable of predicting flexural and shear components of inelastic deformation. Moreover, the model should be capable of simulating the behaviour culminating in different failure modes.

Due to lack of a complete macroscopic model that can be used for the dynamic analysis of reinforced concrete buildings with sufficient accuracy, the development of such a model will be described in this Chapter. This will be done by developing elements that can describe the behaviour of RC columns, beams, beam- column joints and shear walls. The model should adequately describe the hysteretic behaviour of reinforced concrete elements and be capable of predicting both the flexural and shear components of inelastic deformation. The model should be able to detect the failure mechanism.

5.2 FLEXURAL MEMBERS

5.2.1 Introduction

Lai et al. (1984) developed an analytical model to simulate the hysteretic and stiffness degrading behaviour of reinforced concrete members subjected to axial load and biaxial bending interaction. The member is separated into two inelastic elements, as shown in figure 5.1, each composed of individual spring elements to simulate the inelastic effects of the member as well as the cumulative slip of the anchored bars in the beam-column joint. Each element consists of five inelastic springs, as shown in figure 5.1. Each of the four exterior springs represents the stiffness of the reinforcing steel bars and the effective compression concrete. The center spring represents only the concrete in the central region of the section.

The calculation of the effective concrete spring area for the corner springs, A_{ci}, was based on the balanced condition such that the inelastic element will produce the same magnitude of the balanced load, P_b, as the original section. The central spring area is the remaining area of the section.

$$A_{ci} = \frac{P_b - \sum P_{siy}}{2(0.85 f_c')} \qquad i=1,2,3,4$$
$$A_{c5} = A_g - A_{c1} - A_{c2} - A_{c3} - A_{c4} - A_{st} \qquad (5.1)$$

Where,

P_{siy} : The yield force for the i^{th} effective steel spring.

A_g : The gross cross sectional area of concrete.

A_{st} : The total reinforcing steel area of the section.

The spacings, d_{spx}, d_{spy}, of the corner spring elements are determined from the conditions that the inelastic elements at yielding must produce the same magnitude of bending moments, M_{bx} and M_{by}, of the original section at the balanced condition.

$$d_{spx} = \frac{2M_{bx}}{(A_{s1} + A_{s2} + A_{s3} + A_{s4})f_y + 0.85f_c'(A_{c1} + A_{c2})}$$
$$d_{spy} = \frac{2M_{by}}{(A_{s1} + A_{s2} + A_{s3} + A_{s4})f_y + 0.85f_c'(A_{c2} + A_{c4})} \qquad (5.2)$$

Where,

M_{bx}, M_{by} : Yield moments in the x and y directions at the balanced conditions.

A_{si}, A_{ci} : Effective area of steel and concrete spring respectively, of the quadrant i.

For two dimensional analysis, each inelastic element will consist of three inelastic springs as shown in figure 5.2. The model accounts in a simple way for the Bauschinger and flexural yielding effects of the reinforcement and the compressive deformation of the concrete. It also accounts for the cumulative anchorage slip deformations of the reinforcing bars at the face of the joint. However, the model does not account for strength softening due to bond slip or concrete softening.

Ghusn and Saiidi (1986) used Lai's (1984) model for the dynamic analysis of highway bridges. The hysteretic model for the steel springs was the QHYST model, (Saiidi, 1982). This hysteretic model is considerably simpler than Takeda's model, (Takeda et al., 1970). However, it is still lacking strength softening and deterioration.

Jiang and Saiidi (1990) modified Lai's model (Lai, 1984; Lai et al., 1984). The use of four composite springs instead of five concrete springs and four steel springs was

implemented. This model is still lacking strength softening due concrete softening and bond slip.

Li et al. (1988) tested a series of reinforced concrete columns under varying axial load and biaxial lateral load reversals. They compared the results with the multi-spring model of Lai (1984) and Lai et al. (1984). They showed that the multi-spring model is simple and reliable for use in the analysis of reinforced concrete columns under varying axial load and bidirectional lateral load reversals.

5.2.2 Developed model

Using the balanced condition to define the spring properties as recommended by Lai et al. (1984) will result in misleading results especially near failure. To be able to detect the failure mechanism, the property of the springs should be calculated using the acting axial force.

The capacity of the edge concrete springs is calculated as the concrete compression forces at ultimate condition for a given axial load. The capacity of the central concrete spring is calculated as the difference between the total capacity of the concrete section and the capacity of the exterior springs. The distance between the exterior springs is calculated such that the ultimate moment of the transformed section (consisting of the steel and concrete springs) will be the same as that of the actual section.

5.3 BEAM-COLUMN JOINTS

5.3.1 Introduction

The beam-column joint is one of the critical elements in RC frame structures. Joint deformations make significant contribution to the frame drift or may fail as in the case of frames with non-ductile detailing. When subjected to earthquake loading, failure in RC frame joint might occur due to cumulative crushing of the concrete in the beam section or in the column section, bond slip failure of the embedded bars in the beam-column joint, shear failure or a combination of the various mechanisms of failure. There is a need to include these modes of failure in a simple model that can be used in the analysis of RC frames to predict their response under earthquake loading and determine their failure modes.

In traditional analysis of moment resisting frames, beam-column joints are assumed to be rigid. After observing many cases of joint failures in existing structures during recent earthquakes, modeling of beam-column joints has recently received considerable attention and different modeling techniques were proposed by several researchers. These approaches range from using empirical methods to finite element modeling as explained in the following paragraphs. The two main sources of deformation in beam-column joints are shear and bond slip. A successful analytical model for the beam-column joint should be able to represent these two types of deformation. In addition, the model should be capable of idealizing different failure modes.

A simple approach was presented by Hoffmann et al. (1992). By adjusting the flexural properties of the members framing into the joint, the joint capacity can be represented. This approach has the advantage of simplicity and its ability to describe the joint's global

behaviour. However, the shear deformations in the joint cannot be calculated. Moreover, it is difficult to separate the shear and flexural behaviours because the contribution for each can not be isolated.

A rotational spring model was presented by Alath et al. (1995). In this model, the relative change in rotation between the beam and the column is controlled by a spring which defines the shear distortion of the beam-column joint. The equations used to predict the characteristics of the joint panel are empirical and are applicable to specific cases. The hysteretic model is a crude representation of the shear behaviour. Biddah (1998) modified this model by adding another rotational spring to represent the bond slip, the calculation of the moment-rotation relationship was based on simplified assumptions that limit its applicability. The shear stress-shear strain relation was calculated using the modified compression field theory and transformed to moment-rotation relationship using approximate methods.

Pantazopoulou and Bonacci (1994) modeled the RC beam-column joints by using the finite element method. Bond slip was introduced in this model. The use of this model is limited to montonic loading as it is time consuming.

Elmorsi (1998) represented the beam-column joint by a tweleve node inelastic plane stress element. Ten node inelastic plane stress transition elements were used to provide gradual transition from the cubic displacement field at the beam-column interface to a linear displacement field at their connection with the neighboring beams and columns. The bond slip model did not account for the effect of various confining ratios. Also, it did not account for discontinuous beam bars in the joint panel. Moreover, the application of the model is time consuming.

The principal shortcoming of the available models is their inability to represent strength degradation and thus their inability to represent failure due to concrete crushing, bond slip or shear. An efficient model that is able to distinguish between different types of failures is needed especially for the analysis of existing deficient structures to determine their lateral load carrying capacity and ultimate failure mechanism.

5.3.2 Proposed beam-column joint model

The joint region is represented by four rigid members enclosing the joint as shown in figure 5.3. Beams and columns are idealized using elastic elements. Bond slip and concrete crushing are idealized in the connection between the beam or the column and the rigid members enclosing the joint. The connection between the joint and a beam or a column is idealized using three concrete springs and three steel springs. The connections between these rigid members are assumed pinned with shear springs connecting the diagonals as shown in figure 5.3.

From simple geometry, as shown in figure 5.4, the elongation ($|d1+d2|$) in one of the diagonal springs will be equal to the contraction ($|d3+d4|$) in the other spring.

$$\Delta D = |d1+d2| = |d3+d4| \tag{5.3}$$

Also, the shear deformation γ can be calculated from the following equation,

$$\gamma = \frac{\gamma_{h1} + \gamma_{h2}}{2} + \frac{\gamma_{v1} + \gamma_{v2}}{2} = \frac{2\Delta D}{D\sin(2\phi)} \tag{5.4}$$

where the average of γ_{h1} and γ_{h2} is the horizontal shear deformation, the average of γ_{v1} and γ_{v2} is the vertical shear deformation, D is the undistorted diagonal distance and ϕ is the angle between the diagonal and the horizontal.

During the analysis, the shear force V corresponding to the acting shear deformation on the joint can be calculated as discussed in Section 3.5. Consequently, the force in each of the diagonal springs F can be calculated from simple equilibrium:

$$F = \frac{V}{2\cos(\phi)} \tag{5.5}$$

Idealization of the joint behaviour is achieved in this model by using twelve concrete springs, twelve steel springs and two shear springs. Three concrete and three steel springs are located at the joint interface with each of the beams and columns framing into the joint as shown in figure 5.3. Bond slip, concrete crushing and shear failure are included in the springs behaviour as explained in Sections 2.2.2, 2.3.1 and 3.6.

5.4 RC STRUCTURAL WALLS

5.4.1 Introduction

The reinforced concrete structural wall is an important lateral load resisting element. It is increasingly used by designers in new structures as well as in the rehabilitation of existing ones. There are models that represent the flexural behaviour of walls to various degrees of accuracy. However, an efficient model is needed for accurate representation of the flexural and shear behaviour of these walls.

Vulcano and Bertero (1987) used the model developed by Otani et al. (1985) with

some minor modifications, for the idealization of structural walls. The model is shown in figure 5.5. It idealizes the wall as three vertical line elements with infinitely rigid beams at the top and bottom floor levels. The two outside truss elements represent the axial stiffness of the boundary columns. The central element was a one component model with vertical, horizontal and rotational springs. The adopted hysteretic model did not represent several of the characteristics observed in reinforced concrete walls. The behaviour of the shear spring did not agree with the experimental data.

Linde and Bachmann (1994) developed a model for the idealization of reinforced concrete structural walls. The model has the same deficiencies as the previous models.

All the developed macroscopic models are similar. The only difference between them is the position and type of the springs. All these models are lacking the proper representation of the hysteretic models, especially in the case of the shear springs.

5.4.2 Developed model

A macro wall element is developed as shown in figure 5.6. Four steel and four concrete springs are used to define the plastic hinging region. The two exterior springs represent the boundary elements and the two interior springs represent the remaining section of the wall. If three springs only are used, the flexural behaviour of the wall will be inaccurately estimated to depend only on the boundary elements. The minor enhancement of the response obtained by using more than four springs is not worth the corresponding increase in the degrees of freedom (Ghobarah and Youssef, 1999).

The same idea used in modeling the joint was adopted. Two diagonal shear springs

were used as shown in figure 5.6. By that, the shear strain is assumed to be constant over the wall height.

Two elastic truss elements representing the area of the boundary elements, are used to connect the rigid bars. The location of the truss elements is chosen to be at the centerline of the boundary elements.

The yield strength of the exterior steel and concrete springs is determined according to the boundary element's dimensions and reinforcement. The yield strength of the two interior steel and concrete springs is determined according to the wall dimension and reinforcement. The elastic stiffness of the steel springs is calculated using the methodology described in Chapter 4. The position of the two exterior springs and the two interior springs is determined such that the ultimate moment and curvature of the transformed section (consisting of the steel and concrete springs) will be the same as that of the actual section.

The effect of the normal force on the behaviour of the shear spring is taken into account. The axial force N, acting on the wall is assumed to be equal to the summation of the forces in the four concrete and four steel springs:

$$N = \sum_{i=1}^{4} P_{si} + \sum_{i=1}^{4} P_{ci} \qquad (5.6)$$

where P_{si} and P_{ci} are the forces in the i^{th} steel and concrete springs, respectively.

5.5 SUMMARY

A macro-element is developed to model the flexural behaviour of RC columns. The element consists of a series of three steel and three concrete springs connected by rigid

elements. The use of the proposed hysteretic models for the steel and the concrete springs as presented in Chapter 2, allowed the inclusion of strength deterioration due to concrete softening or bond failure.

The element developed is limited to flexural behaviour and cases with small variations in the axial forces. In developing the element and calculating the element parameters based on a given axial load, the shear behaviour was ignored.

A global model for the beam-column joint is developed. The proposed model represents shear and bond slip deformations in the joint panel as well as the flexural deformations in the plastic hinge regions in the beams and the columns. The model is capable of idealizing the potential failure mechanism due to crushing of concrete or bond slip or beam-column joint shear failure with allowance for the simultaneous progress in each mode.

A macro-element is developed to model the flexural and shear behaviour of structural walls. The wall panel is represented by four steel springs, four concrete springs and a shear spring connected by rigid bars and truss elements. Hysteretic models for the steel and the shear springs include strength deterioration and softening parameters. The envelope curve of the shear spring is defined using the modified compression field theory. The effects of the axial load on the shear behaviour of the structural wall is taken into account.

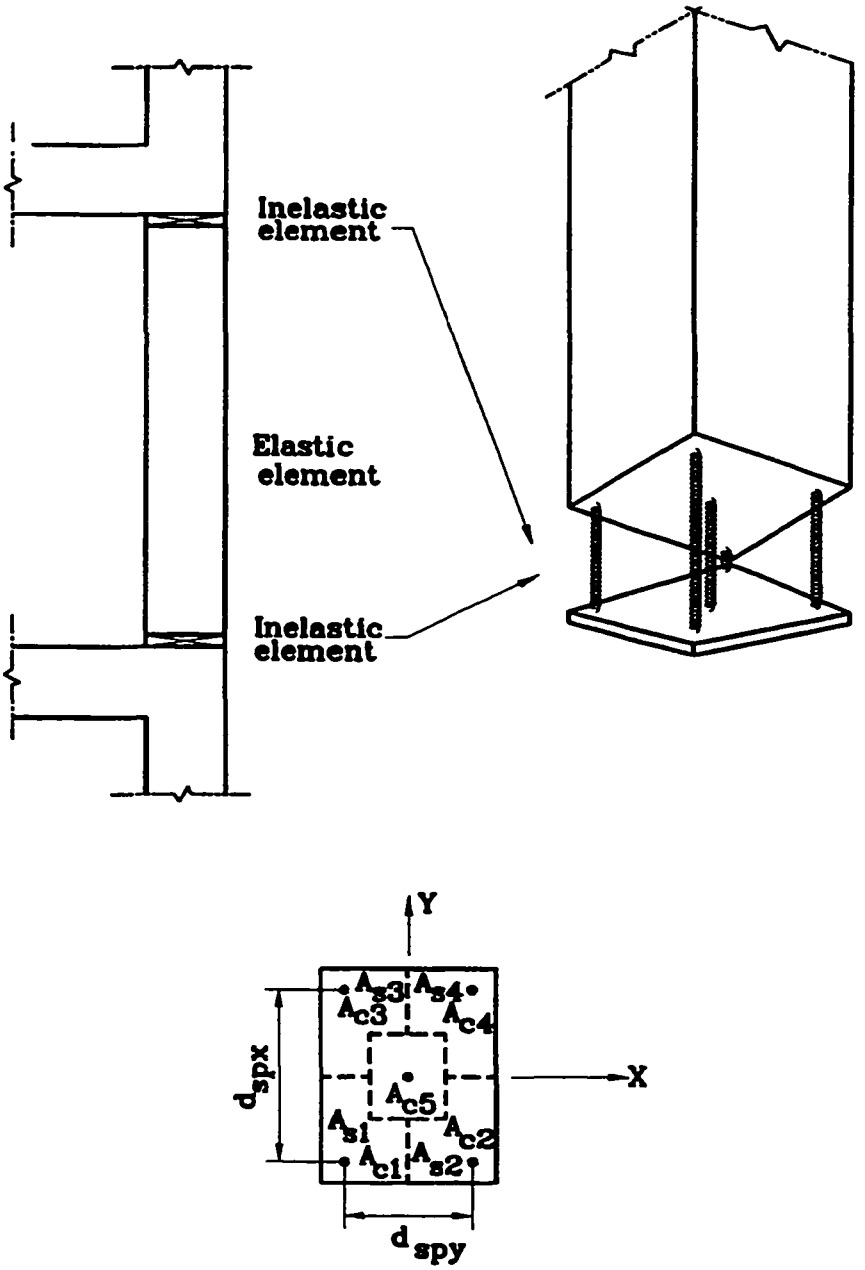

Figure 5.1 Multi–spring element for reinforced concrete frames (Lai et al., 1984)

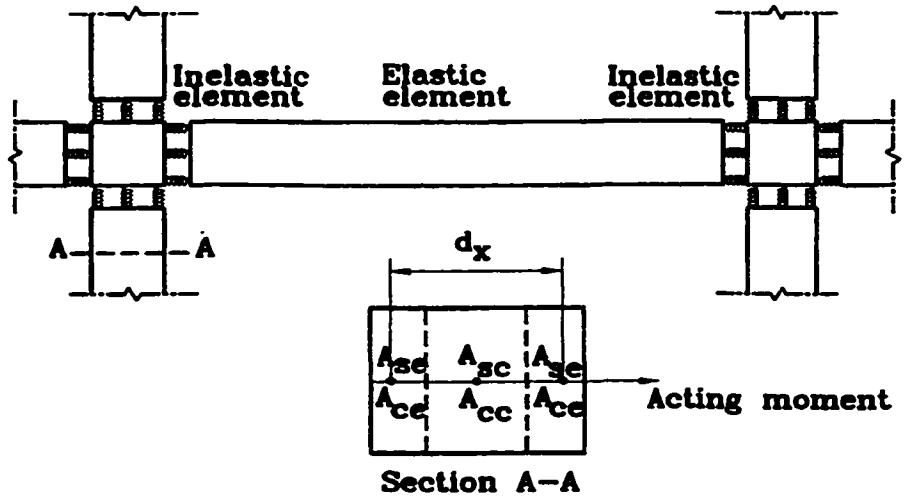

Figure 5.2 Multi–spring element for two dimensional analysis of reinforced concrete frames.

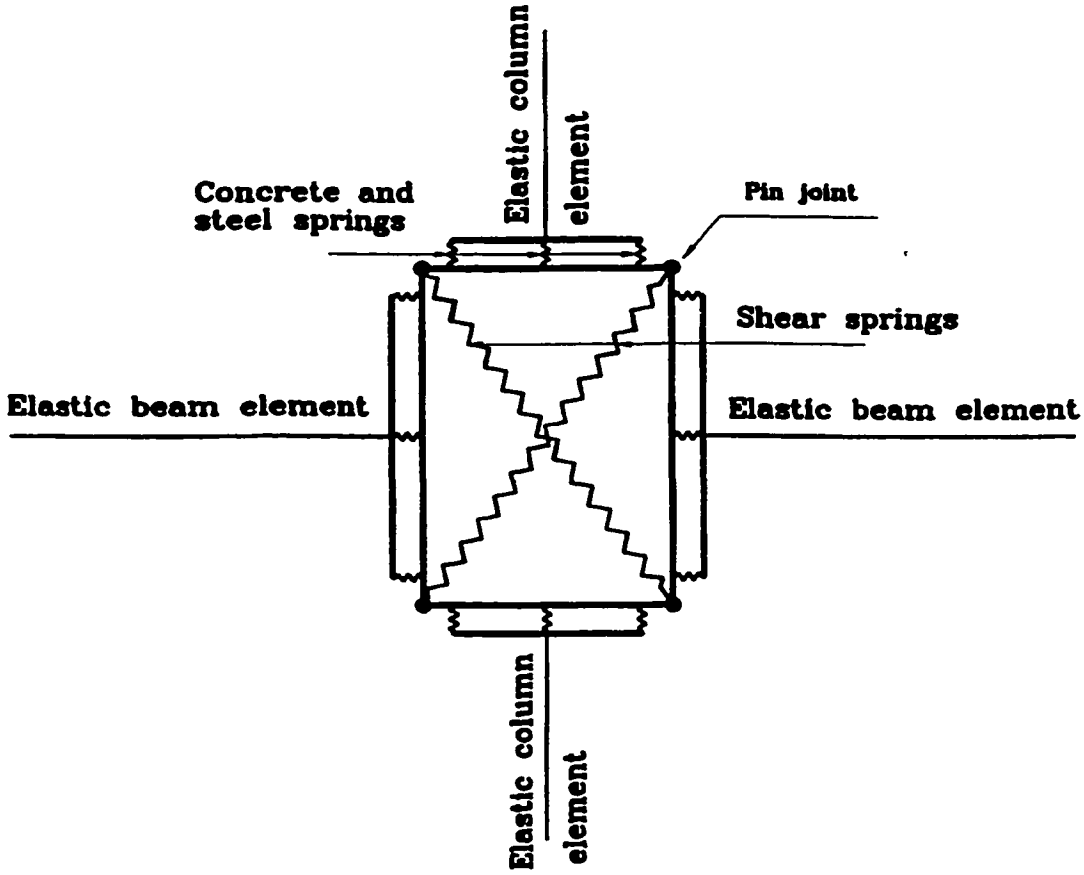

Figure 5.3 Developed joint model

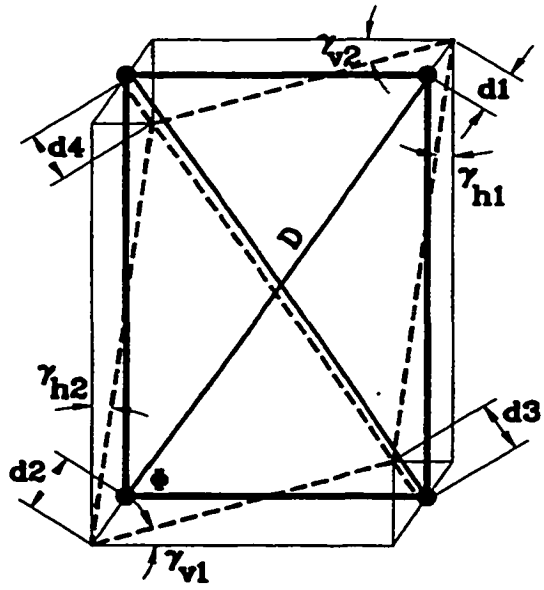

Figure 5.4 Geometry of the model

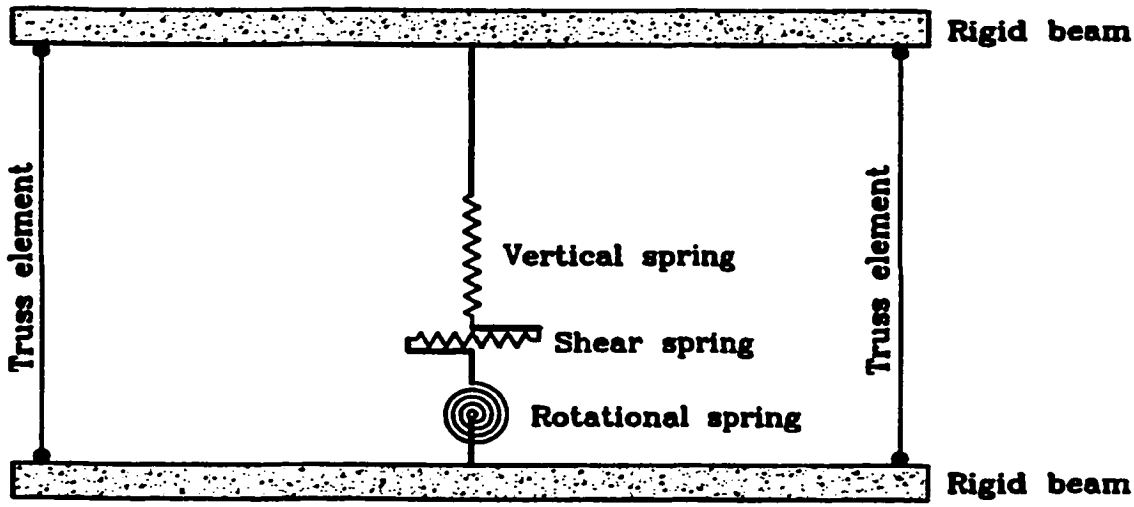

Figure 5.5 Reinforced concrete wall member model (vulcano and Bertero, 1987)

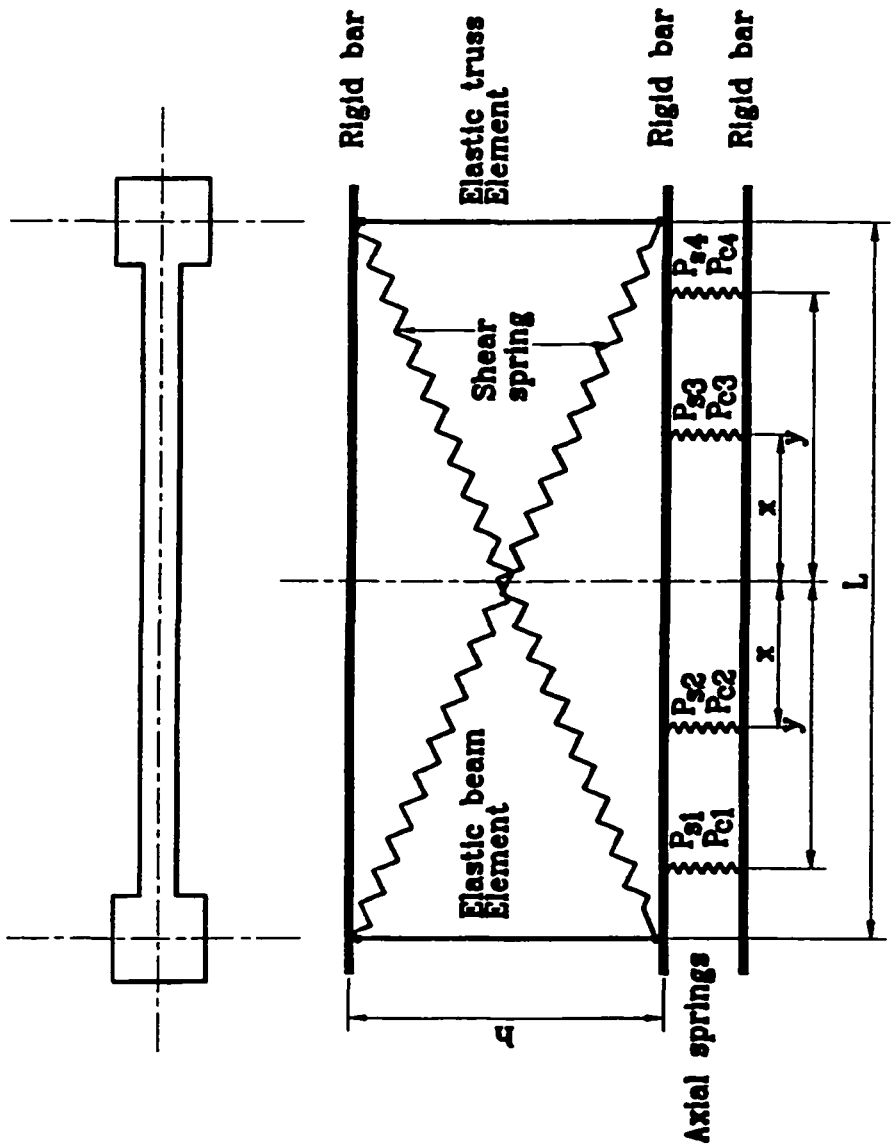

Figure 5.6 Reinforced concrete wall member model

CHAPTER 6

APPLICATIONS

6.1 INTRODUCTION

The developed RC models are incorporated into the general purpose structural analysis program PC-ANSR (Maison, 1992). The modified program is used to analyze a number of columns, joints and RC walls to verify the validity of the model. In choosing the test specimens, care was taken to select those specimens tested to collapse.

6.2 FLEXURAL MEMBERS

The RC columns tested by Ghobarah et al. (1997a) are used for the model validation. The specimens represent a column on a massive base which is loaded laterally by a cyclic load acting at the top of the column. Specimen S1 represents the as built case (designed according to 60's codes) and specimen S3 is designed according to the current codes. The specimens consist of a 2,820 mm high column supported on a concrete base 750 mm deep as shown in figure 6.1. The column width is 610 mm and its depth is 510 mm. The main reinforcement is 12 M15 bars with an average measured value for the yield strength of 437 MPa and strain hardening ratio of 0.025. The average compressive cylinder strength of concrete is 24.0 MPa. The splice length of the main column reinforcement above the foundation is 600 mm (l_d / ϕ_p

= 37.5). The ties in the splice area of specimen S1 (representing the as-built case) are different from those of specimen S3 (representing the specimen designed according to CSA CAN3-A23.3, 1994). For specimen S1, the ties have two legs of diameter 6.35 mm and two legs of diameter 4.7 mm at 150 mm spacing ($\lambda = 0.037$). For specimen S3, the ties have four legs of diameter M10 at 96 mm spacing ($\lambda = 0.118$). A prestressing steel bar installed at the center of the column section is used to apply the axial load of 505 kN. The specimens are tested under cyclic loading by applying a horizontal force at a height equal to 2.55 m from the face of the foundation.

Three concrete and three steel springs are used in the model. Each steel spring represents the area of 4 M15 bars. For calculating the confining width for each bar which will be used to calculate the concrete index of confinement in equation 4.3c in Chapter 4, the width and depth directions are considered for each bar as shown in figure 6.2. In the 610 mm direction, the confining width is taken as the spacing between the longitudinal bars (167.1 mm for specimen S1 and 163.8 mm for specimen S3) or half this distance plus remaining distance to the face of the ties for corner bars (97.9 mm for specimen S1 and 101.2 mm for specimen S3). In the 510 mm direction, the width can be estimated from the height of the effective tension area of concrete surrounding the flexural tension reinforcement given by Clause 10.6.1 of CSA CAN3-A23.3 (1994) after subtracting the concrete cover as it will not have a confining effect after cracking. This distance is equal to 84.7 mm for specimen S1 and 94.6 mm for specimen S3. For the corner bars, this distance should not exceed half the distance to the adjacent bar which is 81.2 mm for specimen S1 and 84.5 mm for specimen S3. Taking the average of the distance of the horizontal and vertical directions for the critical case of the

corner bars, the effective confining width is taken as 89.6 mm for specimen S1 and 92.9 mm for specimen S3. Considering the middle bars, the average confining width is 133.8 mm for specimen S1 and 130.5 mm for specimen S3.

The values of the factors used in equations 4.1 to 4.5 in Chapter 4 are taken the same as those given by equation 4.8 except for f_{cio}, τ_{o2}, τ_o and τ_{mo} which need to be modified by a factor of $\sqrt{\frac{f_c'}{30}}$ (with f_c'=24 MPa) to account for the difference in concrete strength. Using the methodology described in Chapter 4, the element parameters for specimens S1 and S3 are listed in tables 6.1 and 6.2, respectively.

The comparison between the experimental and analytical results for specimens S1 and S3 are shown in figures 6.3 and 6.4, respectively. There is good correlation (ultimate and degraded strength, initial and degraded stiffness) between the experimental (figures 6.3a and 6.4a) and analytical results (figures 6.3b and 6.4b). The major advantage of this model is the representation of the failure mechanism as the results show that both specimens failed first in compression of the concrete springs at displacement of 34 mm for specimen S1 and 46 mm for specimen S3. The failure is more severe for specimen S1 than for specimen S3 because of inadequate confinement. The concrete compressive failure is followed by bond slip failure in specimen S1 at displacement 103 mm. This failure mechanism is the same as that observed by Ghobarah et al. (1997a).

The element parameters for specimens S1 and S3 may also be taken from table 4.3 as listed in tables 6.1 and 6.2, after making corrections to account for the different concrete compressive strength and the different strain hardening ratio for the steel bars as discussed in Chapter 4. Tables 6.1 and 6.2 show that the calculated parameters are different than the

estimated parameters using table 4.3. The value of α_s was totally different. α_s determines the shape of the degrading curve and is not expected to cause much difference in the response as it is very sensitive to the other parameters values. Figures 6.3c and 6.4c show the model prediction for both specimens S1 and S3 when using the parameter values obtained from table 4.3 after correction to account for the different concrete compressive strength and the different strain hardening ratios for the steel bars. The figures show that these values give close representation to that obtained by using the calculated parameters (figures 6.3b and 6.4b). However, the bond slip is determined to occur at a higher displacement than that observed experimentally or determined using the calculated parameters, this comparison indicates that the tables developed in Chapter 4 give good results based on reasonably good estimates of the bond slip parameters.

6.3 BEAM-COLUMN JOINTS

The joints used for the model verification process are those tested by Ghobarah et al. (1997b). These specimens represent an exterior joint of an existing two storey frame. Two specimens were chosen for the comparison with the analytical results, J1 and J2. The specimen J1 represents the joint of the existing frame which was designed in 1969 before the availability of the current seismic codes. The specimen J2 represents the same joint but designed according to the current Canadian Standard (CSA A23.3-94, 1994). The concrete dimensions and the reinforcement details of the specimens tested are shown in figure 6.5.

The two joints are tested under reversed cyclic loading. An initial axial load of 505 kN is applied to the column to simulate the gravity load. In the analysis, the axial load is applied

first and then the lateral load. Each of the two specimens is analyzed twice, once ignoring joint shear deformation (rigid joint) and once taking shear deformation into consideration (flexible joint).

The model properties for specimen J1 are listed in table 6.3. Figure 6.6 shows the comparison between analytical and experimental results. Ignoring the shear deformation when analyzing the joint leads to bond slip softening and concrete softening starting earlier than in the case where shear deformation is considered. This indicates that including joint shear deformation delays the bond slip as the forces and displacements are shared between flexural and shear and thus less demands are imposed on the flexural behaviour. As shown in figure 6.6b, the shear failure occurs before concrete softening and bond slip softening. In the analysis of frames, the assumption of rigid joints will lead to false results as the distribution of plastic hinges at failure will be different from the case of flexible joint assumption.

The model properties for specimen J2 are listed in table 6.4. Figure 6.7 shows the comparison between the analytical and experimental results. Ignoring the shear deformations when analyzing the joint have minor effect on the results. This could be attributed to good detailing and confinement of this joint.

Figures 6.6 and 6.7 show that the analytical model is capable of predicting the pinching, stiffness deterioration, and strength degradation resulting from the application of cyclic loading with reasonable accuracy. The developed hysteretic models and the proposed macro-element result in accurate representation of the behaviour of RC joints when subjected to cyclic loading.

6.4 STRUCTURAL WALLS

The structures used for the validation of the developed model are the three-storey RC walls tested by Vallenas et al. (1979). These walls are intended to idealize the three lower storeys of both a framed wall (specimen 3 and 4) and rectangular walls (specimen 5 and 6) designed for ten-storey and seven-storey prototype buildings shown in figure 6.8, respectively. These specimens are selected for the verification process because they experience high shear deformation and will provide a suitable case for testing the shear model. Cross-sectional details and loading patterns of the four specimens are shown in figures 6.9, 6.10, 6.11 and 6.12. The properties of the steel reinforcement in these tests can be found in table 6.5. The concrete compressive strength determined from cylinder tests range from 32.4 MPa to 38.0 MPa.

The selected RC walls are tested under two loading conditions: monotonic and reversed cyclic loads. Four concrete springs, four steel springs and two diagonal shear spring are used to model each floor of the wall. The wall model properties used in representing the walls are given in tables 6.6 and 6.7. Details of the testing program and the analytical predictions for the two loading conditions are discussed in the following sections.

6.4.1 Monotonic loading

Specimens 3 and 5 are subjected to monotonically increasing loads. Specimen 3 is subjected to an initial axial load of 434 kN on each of its end columns to simulate the gravity load effects. A varying axial load of 0.644 V and -0.644 V is applied to its end columns to produce an overturning moment in the same direction as that caused by the horizontal force

V, acting at the third floor level. The applied axial load for specimen 5 is 299 kN and the varying axial load is 0.522 V where V is the base shear. Of the total base shear, 79.9% is applied at the third floor, 10.4% at the second floor and 9.7% at the first floor. In the analysis, the initial axial load is applied first and then the lateral load and the varying axial load are applied simultaneously.

Figures 6.13a and 6.14a compare the experimental results and the analytical predictions for the third floor load-displacement relationship of specimen 3 and 5, respectively. Figures 6.13b, 6.13c, 6.14b and 6.14c show the load versus flexural displacement and the load versus shear displacement for both specimens. These figures show good correlation between the experimental and analytical results. The load-shear deformation plot shows a maximum shear deformation of about 31% of the total deformation for specimen 3 and about 25% of the total deformation for specimen 5. The analytical model is able to predict these deformation with reasonable accuracy for both specimens. The maximum flexural deformation reached in specimen 3 is about 69% of the total deformation and about 75% of the total deformation for specimen 5.

The analytical model is able to predict the failure mechanism as shear failure followed by bond slip softening for specimen 3 and shear failure, bond slip softening and concrete softening occurring almost simultaneously for specimen 5.

6.4.2 Cyclic loading

Specimen 4 is subjected to an initial axial load of 434 kN on each of its boundary elements to simulate the gravity load. A varying axial load of 0.644 V and -0.644 V is applied to its boundary elements to produce an overturning moment in the same direction as that

caused by the horizontal force V, acting at the third story level. The load history for specimen 6 is applied in the same manner as the monotonic load on specimen 5 with the exception that the lateral load is cyclic, applied using displacement control program (Vallenas et al., 1979). Figures 6.15 and 6.16 compare the analytical and the experimental load-deflection relationship under reversed cyclic loading for specimens 4 and 6, respectively. The two curves are in good agreement with the experimental results. The analytical model is capable of predicting the pinching, stiffness deterioration, and strength degradation resulting from the application of cyclic loading with reasonable accuracy. The analytical curve shows an increase in the stiffness just before reaching the envelope curve. This is due to the sudden increase in the shear stiffness when reaching the unloading branch of the previous cycle as represented by the shear spring model. The hysteretic models developed and the proposed macro-element resulted in a reasonably accurate representation of the behaviour of the structural walls when subjected to cyclic loading.

6.5 SUMMARY

The RC models developed are validated by comparison with column, joint and wall tests. The element model includes strength deterioration and softening parameters. These parameters are calculated based on the bond slip in the steel springs and the confining ratios.

The elements are tested using the experimental results and are shown to be sufficiently accurate in predicting the behaviour of the specimens up to the failure load. Moreover, the model is capable of accurately predicting the failure mechanism. The model is particularly effective in representing brittle modes of failure characteristic of existing nonductile RC

Table 6.1 Model properties for the specimen S1 tested by Ghobarah et al. (1997a)

		Calculated	Estimated using table 4.3*
Exterior steel spring parameters	d_{ss} (mm)	7.91	11.59
	f_{iy} (MPa)	517.60	460.80
	α_s (mm^{-2})	14.54	514.40
	R_{so}	0.49	0.50
	r	0.013	0.038
	P_{sy} kN	416.30	370.60
	K_s N/mm	965100.00	1135682.20
	λ	0.01	0.01
Central steel spring parameters	d_{ss} (mm)	16.99	23.81
	f_{iy} (MPa)	586.20	536.90
	α_s (mm^{-2})	2.81	283.00
	R_{so}	0.53	0.53
	r	0.011	0.011
	P_{sy} kN	471.50	431.80
	K_s N/mm	965100.00	1052612.30
	λ	0.01	0.01
Exterior concrete springs	P_{cy} kN	974.00	974.00
	d_{cy} mm	2.22	2.14
	K_h	1.05	1.05
	Z	88.75	88.75
Central concrete spring	P_{cy} kN	4349.00	4349.00
	d_{cy} mm	0.01	0.01
	K_h	1.05	1.05
	Z	88.75	88.75
Distance between exterior springs (mm)		390.00	411.00

* After modification for concrete compressive strength and steel hardening ratio.

Table 6.2 Model properties for the specimen S3 tested by Ghobarah et al. (1997a)

		Calculated	Estimated using table 4.3*
Exterior steel spring parameters	d_{ss} (mm)	29.33	24.11
	f_{sy} (MPa)	653.10	574.70
	α_s (mm^{-2})	0.11	282.40
	R_{so}	0.49	0.52
	r	0.011	0.027
	P_{sy} kN	525.20	462.20
	K_s N/mm	514719.00	891106.50
	λ	0.01	0.01
Central steel spring parameters	d_{ss} (mm)	34.90	29.39
	f_{sy} (MPa)	707.30	622.70
	α_s (mm^{-2})	0.09	170.60
	R_{so}	0.50	0.53
	r	0.007	0.021
	P_{sy} kN	568.90	500.80
	K_s N/mm	514719.00	848400.90
	λ	0.01	0.01
Exterior concrete springs	P_{cy} kN	974.00	974.00
	d_{cy} mm	2.28	2.25
	K_h	1.29	1.29
	Z	18.49	18.49
Central concrete spring	P_{cy} kN	4349.00	4349.00
	d_{cy} mm	0.01	0.01
	K_h	1.29	1.29
	Z	18.49	18.49
Distance between exterior springs (mm)		348.00	371.00

* After modification for concrete compressive strength and steel hardening ratio.

Table 6.3 Model properties for specimen J1 tested by Ghobarah et al. (1997b)

		Beam	Lower Column	Upper Column
Exterior steel spring parameters	d_{su} (mm)	5.13	35.71	8.01
	f_{iy} (MPa)	476.40	573.40	500.50
	R_s	0.47	0.70	0.47
	α_s	107.39	84.47	11.01
	r	0.016	0.007	0.015
	P_{sy} kN	667.00	458.70	400.40
	K_s kN/mm	1680.00	960.00	960.00
	λ	0.01	0.01	0.01
Central steel spring parameters	d_{su} (mm)	43.56	61.40	18.14
	f_{iy} (MPa)	854.00	633.80	566.40
	R_s	0.54	0.72	0.53
	α_s	0.14	5.01	2.18
	r	0.013	0.006	0.011
	P_{sy} kN	341.60	507.10	453.10
	K_s kN/mm	380.00	960.00	960.00
	λ	0.01	0.01	0.01
Exterior concrete springs	P_{cy} kN	549.00	856.00	856.00
	d_{cy} mm	0.73	1.31	0.96
	K_h	1.06	1.07	1.07
	Z	73.44	72.71	72.71
Central concrete spring	P_{cy} kN	6302.00	4480.00	4480.00
	d_{cy} mm	0.01	0.01	0.01
	K_h	1.06	1.07	1.07
	Z	73.44	72.71	72.71
Distance between exterior springs (mm)		466.90	383.40	410.40

Table 6.4 Model properties for specimen J2 tested by Ghobarah et al. (1997b)

		Beam	Lower Column	Upper Column
Exterior steel spring parameters	d_{ss} (mm)	28.18	90.18	28.48
	f_{sy} (MPa)	608.64	780.40	688.30
	R_s	0.48	0.61	0.48
	α_s	0.14	0.15	0.11
	r	0.017	0.010	0.015
	P_{sy} kN	852.00	624.30	550.60
	K_s kN/mm	869.00	544.00	544.00
	λ	0.001	0.001	0.001
Central steel spring parameters	d_{ss} (mm)	40.14	108.44	35.64
	f_{sy} (MPa)	810.70	820.20	679.50
	R_s	0.53	0.63	0.50
	α_s	0.14	0.11	0.08
	r	0.014	0.009	0.017
	P_{sy} kN	324.290	656.20	543.60
	K_s kN/mm	360.00	544.00	544.00
	λ	0.001	0.001	0.001
Exterior concrete springs	P_{cy} kN	549.00	856.00	856.00
	d_{cy} mm	0.82	1.71	1.61
	K_h	1.12	1.41	1.41
	Z	32.10	13.86	13.86
Central concrete spring	P_{cy} kN	6302.00	4480.00	4480.00
	d_{cy} mm	0.01	0.01	0.01
	K_h	1.12	1.41	1.41
	Z	32.10	13.86	13.86
Distance between exterior springs (mm)		385.60	350.00	347.40

Table 6.5 Properties of steel used in Vallenas et al. (1979) specimens

Reinforcement	Bar diameter (mm)	Bar Area (mm^2)	Elasticity modulus (MPa)	Yield strength (MPa)
Gage No. 7 wire	4.55	16.28	$190x10^3$	440
No. 2 reinforcing bar	6.35	31.67	$211x10^3$	507
No. 5 reinforcing bar	15.90	198.00	$216x10^3$	482
No. 6 reinforcing bar	19.00	281.00	$211x10^3$	444

Table 6.6 Concrete spring parameters used to represent Vallenas et al. (1979) specimens.

Model Parameters		Specimens 3&4	Specimens 5&6
Exterior	P_{cy} kN	1908.00	941.00
Concrete	d_{cy} mm	4.80	6.00
Springs	K_h	1.21	1.19
	Z	16.32	26.69
Interior	P_{cy} kN	2840.00	3130.00
Concrete	d_{cy} mm	0.48	0.57
Springs	K_h	1.00	1.00
	Z	154.50	154.50
Eccentricity of interior springs (mm)		273.00	332.00
Eccentricity of exterior springs (mm)		813.00	974.00

Table 6.7 Steel springs parameters used to represent Vallenas et al. (1979) specimens.

Model Parameters		Specimens 3&4	Specimens 5&6
Exterior Steel Spring parameters	d_{ss} (mm)	67.00	18.62
	f_{sy} (MPa)	652.40	584.50
	R_s	0.57	0.45
	α_s	0.11	0.24
	r	0.014	0.016
	P_{sy} kN	1466.60	1041.60
	K_s kN/mm	1461.20	1024.70
	λ	0.001	0.001
Interior Steel Spring	d_{ss} (mm)	9.89	10.13
	f_{sy} (MPa)	621.12	622.08
	R_s	0.56	0.57
	α_s	38.65	475.00
	r	0.009	0.008
	P_{sy} kN	491.77	354.96
	K_s kN/mm	2533.60	1825.90
	λ	0.001	0.001
Eccentricity of interior springs (mm)		273.00	332.00
Eccentricity of exterior springs (mm)		813.00	974.00

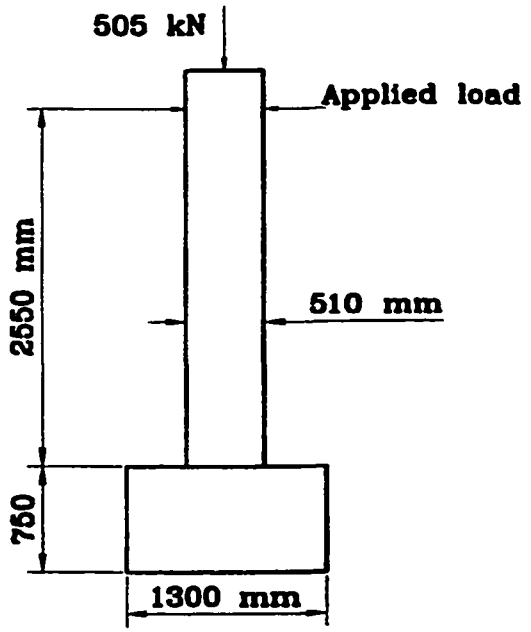

Figure 6.1 Specimen dimensions and applied load for reinforced concrete columns tested by Ghobarah et al (1997a).

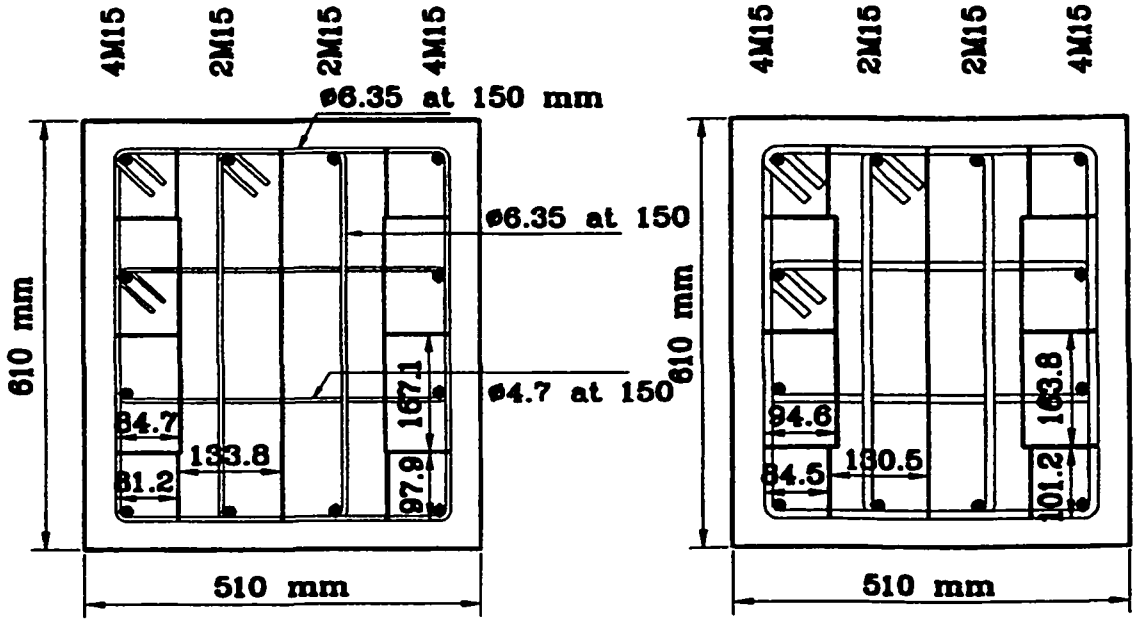

Diameter 6.35 mm and 4.70 mm ties at 150 mm spacing.

Specimen S1

M10 ties at 96 mm spacing.

Specimen S3

Figure 6.2 Reinforcement details and concrete confining width for each bar.

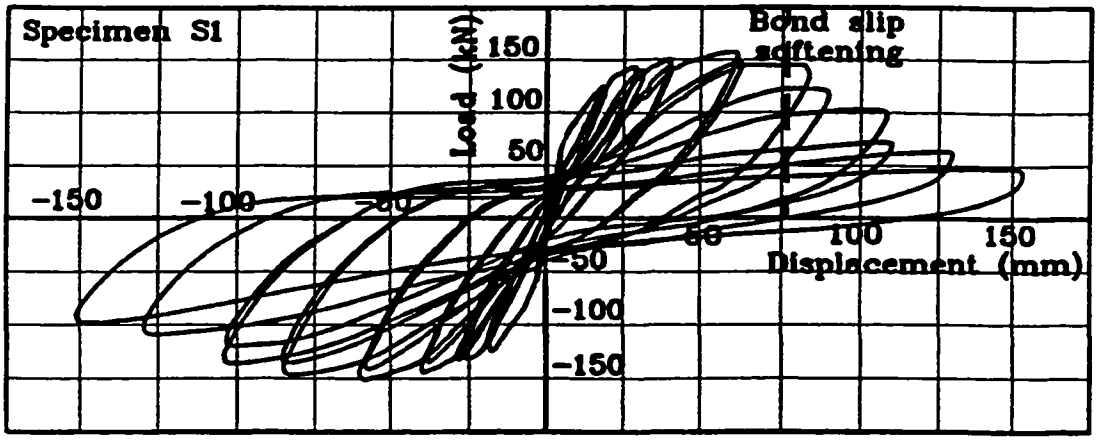

(a) Experimental (Ghobarah et al., 1997)

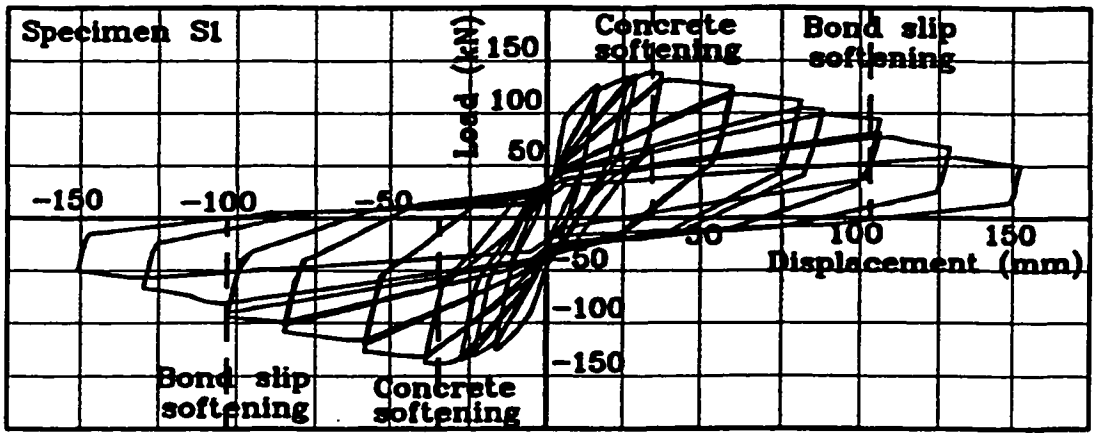

(b) Analytical using calculated parameters.

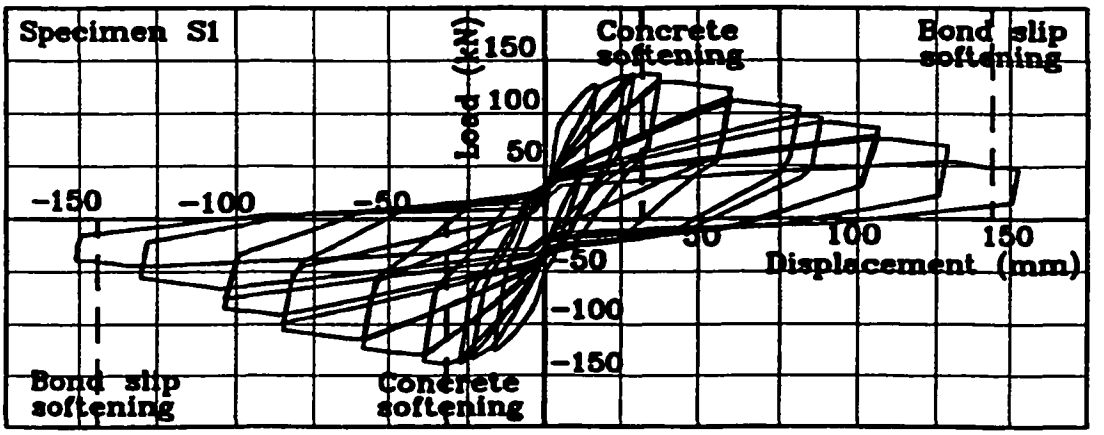

(c) Analytical using approximate parameters from table 4.3.

Figure 6.3 Experimental and analytical results for specimen S1.

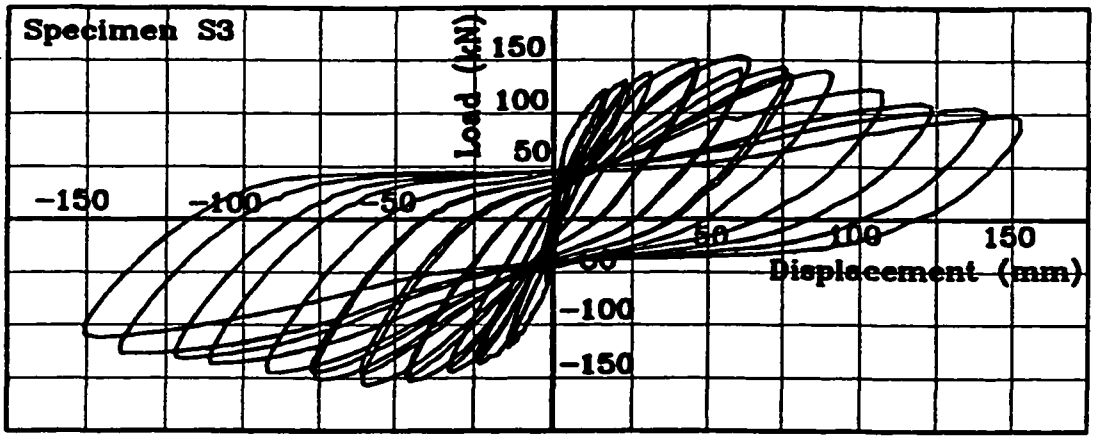

(a) Experimental (Ghobarah et al., 1997a)

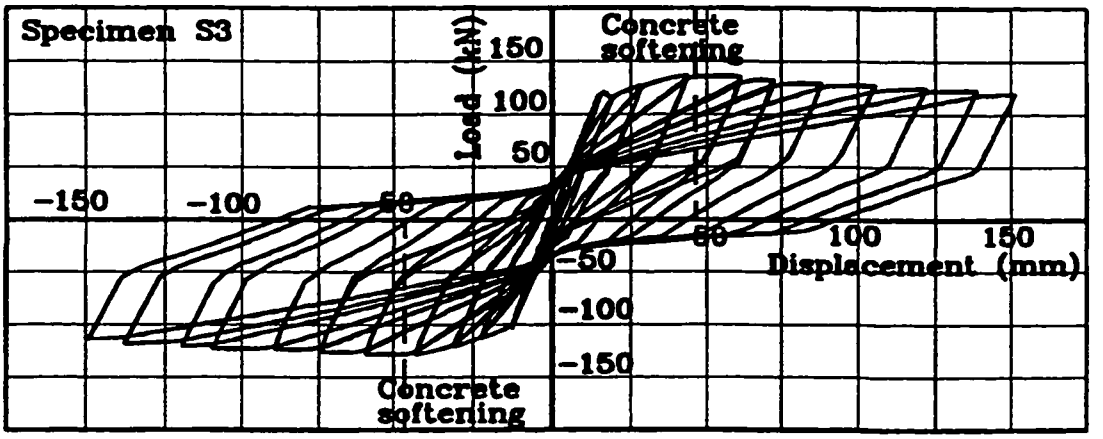

(b) Analytical using calculated parameters.

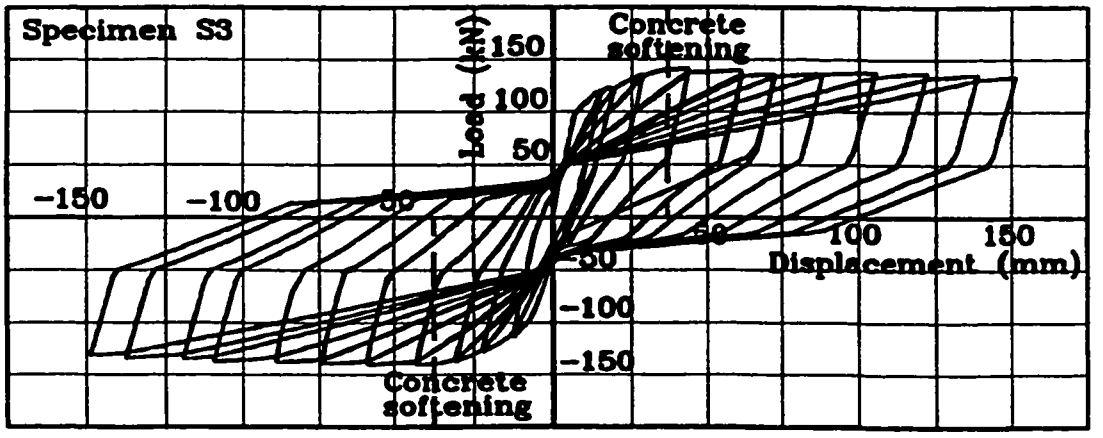

(c) Analytical using approximate parameters from table 2.

Figure 6.4 Experimental and analytical results for specimen S3.

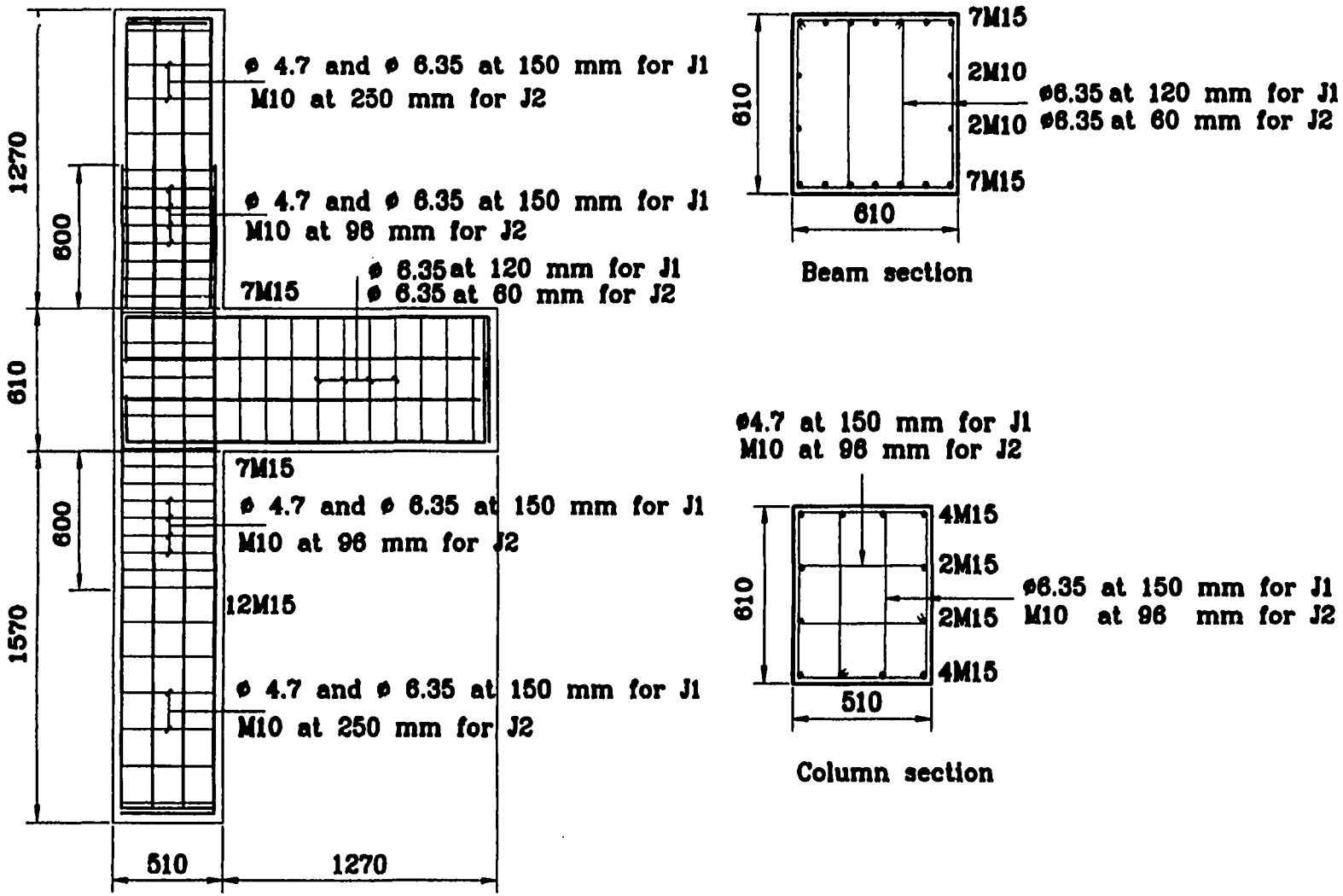

Figure 6.5 Details of specimens J1 and J2 tested by Ghobarah et al (1997b)

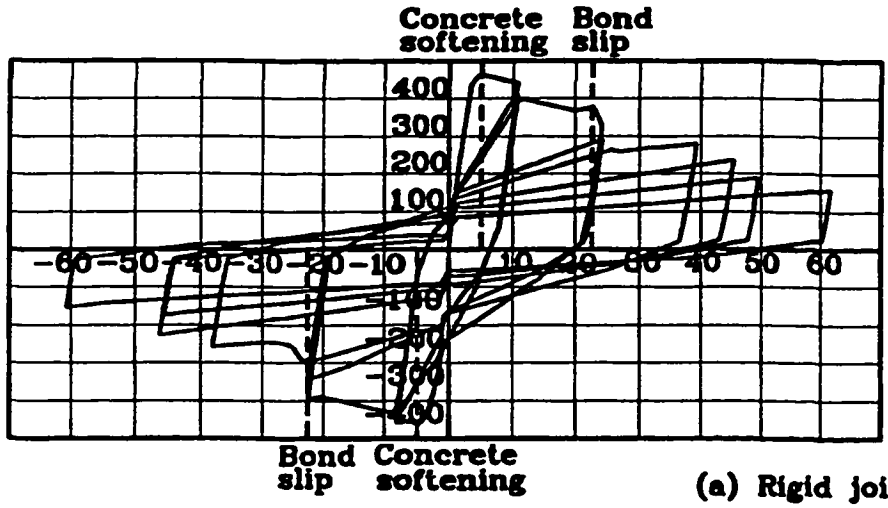

(a) Rigid joint.

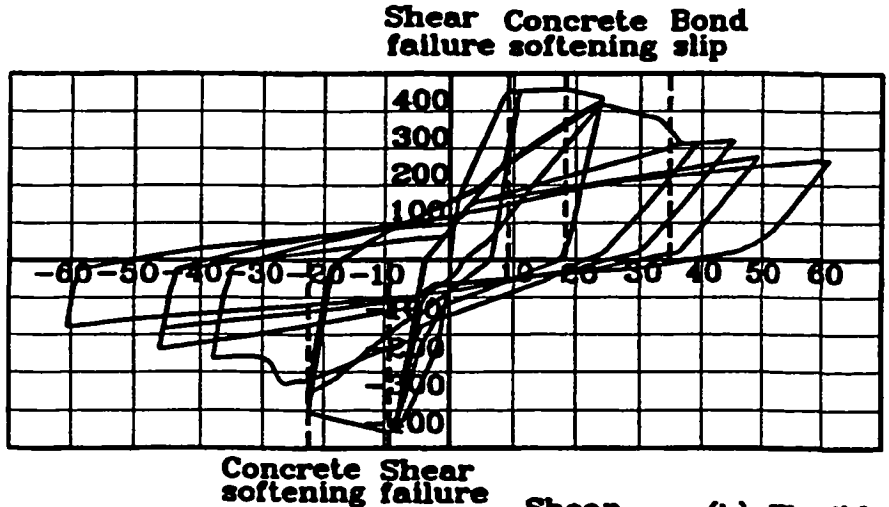

(b) Flexible joint.

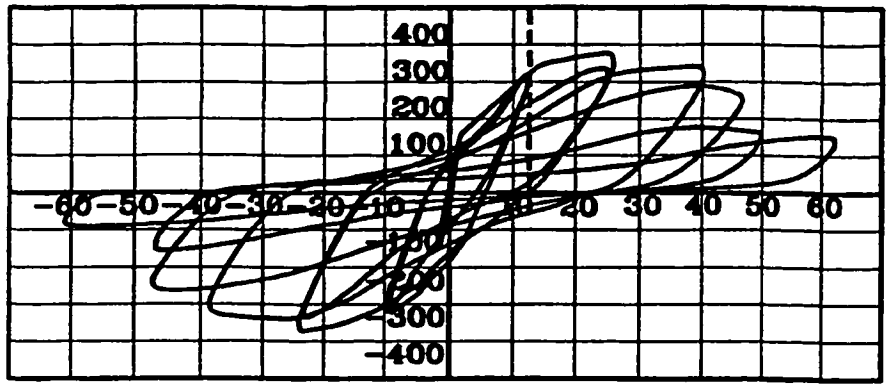

(c) Experimental.

Figure 6.6 Comparison between the experimental and analytical results for specimen J1 tested by Ghobarah et al. (1997b)

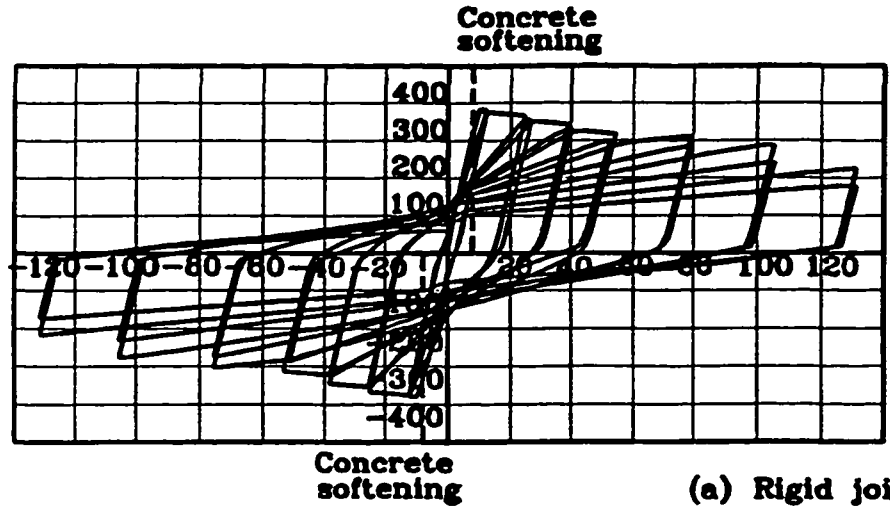

(a) Rigid joint.

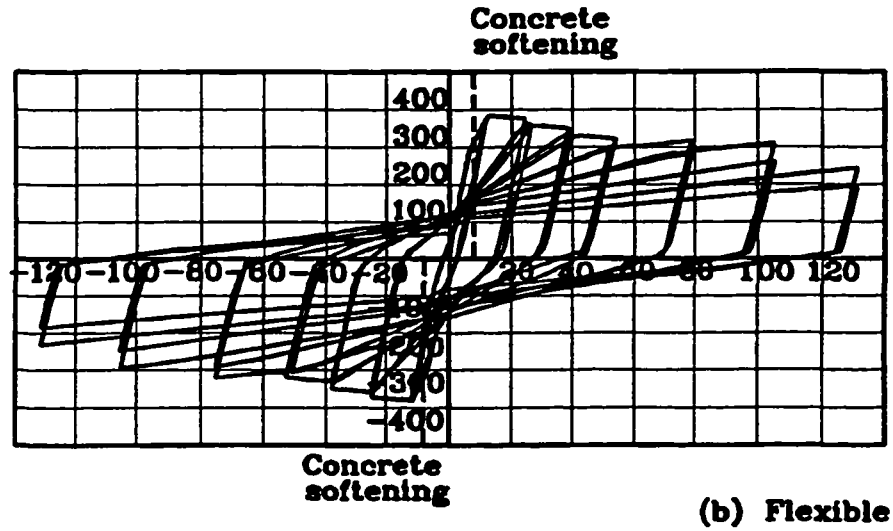

(b) Flexible joint.

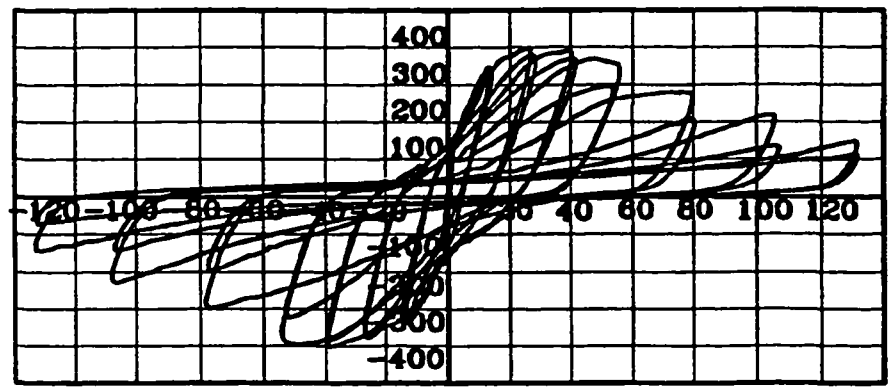

(c) Experimental.

Figure 6.7 Comparison between the experimental and analytical results for specimen J2 tested by Ghobarah et al. (1997b)

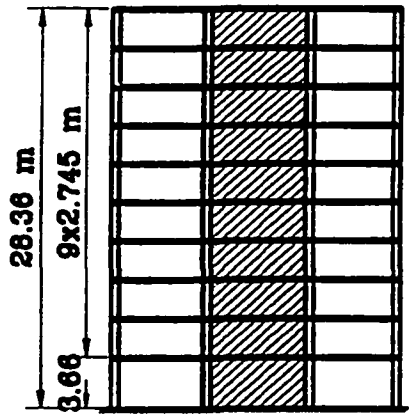

Elevation
Ten-storey building

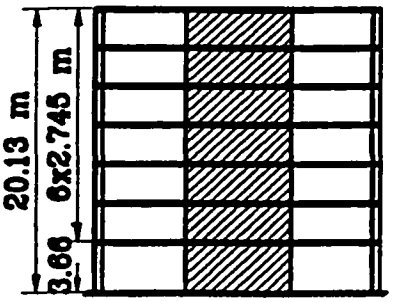

Elevation
Seven-storey building

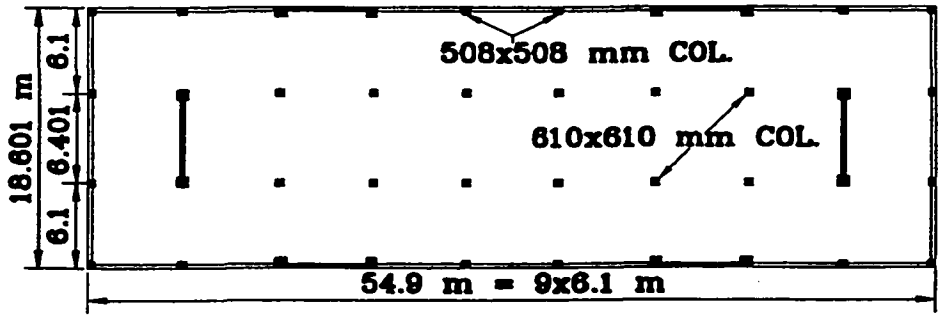

Typical floor plan
Ten-storey building

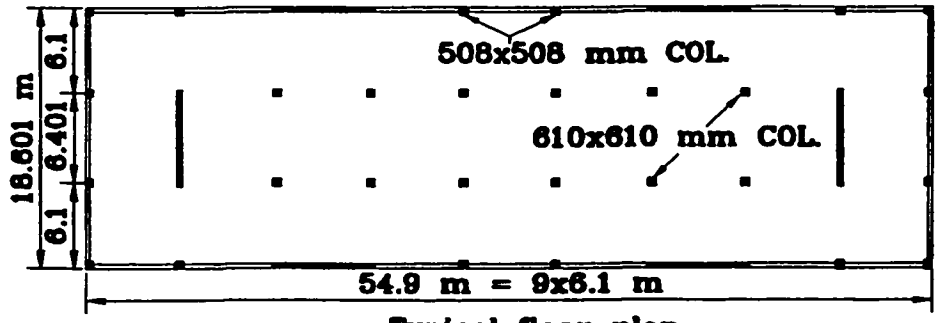

Typical floor plan
Seven-storey building

Figure 6.8 Prototype buildings (Vallenas et al., 1979)

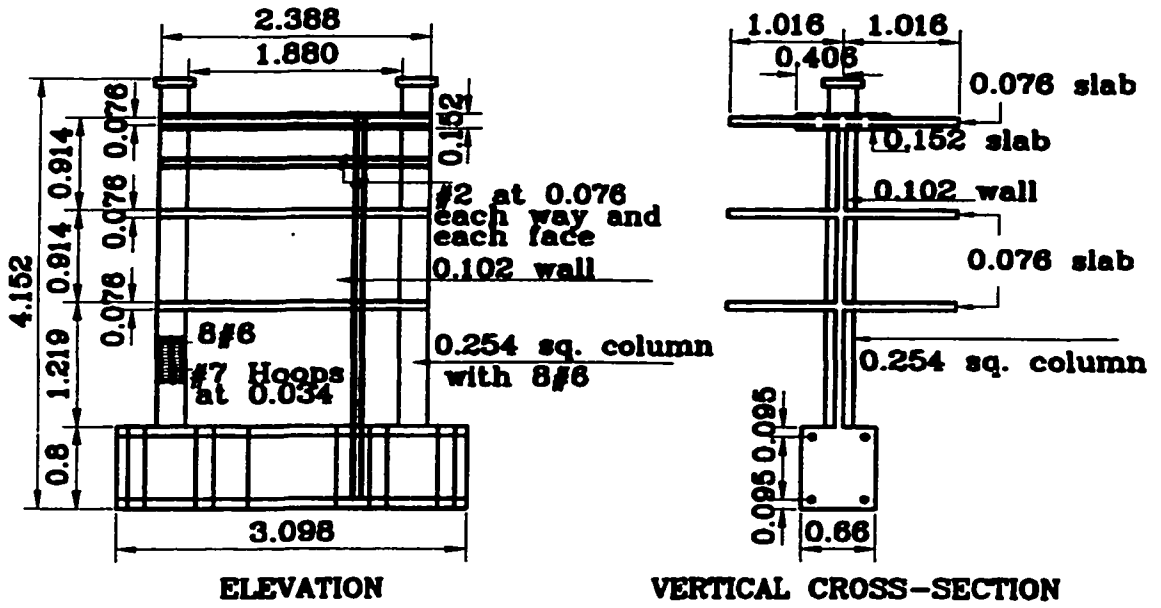

All dimensions are in metres

Figure 6.9 Dimensions and details of the framed wall (Specimens 3 and 4). (Vallenas et al., 1979).

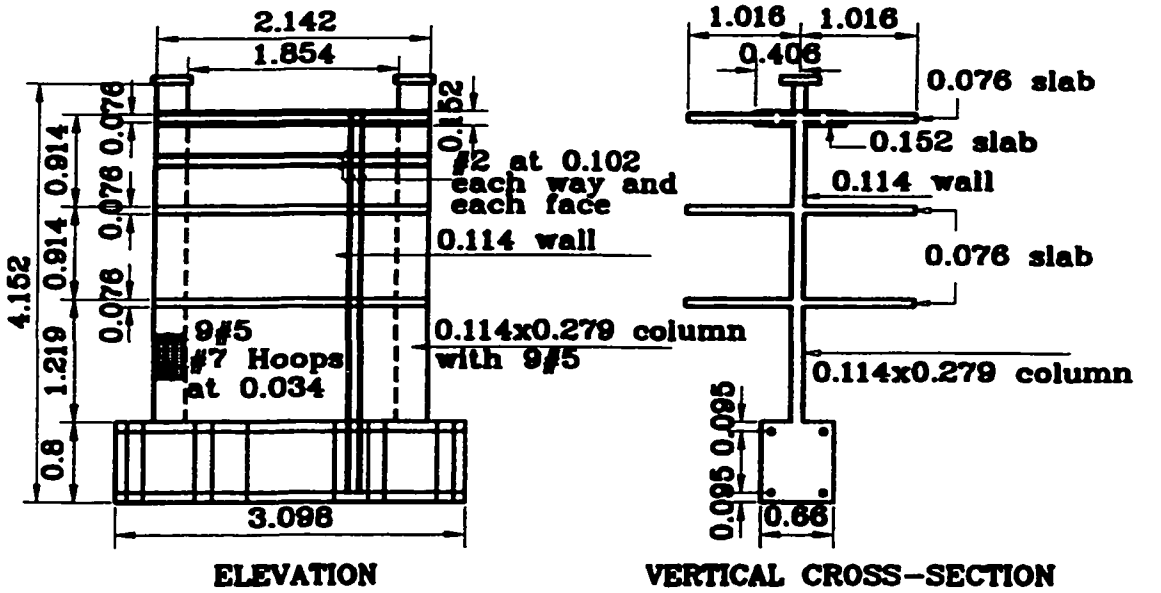

All dimensions are in metres

Figure 6.10 Dimensions and details of the rectangular wall (Specimens 5 and 6). (Vallenas et al., 1979)

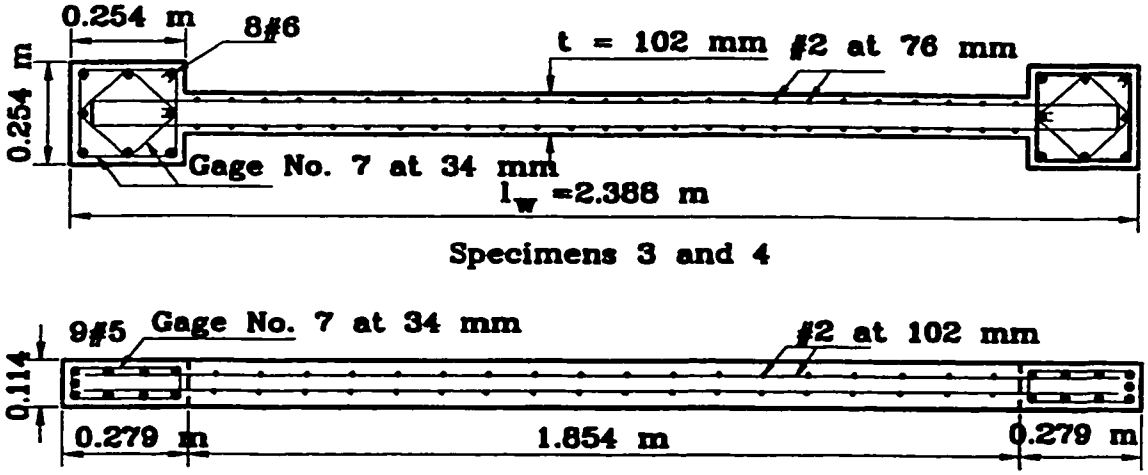

Figure 6.11 Detailed cross section of framed and rectangular walls (Vallenas et al, 1979)

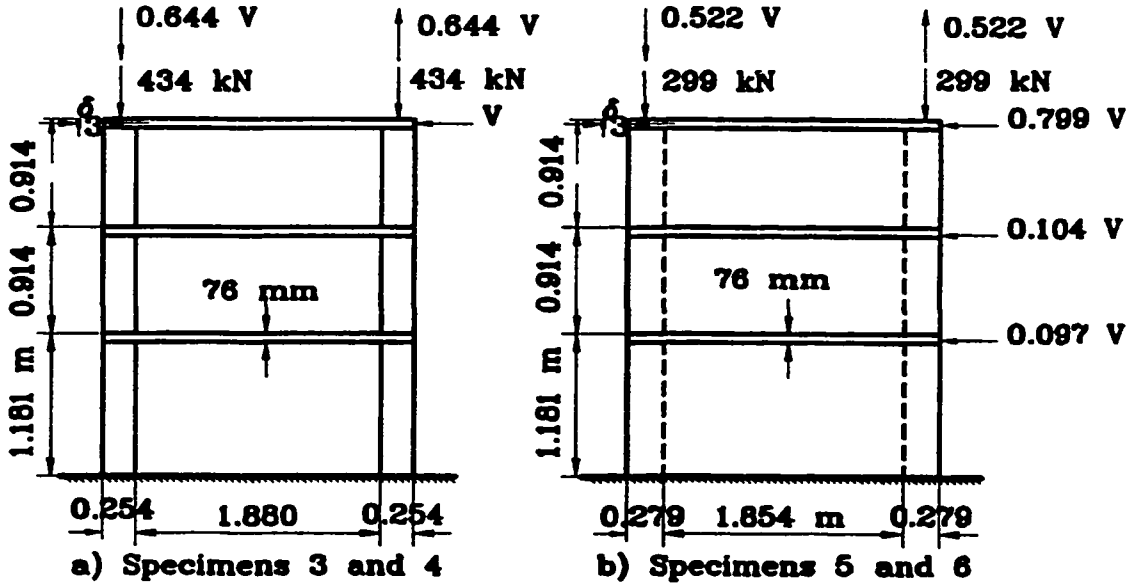

all dimensions in metres

Figure 6.12 Test setup (Vallenas et al., 1979)

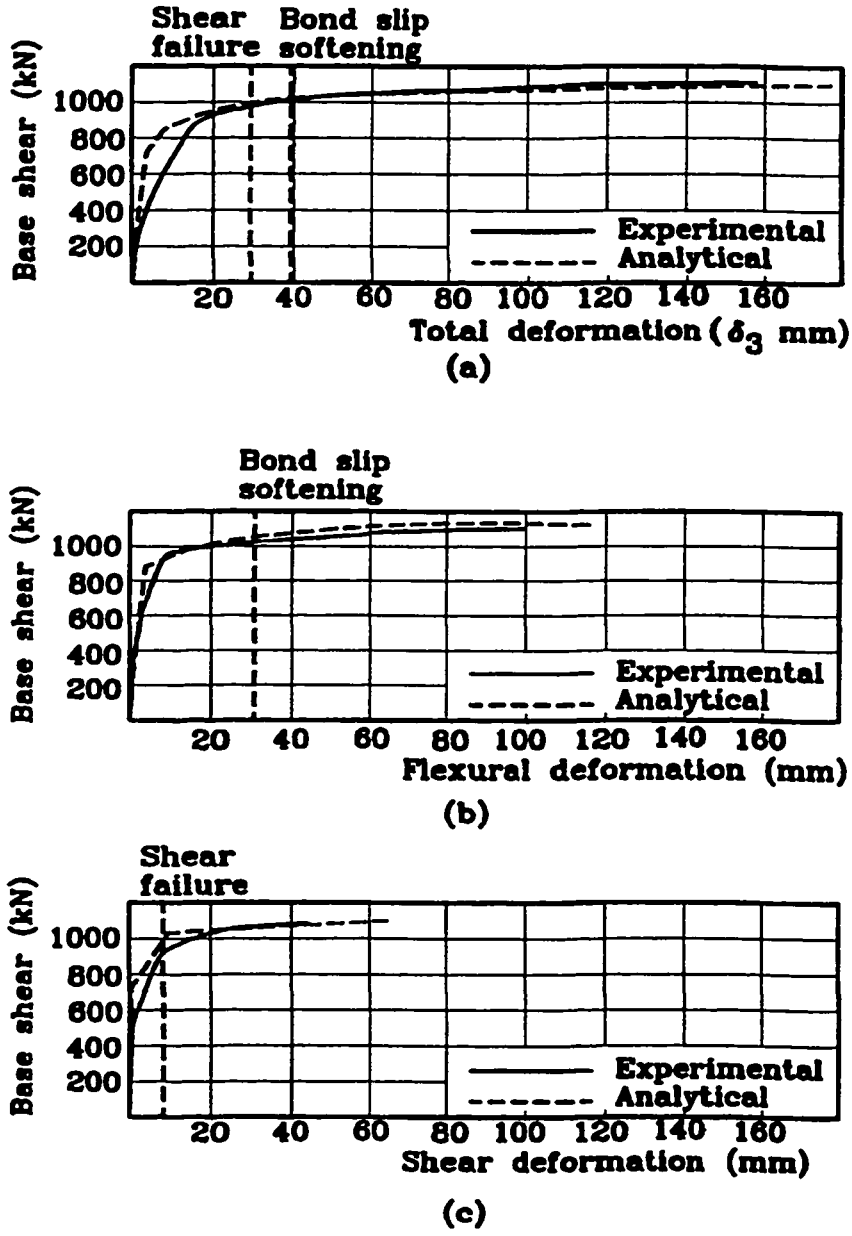

Figure 6.13 Comparison between the experimental and analytical results for specimen 3 tested by Vallenas et al. (1979)

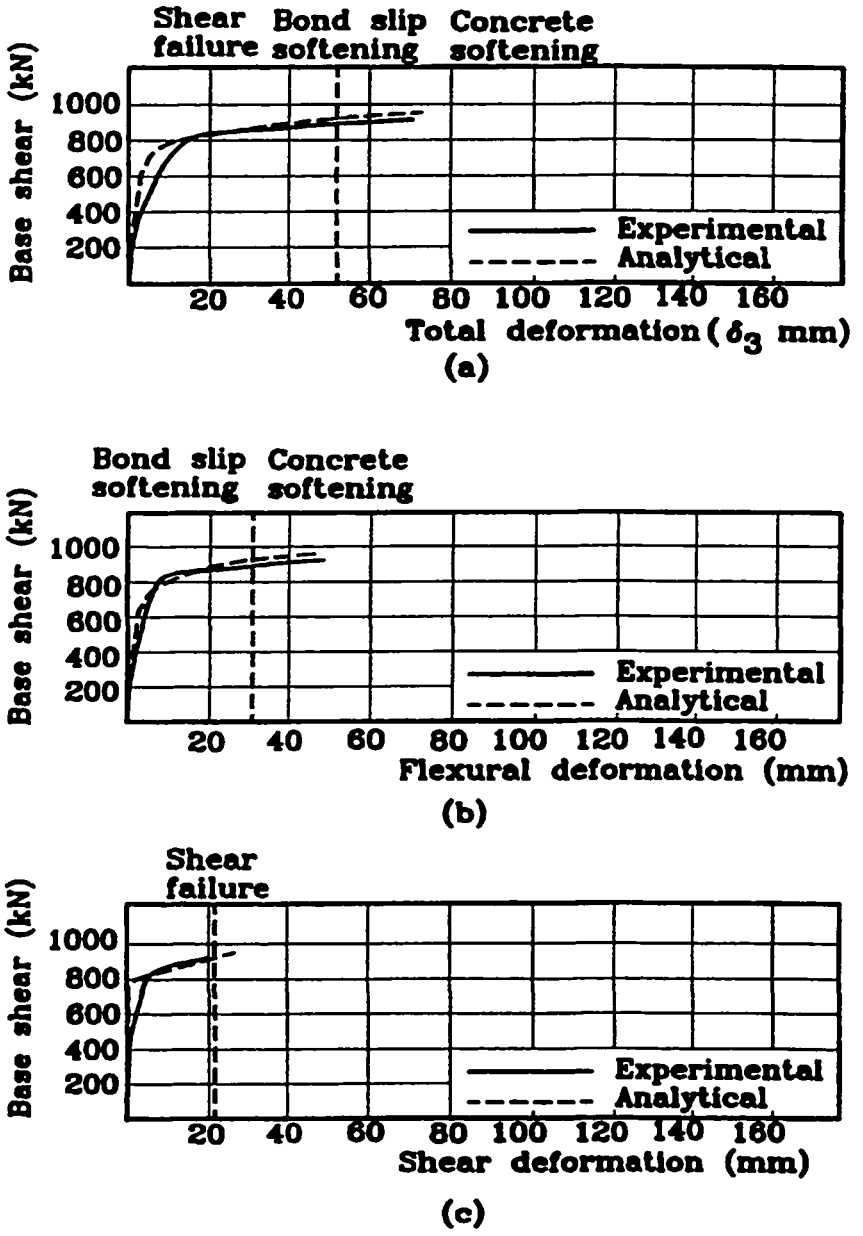

Figure 6.14 Comparison between the experimental and analytical results for specimen 5 tested by Vallenas et al. (1979)

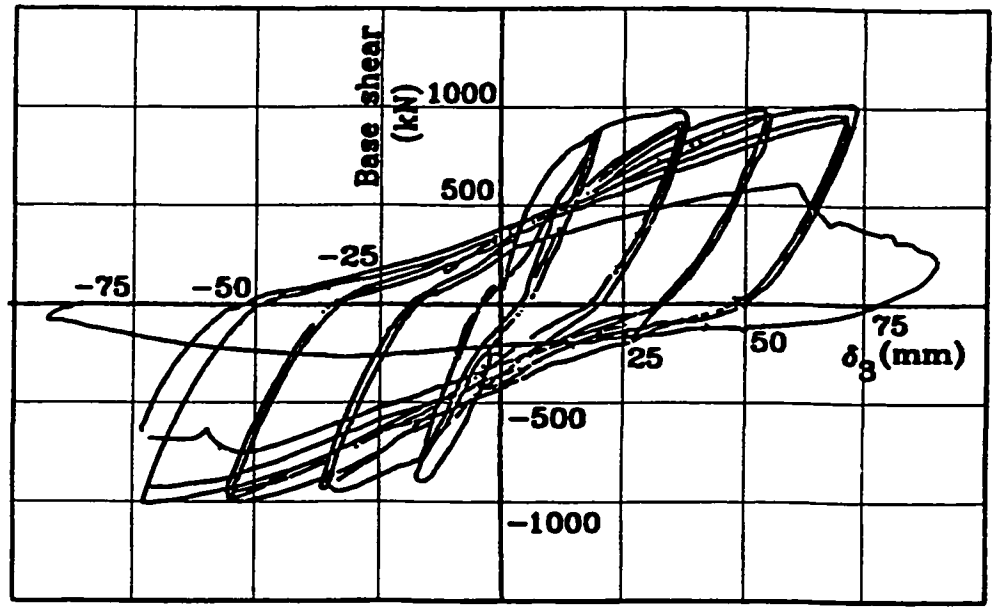

(a) Experimental

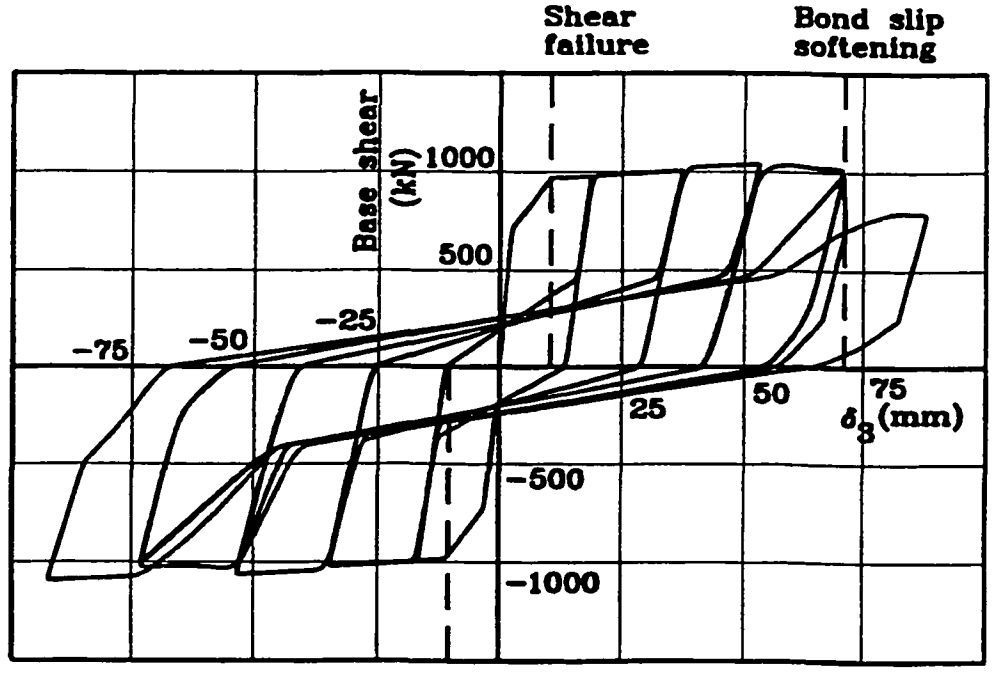

(b) Analytical

Figure 6.15 Comparison between the experimental and analytical results for specimen 4 tested by Vallenas et al. (1979)

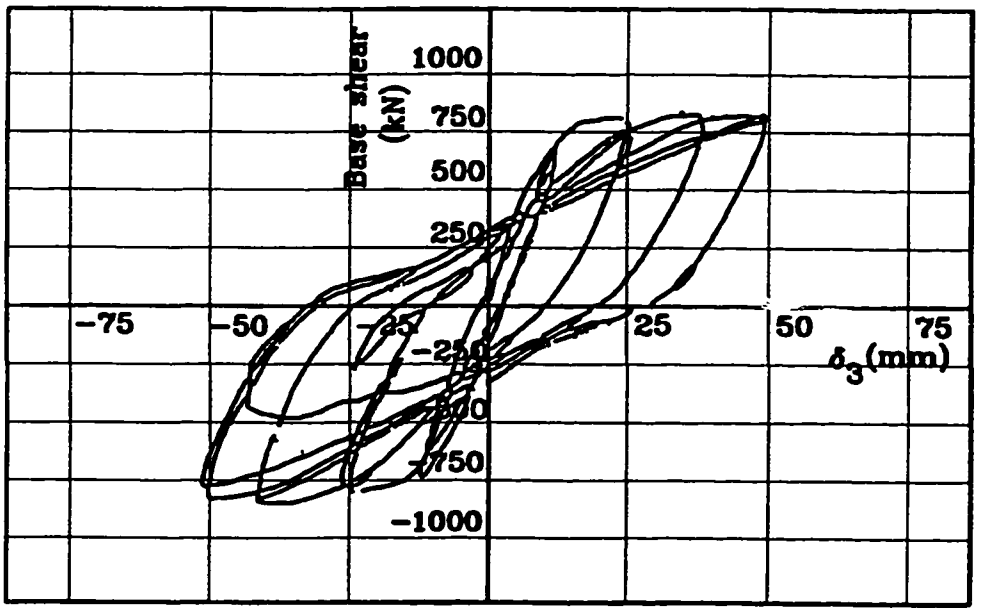

(a) Experimental

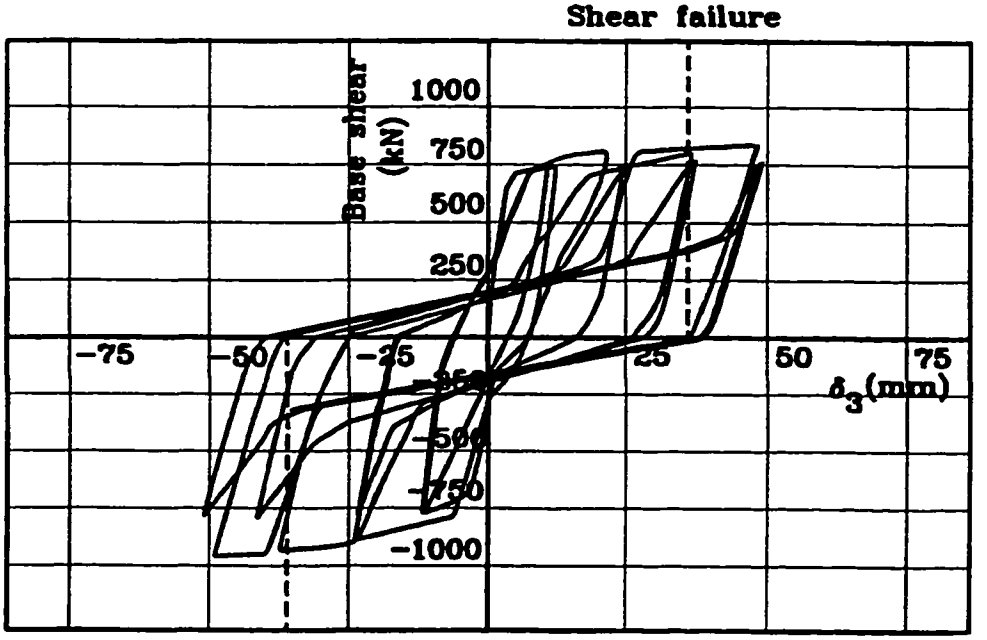

(b) Analytical

Figure 6.16 Comparison between the experimental and analytical results for specimen 6 tested by Vallenas et al. (1979)

CHAPTER 7

SIMULATED RESPONSE OF AN EXISTING RC BUILDING BEFORE AND AFTER REHABILITATION

7.1 INTRODUCTION

In this chapter, the shear and bond slip elements developed are applied to the analysis of an example structure to demonstrate the use and advantages of the models. The lateral capacity of a three-storey reinforced concrete (RC) building before and after rehabilitation was assessed using pushover analysis and nonlinear dynamic analysis. In the pushover analysis, several cases were studied to determine the effect of including concrete crushing, bond slip failure and beam-column joint shear deformation. The nonlinear dynamic time history analysis was conducted using the 1940 El Centro record during the Imperial Valley earthquake scaled to different peak ground accelerations (PGA). A rehabilitation technique using structural walls was designed and tested using pushover analysis and nonlinear dynamic analysis with the El Centro record as the ground motion time history input.

7.2 BUILDING DESCRIPTION

A three-storey reinforced concrete office building was designed to represent existing nonductile buildings. The building consists of three bays by five bays. Each bay is 6 m wide.

The floor height is 3.6 m. The building was designed for gravity loads only according to the ACI code (ACI 318-63). The concrete strength is 21 MPa and the steel yield strength is 300 MPa. Typical floor plan, elevation and cross sections of the office building are shown in figures 7.1, 7.2 and 7.3.

Nonductile reinforcement details in the building include: beam bottom longitudinal reinforcement embedded 150 mm into the beam-column joint, widely spaced transverse reinforcement in beams and columns (M10 at 300 mm), column lap splices (20 bar diameter) located just above the floor level and no transverse reinforcement in the joints.

An interior frame in the short direction of the building was chosen for the analysis. The weight due to the dead load of structural and nonstructural elements on the frame was calculated to be equal to 1416.4 kN. The fundamental period of the frame is analytically predicted to be 0.80 second.

7.2.1 Pushover analysis

The building was modeled using the elements developed as shown in figure 7.4. To evaluate the effect of various behavioural parameters and the potential mode of failure on the response of the building, a number of cases of three-storey frames were analyzed. The effect of ignoring each of the failure criteria was studied. Bond slip softening was not accounted for by assuming the steel spring element to remain bilinear and the yield force is calculated based on the bond slip behaviour. Concrete softening was ignored by assuming the degrading slope Z of the concrete springs to be equal to zero. The three-storey frame was analyzed six times, each case representing the effect of ignoring one or more of the joint shear deformation,

concrete softening and bond slip softening. To differentiate between the different cases in the text and figures, the following notations are used, R for rigid joints; F for flexible joints (including joint shear deformation); B representing inclusion of bond slip softening; NB for ignoring bond slip softening; S for including concrete softening and NS for ignoring concrete softening. For example, frame R-NB-S means that this frame was analyzed using rigid joints, bond slip softening was not included and concrete softening was considered.

The purpose of the nonlinear pushover analysis was to identify the lateral strength of the structure and its behaviour under static load. The three-storey frame was subjected to an increasing monotonic lateral load of an inverted triangular distribution. The lateral load was distributed over the height of the building as shown in figure 7.5.

7.2.1.1 Overall displacement and drift

Figure 7.6 shows the base shear-roof drift relationships for the six cases studied. The figure shows that the six cases are divided into two groups depending on whether bond slip softening is considered or not. The top group represents the two cases R-NB-S and F-NB-S. Ignoring bond slip softening increased the ultimate load by about 24%. It is concluded that the bond slip softening has a major effect on the behaviour of this frame. The effect of joint shear deformation and concrete softening on the overall displacement behaviour is small especially after reaching the yield load. This could be attributed to the high deformation that developed due to the flexural behaviour in the columns. The pushover analysis was carried out using load control and that is why figure 7.6 does not show any strength degradation. For all cases, the analysis was stopped at drift equal to 2.25% of the building height.

Figures 7.7a and 7.7b show the distribution of storey drift and interstorey drift along the height of the building for cases in which bond slip softening was taken into account at an arbitrary load level of 234 kN. Figure 7.7a shows that the F-B-S case incurred the highest storey displacements followed by F-B-NS then R-B-NS then R-B-S. Contrary to expectations, the R-B-S case incurred less displacements than R-B-NS case. This is because the concrete softening in an element results in decreased demands on bond slip softening as a result of decreasing the total stiffness of the two steel and concrete elements combined. This will result in a change in the failure mechanism. This conclusion is supported by figure 7.7b where the R-B-S frame showed less interstorey drift than the R-B-NS in the first floor and higher interstorey drift in the second floor. This is a consequence of the change in the failure mechanism. It is concluded that ignoring any of the failure mechanisms might lead to higher or lower displacements. The effect of concrete softening was observed to be higher than the effect of joint shear deformations in the frame analyzed.

Figures 7.8a and 7.8b show the distribution of storey drift and interstorey drift along the height of the building for cases in which bond slip softening was not taken into account at load level of 262.5 kN. The figure shows that in this particular frame design, the effect of the joint shear deformation on the overall behaviour was small.

For the F-B-S case, it is observed that the interstorey drift in the first two floors is much higher than in the third floor. This means that damage is mainly concentrated in the first two floors.

7.2.1.2 Failure mechanisms

Several investigations have been conducted on the modeling and behaviour of reinforced concrete (RC) buildings. However, the definition of failure is still a deficiency in most available models. Near collapse, it is often difficult to distinguish between numerical instability and structural instability (Ghobarah, 1998). In frame analysis, failure is defined by most researchers (Abouelfath, 1998; Elmorsi, 1998) to be steel yielding. On the basis of this concept, plastic hinge distribution is defined. This is a crude assumption as concrete sections can carry loads after steel yielding. Failure is defined in this research work as the point at which strength degradation starts in any of the elements. By this definition, bond slip failure can be detected from the steel springs, cumulative concrete crushing from the concrete springs and shear failure from the shear springs.

Figure 7.9 shows the failure mechanism for the six studied cases. For cases with bond softening, the failure mechanism is mainly a soft first storey. For cases without bond softening, local failure due to concrete softening occurred at several locations. This combined with the high displacements incurred by the steel springs, led to high roof drifts of (2.25% of the building height). A failure mechanism of the building could not be detected. In frames R-B-S, F-B-S, R-B-NS and F-B-NS, it is observed that bond slip softening is concentrated in the columns despite the fact that beam lap splices are shorter than column lap splices. This could be attributed to the fact that flexural capacities of the beams are higher than those of the columns and the frame is essentially of strong beam-weak column design. Failure in beams was limited to those beams connecting to exterior columns due to the high demands on those beams relative to the interior ones. For the F-B-S case, the first two floors suffered much

more damage than the third floor which was detected from the interstorey drift diagram as was discussed in the previous section. Comparing the failure mechanism of the R-B-S case with that of R-B-NS case, it is observed that the second floor suffered some damage in the case of R-B-S and none in the case of R-B-NS. This resulted in a higher interstorey drift in the second floor for R-B-S than R-B-NS. However, as damage is only concentrated in the first floor for the case of R-B-NS, first floor interstorey drifts are higher for R-B-NS than R-B-S.

7.2.2 Dynamic analysis (frame F-B-S)

This section describes the response of the three-storey frame structure to earthquake excitations. The masses of slabs, beams, columns and nonstructural walls are assumed to be lumped at the beam-column joints. The analyzed frame was assumed to carry one fifth of the building mass. The dynamic analysis of the building when subjected to earthquake ground motion is carried out by solving the equation of motion using step by step Newmark constant average acceleration integration procedure. Integration time step of 0.005 second is found to produce accurate results.

The acceleration time history selected as input ground motion is El Centro record (component S00E) of the 1940 Imperial Valley earthquake, California with PGA of 0.348g and PGV of 0.334 m/s. The El Centro acceleration time history record is shown in figure 7.10 and its response spectrum is shown in figure 7.11. The fundamental frequency of the building of 0.80 second is marked on the response spectrum.

7.2.2.1 Roof displacement time histories

Figures 7.12 and 7.13 show the roof displacement time histories for the frame (F-B-S) subjected to El Centro record scaled to PGA of 0.05g ,0.10g, 0.15g and 0.20g. When the record scaled to PGA of 0.20g is used as input ground motion, failure of the building occurred 13.02 seconds into the earthquake record. The maximum roof displacements were 18.21 mm (0.17% drift), 32.58 mm (0.30% drift), 42.84 mm (0.40% drift) and 57.83 mm (0.54% drift) for peak ground accelerations of 0.05g, 0.10g, 0.15g and 0.20g, respectively.

By comparing the maximum roof drift with the drift obtained from pushover curve shown in figure 7.6 for frame F-B-S, it is found that under the effect of earthquake loading, the building behaved with very limited ductility as brittle failure occurred when the peak strength was reached.

7.2.2.2 Envelopes of lateral drift and interstorey drift

The envelopes of maximum storey drift and interstorey drift for the frame are shown in figures 7.14 and 7.15. The building response was in the first mode until failure. The interstorey drift is higher at the first floor than the second floor with the third floor showing the lowest drift. This indicated that damage is decreasing towards the top of the building.

7.2.2.3 Damage to the three-storey building due to El Centro record

Figure 7.16 shows the damage to the building when subjected to the ground motion record. For peak ground acceleration up to 0.10g, there was no damage. Some of the elements yielded but none of them reached the strength degradation part. According to this

definition the building is still in a repairable condition and damage is minor. For the case of PGA of 0.15g, bond slip failure occurred at the base of the two interior columns. The damage at this stage will be more difficult to repair. For peak ground acceleration of 0.20g, extensive damage and collapse of the building occurred before the completion of the earthquake record as can be seen in figure 7.16. It is observed that beam-column joint shear failure occurred in five of the joints. That is different from the case of pushover analysis where there was no identified beam-column joint shear failure. This is due to the fact that the shear rigidities of the joints have significantly deteriorated due to the cyclic load application. A behaviour which cannot be captured by the pushover analysis. This deterioration combined with deterioration due to bond slip softening and concrete softening due to the cyclic behaviour resulted in limited ductility that appeared in the dynamic analysis.

7.3 PROPOSED REHABILITATION SYSTEM

The seismic design load for the building was calculated assuming that the building is located in the City of Victoria, British Columbia. The force modification factor, R, was taken equal to two assuming that the lateral load resisting system is RC walls with nominal ductility. Walls were not assumed to be ductile to limit the damage to the original structure which has very limited ductility. The system of walls used for the rehabilitation process is shown in figure 7.17. Including the effect of torsion due to incidental eccentricity, the total base shear to be carried by an exterior wall is calculated to be equal to 0.14 of the total weight of the building.

The wall thickness is assumed to be 200 mm, and assuming that the original columns

are acting with the wall as a boundary element, the wall reinforcement was calculated according to the CSA Standard (A23.3-94, 1994) and is shown in figure 7.18. Sufficient dowels to resist the shear flow are to connect the wall with the columns. The computer model used to analyze the three-storey building after rehabilitation is shown in figure 7.19. The fundamental period of the rehabilitated frame is predicted to be 0.14 second. This frequency is marked on the response spectrum of El Centro record shown in figure 7.11.

7.3.1 Pushover analysis

The rehabilitated three-storey frame was subjected to an monotonically increasing lateral load of an inverted triangular distribution. The lateral load was distributed over the height of the rehabilitated building in the same way as that of the original building.

7.3.1.1 Overall displacement and drift

Figure 7.20 shows the base shear-roof drift relationship. The lateral strength of the rehabilitated frame is 1500 kN and thus the lateral strength of the rehabilitated building, assuming that the lateral resisting system is the four walls and ignoring the effect of torsion, is 6000 kN which is about 4 times larger than the original building which consists of six frames each with capacity of 250 kN. The rehabilitation system resulted also in increasing the initial stiffness.

Figures 7.21 and 7.22 show the distribution of storey drift and interstorey drift along the height of the building. The interstorey drift in the three floors in nearly equal which implies that the rehabilitation system is effective in distributing the damage along the building height.

7.3.1.2 Failure mechanisms

Figure 7.23 shows the failure mechanism. The failure is distributed between beams, columns and the added structural wall. The same conclusion was reached in the previous section from the interstorey drift diagram. At the end of loading, failure occurred due to the soft first storey.

7.3.2 DYNAMIC ANALYSIS

This section describes the response of the rehabilitated three-storey frame structure to earthquake excitations. The masses are assumed to be lumped at the beam column-joints. The acceleration record selected as input ground motion is the same as that used for the original building.

7.3.2.1 Roof displacement time histories

Figures 7.24 and 7.25 show the roof displacement-time histories for the frame when subjected to the El Centro record scaled to PGA of 0.30g ,0.50g, 0.70g and 0.75g. When the record scaled to PGA of 0.75g is used as input ground motion, failure of the building occurred at 0.3 second into the earthquake record. The maximum roof displacements were 2.24 mm (0.02% drift), 3.61 mm (0.03% drift), 5.08 mm (0.05% drift) and 22.15 mm (0.21% drift) for peak ground accelerations of 0.30g, 0.50g, 0.70g and 0.75g, respectively. The rehabilitated building was able to sustain an earthquake with a peak ground acceleration about 4 times greater than the original building.

By comparing the maximum roof displacements with the displacements obtained from

the pushover curve shown in figure 7.20, it is evident that the behaviour of the rehabilitated building was not ductile as brittle failure occurred when the peak strength was reached. This is expected because of the use of strong lateral load resisting elements such as the structural walls.

7.3.2.2 Envelopes of lateral displacement and interstorey drift

The envelopes of maximum displacements and interstorey drift for the frame are shown in figures 7.26 and 7.27. The behaviour was mainly in the first mode except near collapse, as the effect of higher modes appeared. This could be due to major damage in the first floor.

7.3.2.3 Damage to the three-storey building due to El Centro record

Figure 7.28 shows the damage to the building when subjected to the ground motion record. For peak ground acceleration up to 0.50g, there was no damage. Some of the elements yielded but none of them reached the strength degradation part. According to this definition, the building is still in a repairable condition, and the damage is minor. For the case of PGA of of 0.70g, bond slip failure and concrete crushing occurred in the external columns. The damage at this stage will be more difficult to repair. For peak ground acceleration of 0.75g, extensive damage and collapse of the building occurred before the completion of the earthquake record as can be seen in figure 7.28. It is noticeable that beam-column joint shear failure occurred in two of the joints and shear failure occurred in the first story of the shear wall. That is different from the results of the pushover analysis where there was no identified

shear failure. This is due to the fact that the shear rigidities of the joints have significantly deteriorated due to the cyclic load application. A behaviour which can not be captured by the pushover analysis.

7.4 SUMMARY

The results from the pushover analysis of the three-storey frames indicated that the failure mode is mainly due to bond slip failure. Concrete softening and beam-column joint shear deformation did not affect the lateral strength and there was no identified beam-column joint shear failure. It should be noted that the shear forces in the joints were low due to bond slip failure. Considering concrete softening, it is expected that it will have a major effect if the section is over reinforced or subjected to high axial loads. But most importantly, considering concrete softening is necessary to define the failure mechanism which will help in defining a suitable rehabilitation technique.

The results demonstrate the importance of including all potential modes of failure due to concrete crushing, bond slip and beam-column joint shear in the seismic assessment of structures. This is particularly important in the analysis of existing buildings with recognized inadequate lateral load resistance and nonductile reinforcement detailing. In general, a reasonable estimate of the lateral load carrying capacity of the building can be obtained using the pushover analysis.

Time-history analysis of the original frame shows that it has a very limited ductility and that a brittle failure is expected. The pushover analysis does not give a good estimate of the building ductility because it does not take into account the effect of the cyclic loading on

the stiffness and strength of individual elements.

Shear failures were observed during the time-history analysis. this is mainly due to the cyclic degradation of stiffness. In order to assess the behaviour of existing buildings and determine their failure mechanism, time-history analysis is needed.

The designed rehabilitation system increased the ultimate strength of the building to about four times than of the original building. However, it did not affect its ductility.

Finally, the results presented are based on a limited number of analyses on a specific frame. To attempt to establish general conclusions on the behaviour of gravity load designed frames, a more comprehensive study of several frame designs subjected to different ground motion records, is necessary.

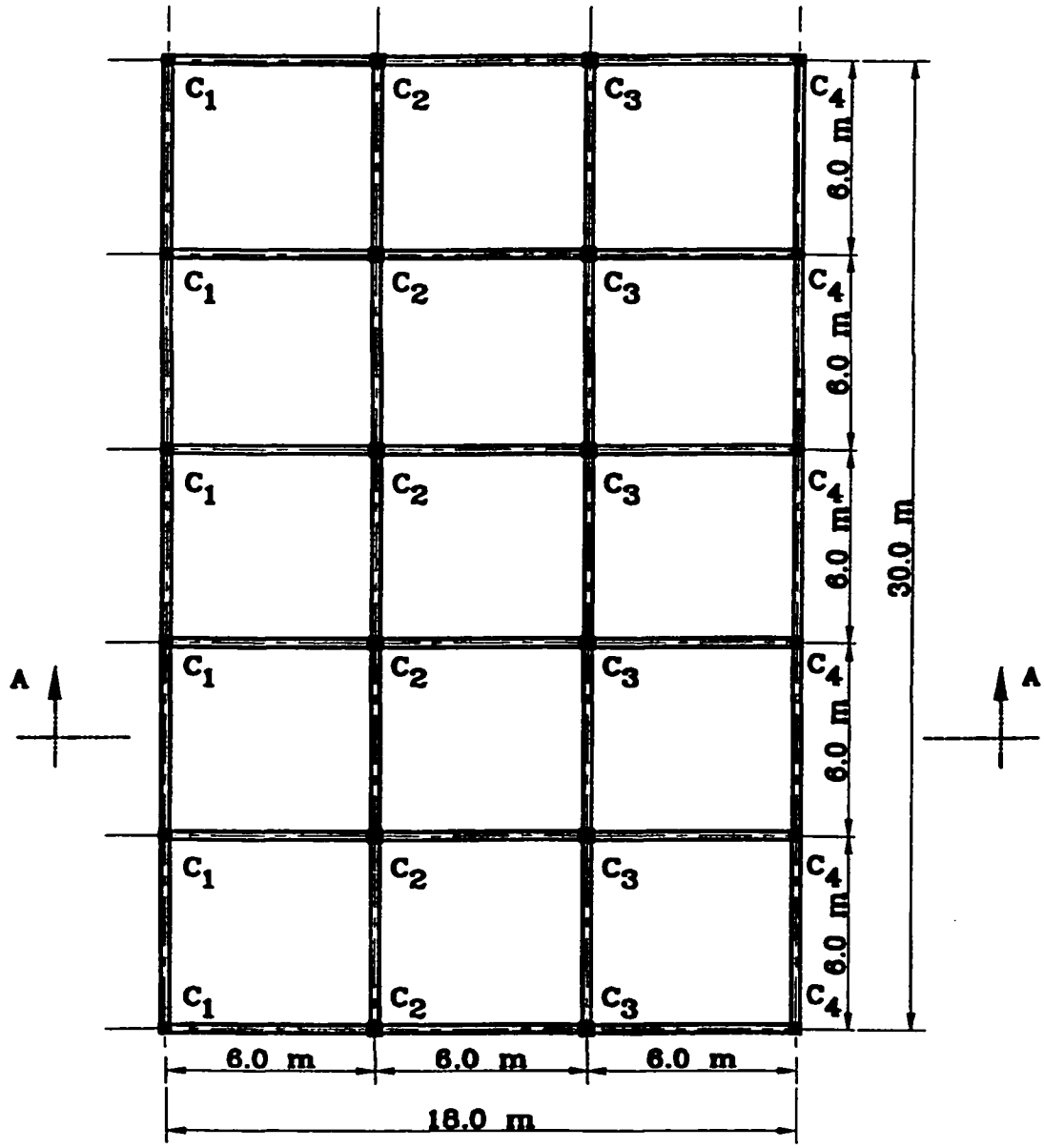

All beams are 250 x 600 mm.
Floor slab thickness is 150 mm.
Exterior columns C_1 and C_4 are 300 x 300 mm.
Interior columns C_2 and C_3 are 400 x 400 mm.

Figure 7.1 Typical floor plan for the three-storey building.

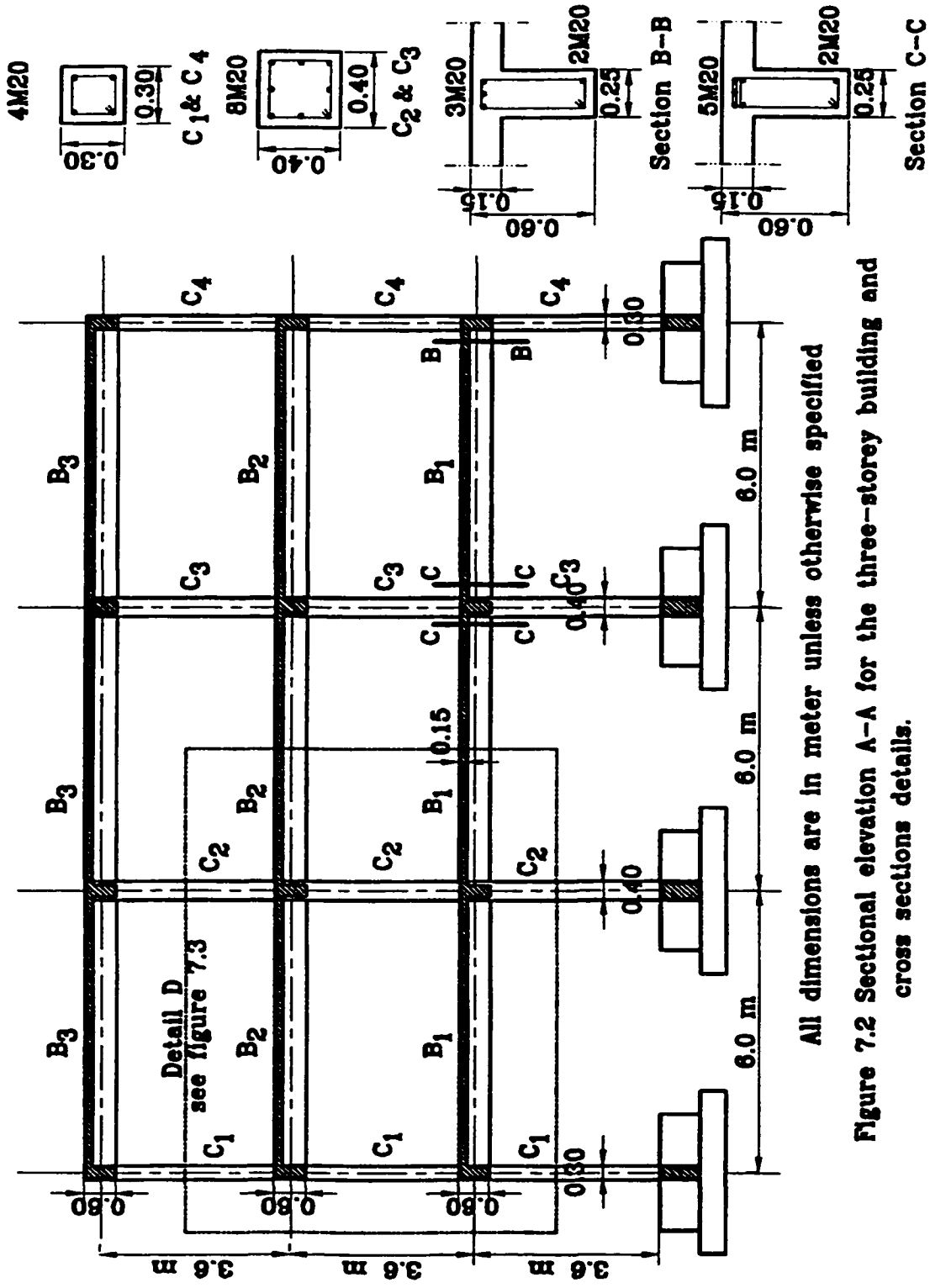

All dimensions are in meter unless otherwise specified

Figure 7.2 Sectional elevation A-A for the three-storey building and cross sections details.

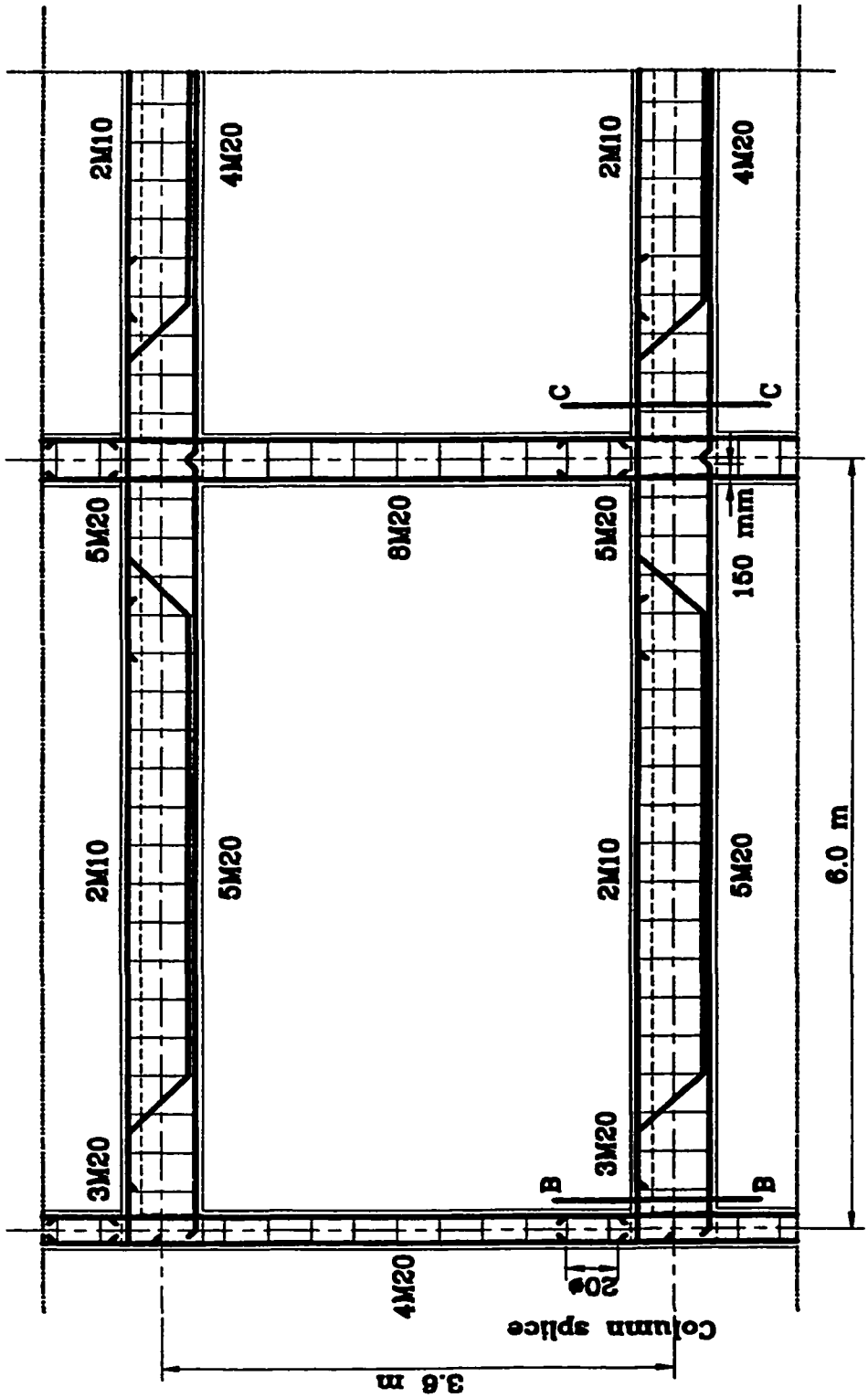

All stirrups and ties are M10@300 mm

Figure 7.3 Reinforcement details for the three-storey frame (Detail D of figure 7.2)

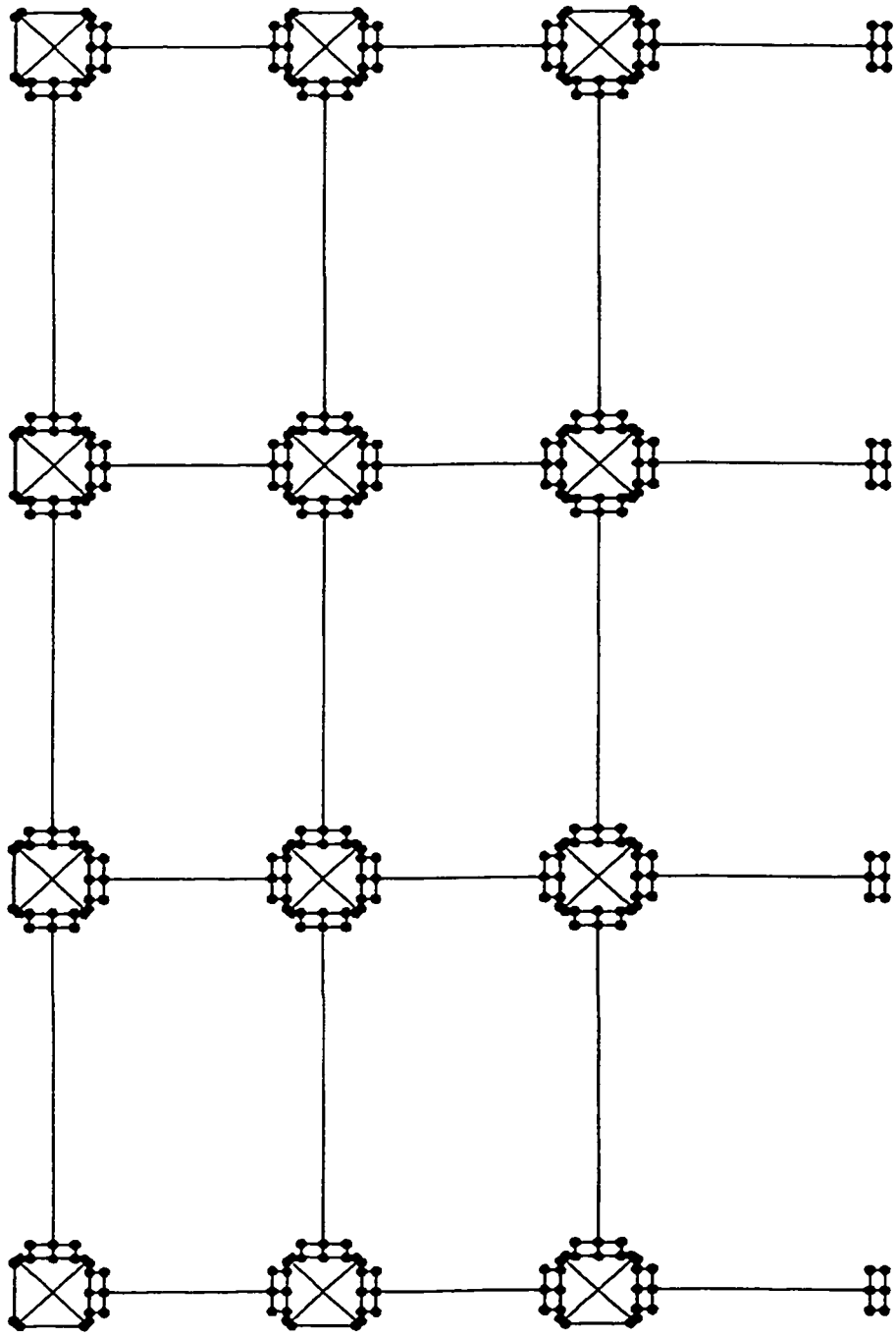

Figure 7.4 Computer model for the three-storey frame

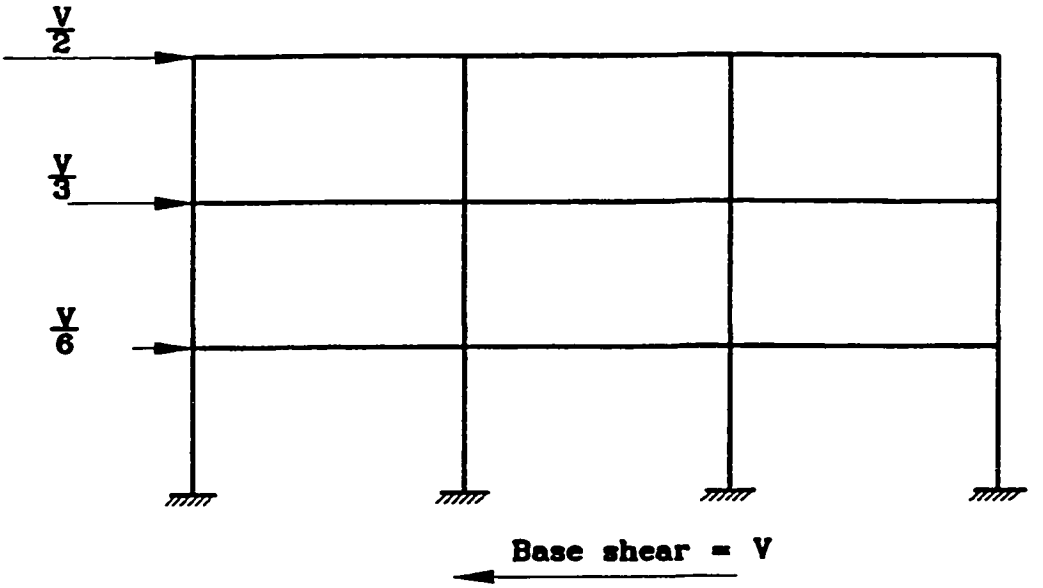

Figure 7.5 Lateral load distribution for pushover analysis.

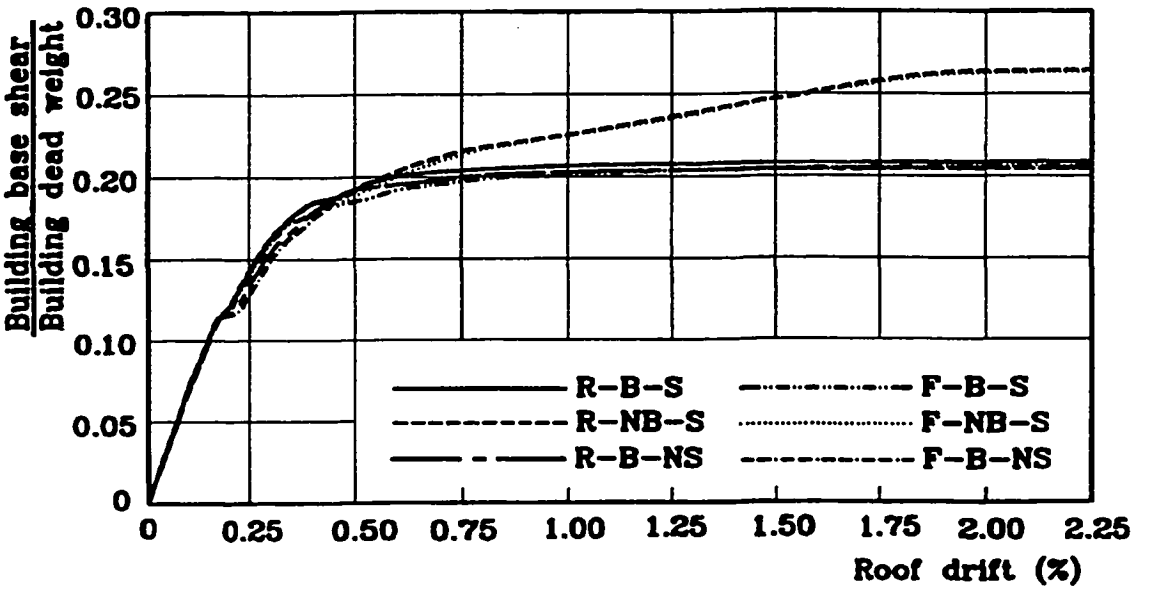

Figure 7.6 Base shear–roof drift relationship from pushover analysis.

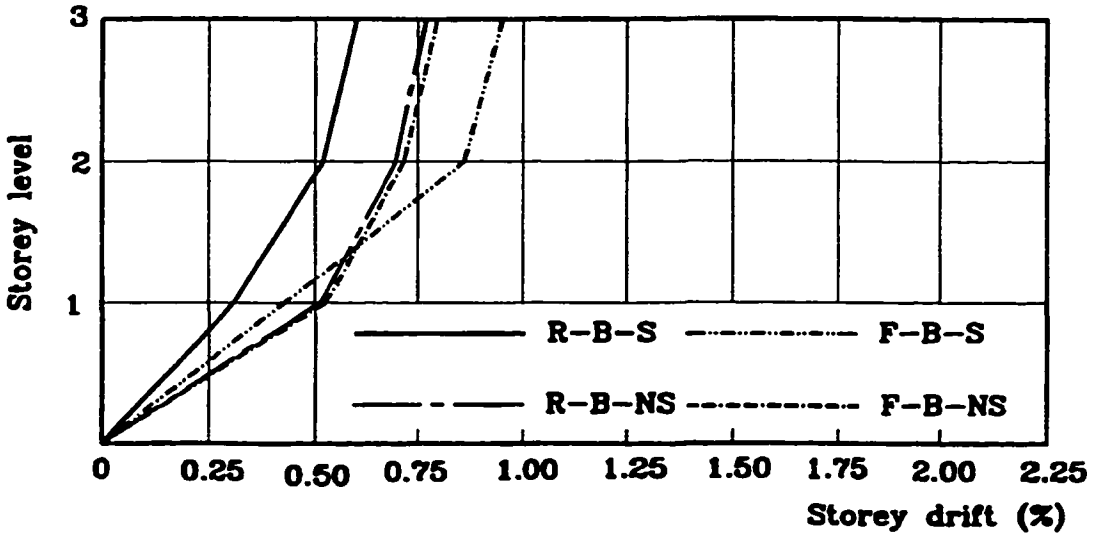

Figure 7.7a Storey drift at load level 234 kN of the pushover analysis.

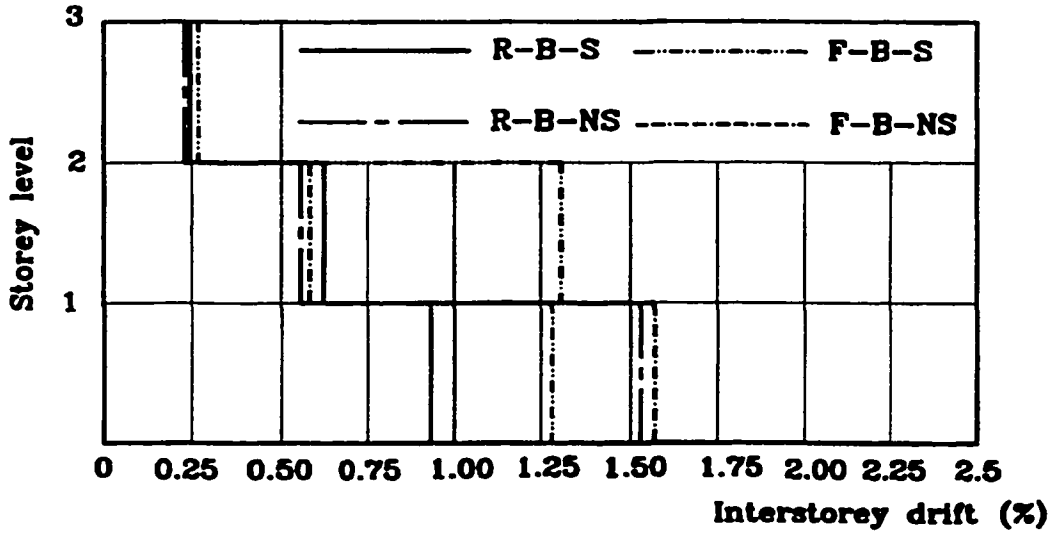

Figure 7.7b Interstorey drift at load level 234 kN due to the pushover analysis.

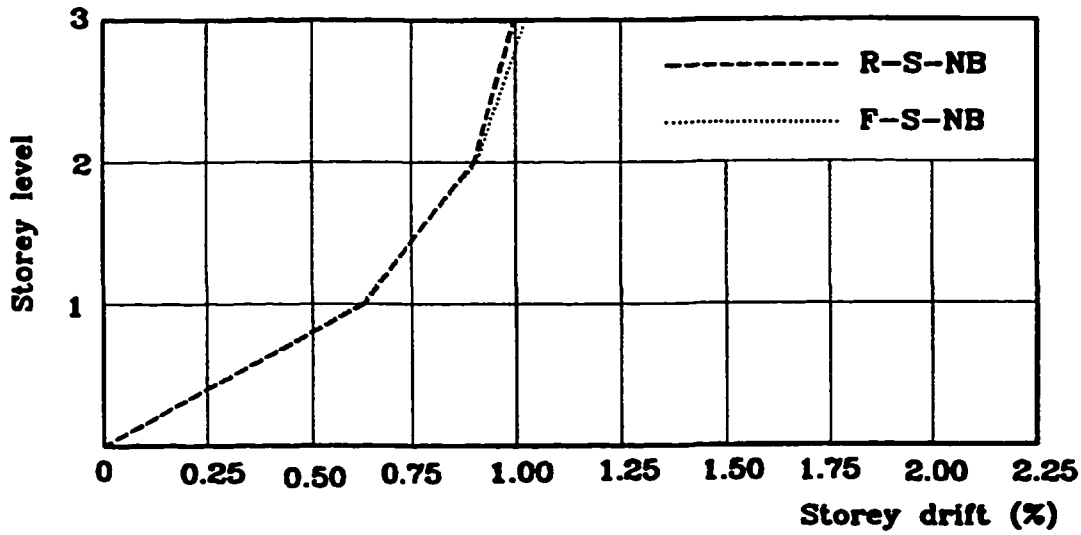

Figure 7.8a Storey drift at load level 262.5 kN of the pushover analysis.

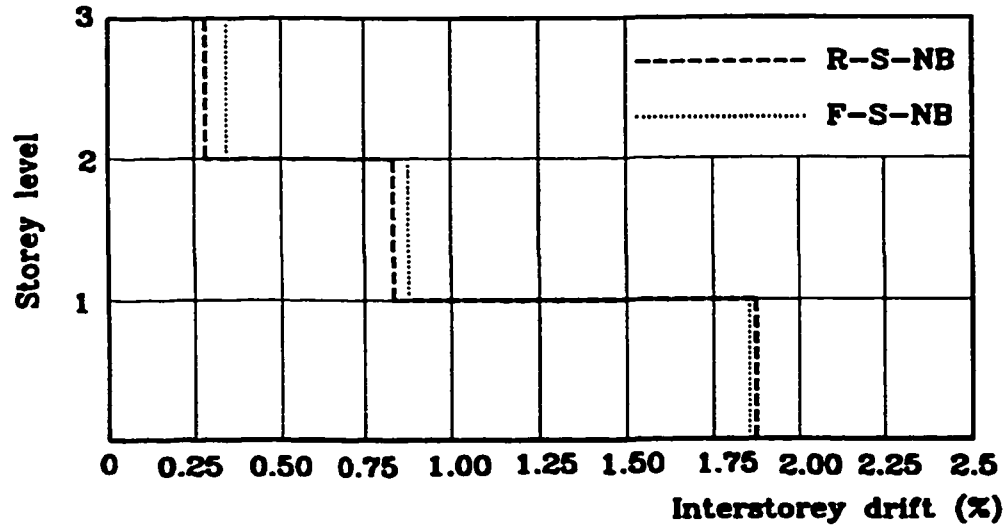

Figure 7.8b Interstorey drift at load level 262.5 kN due to the pushover analysis.

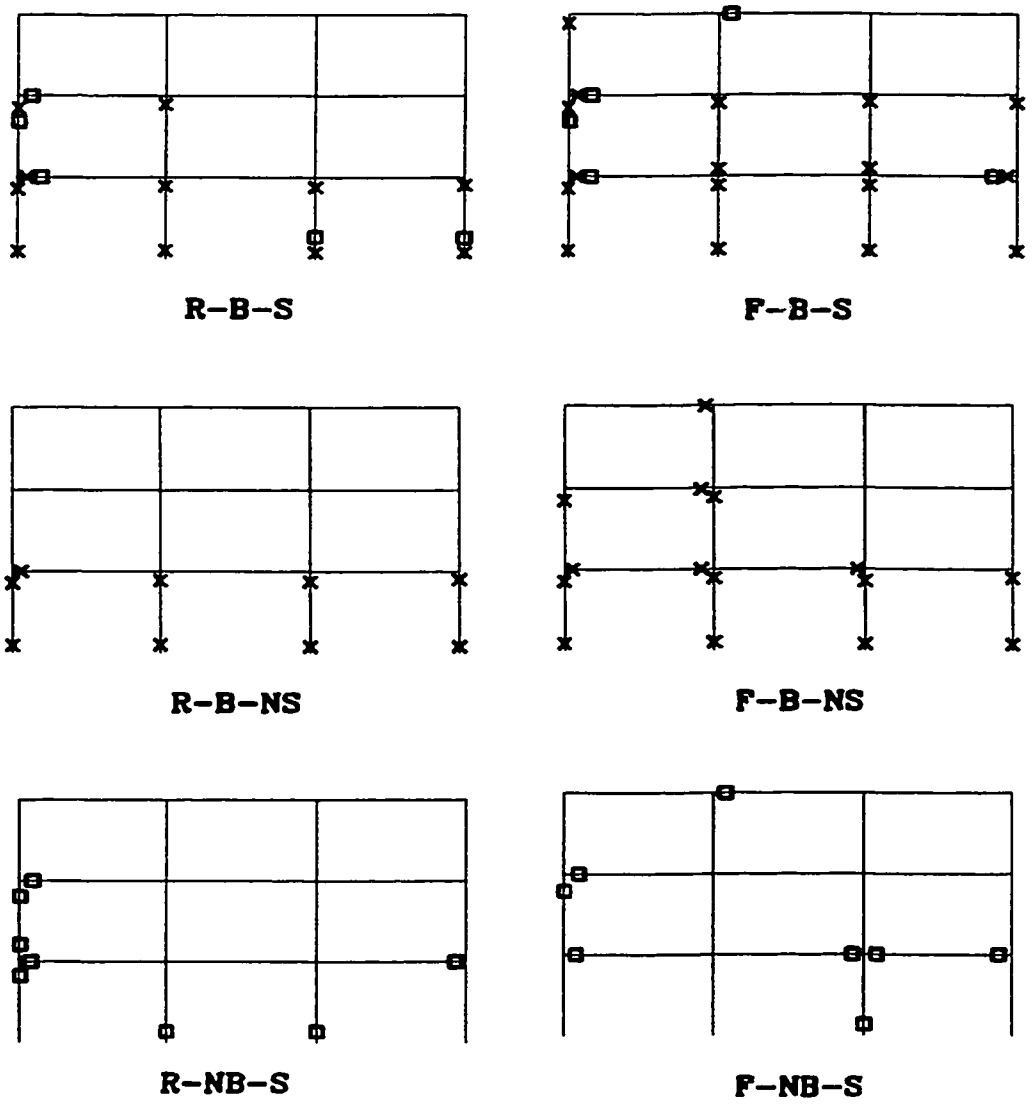

Figure 7.9 Failure mechanism from the pushover analysis.

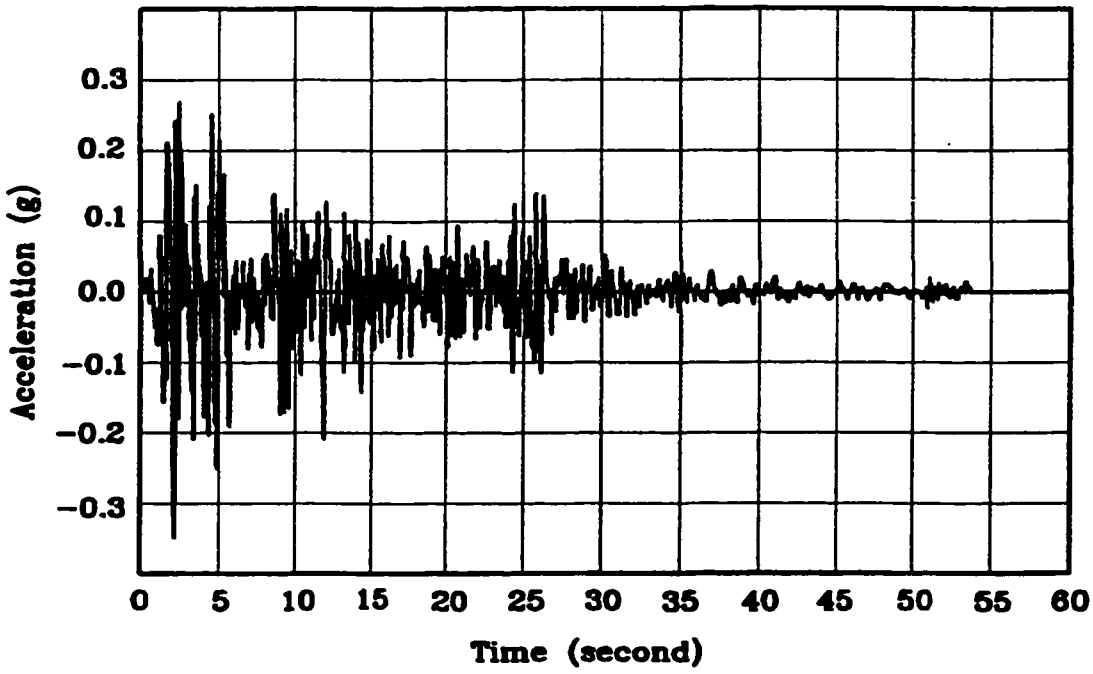

Figure 7.10 El Centro acceleration time history record

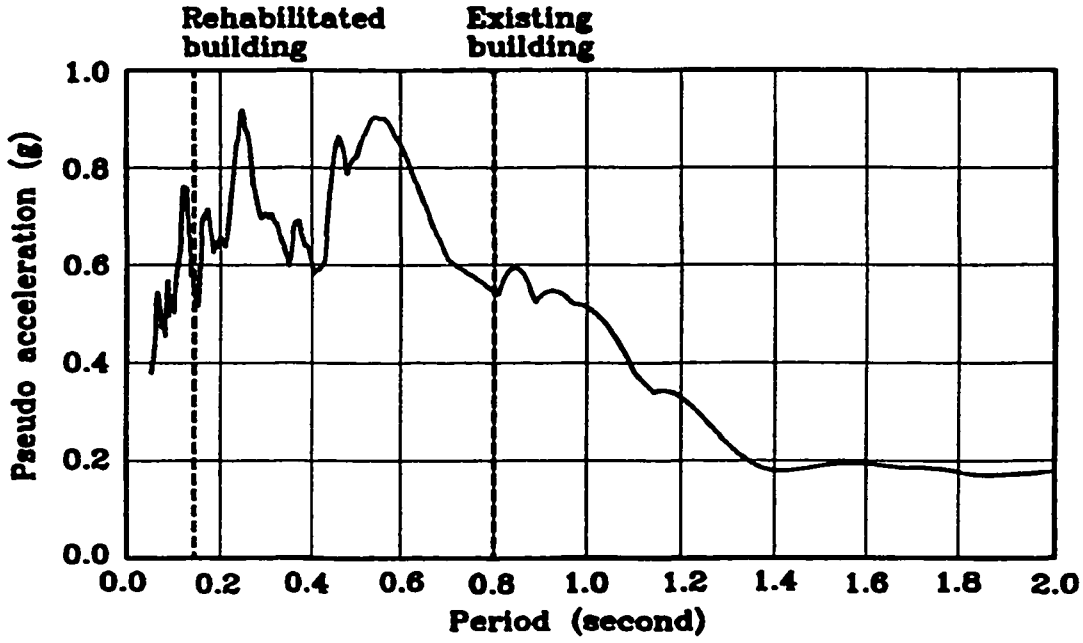

Figure 7.11 Response spectrum for El Centro record

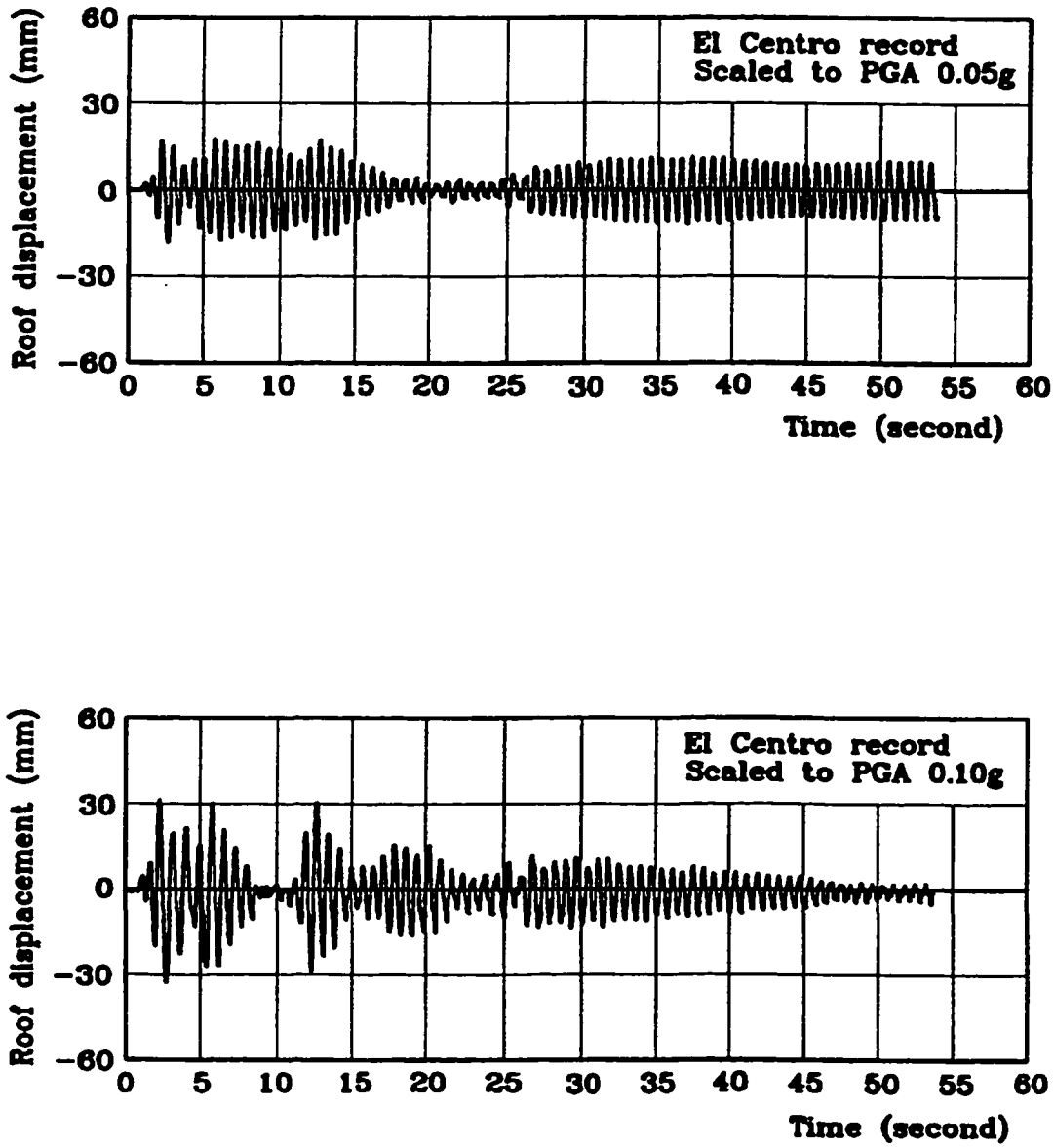

Figure 7.12 Roof displacement time histories for the 3-storey frame due to El Centro record.

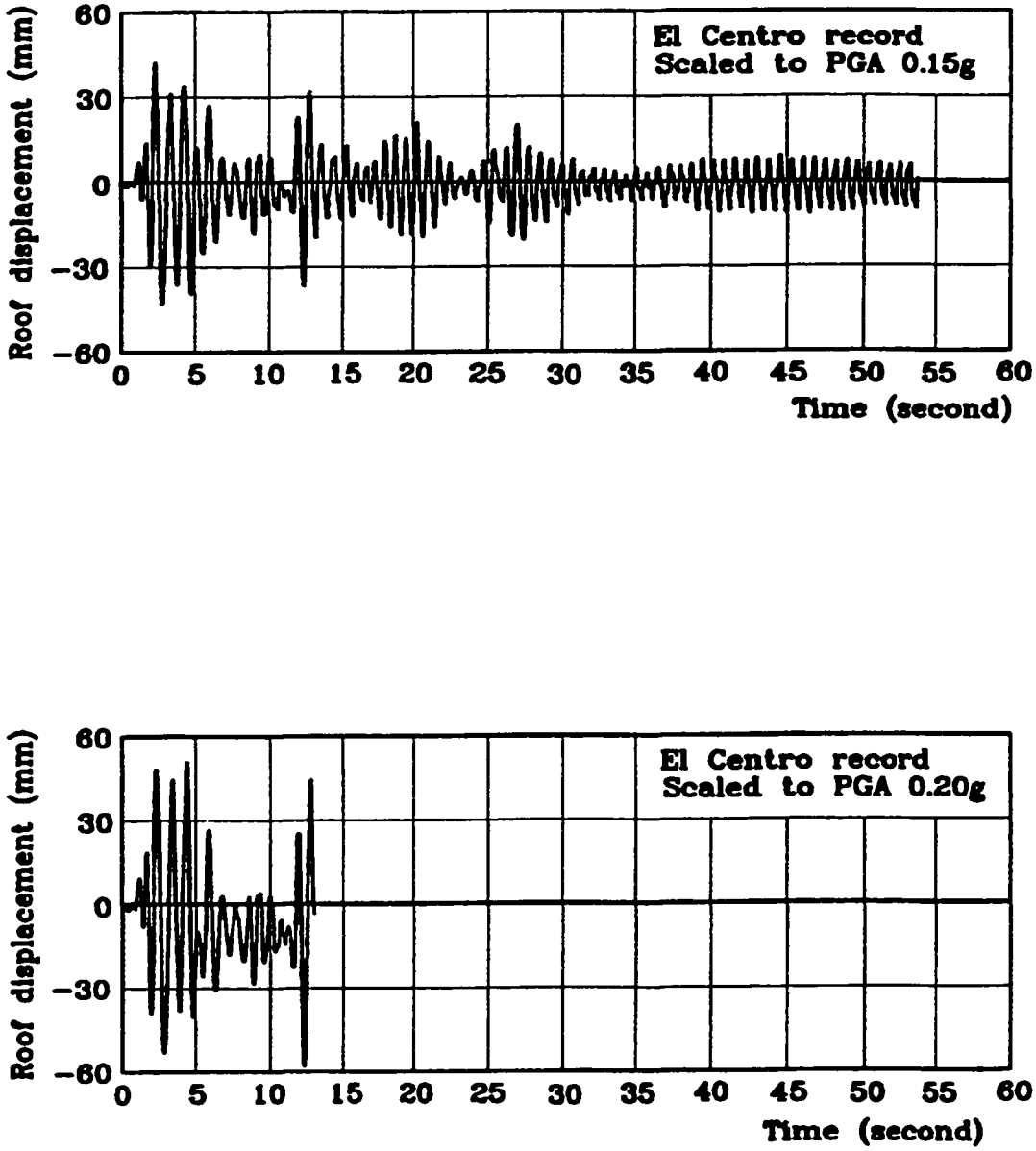

Figure 7.13 Roof displacement time histories for the 3-storey frame due to El Centro record.

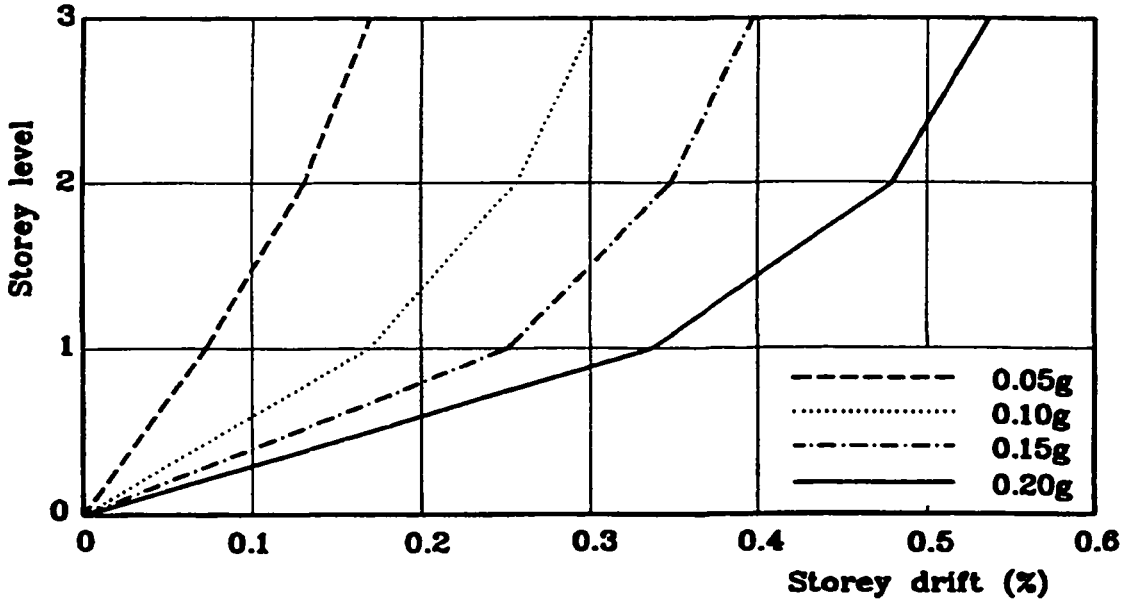

Figure 7.14 Maximun storey drift due to El Centro record

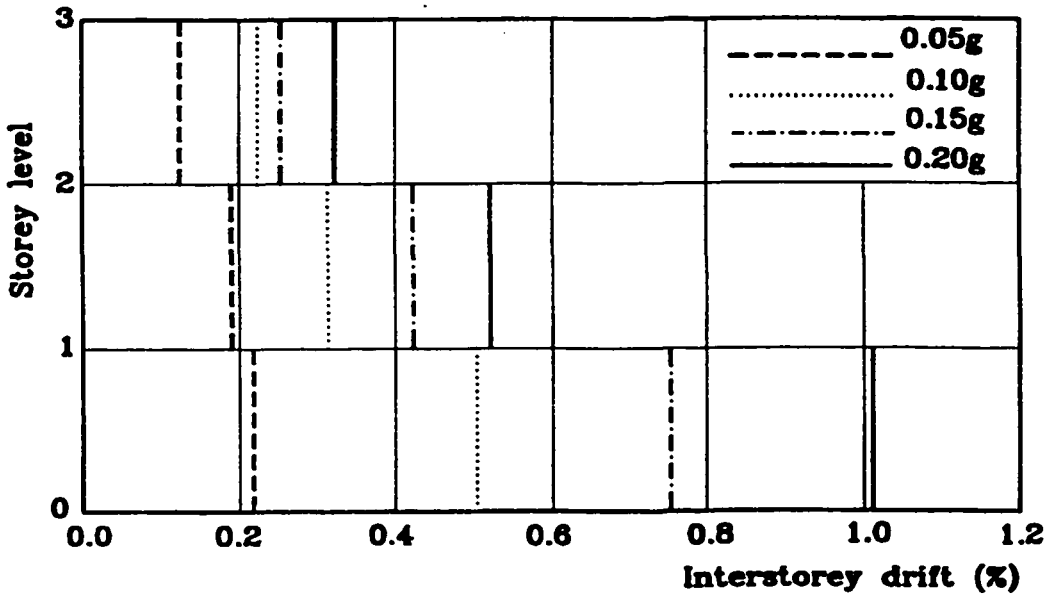

Figure 7.15 Maximum interstorey drift due to El Centro record

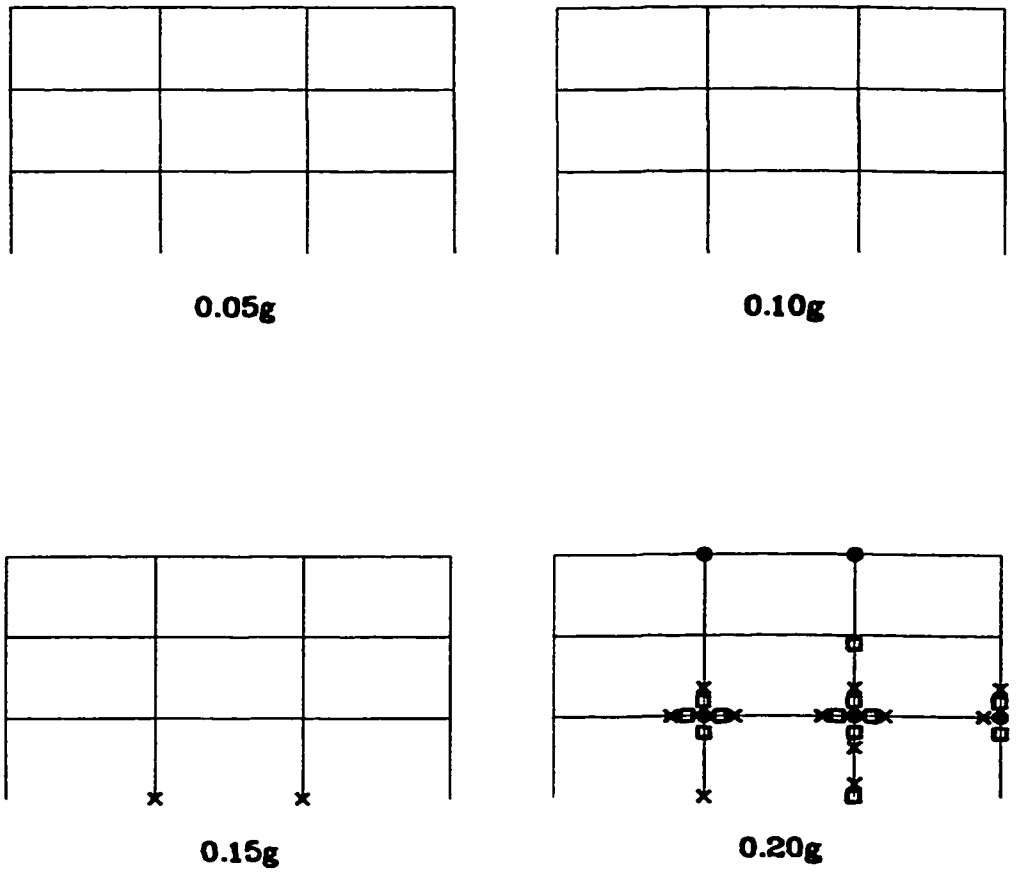

Figure 7.16 Damage to the 3–storey building due to El Centro record scaled to the shown PGA values

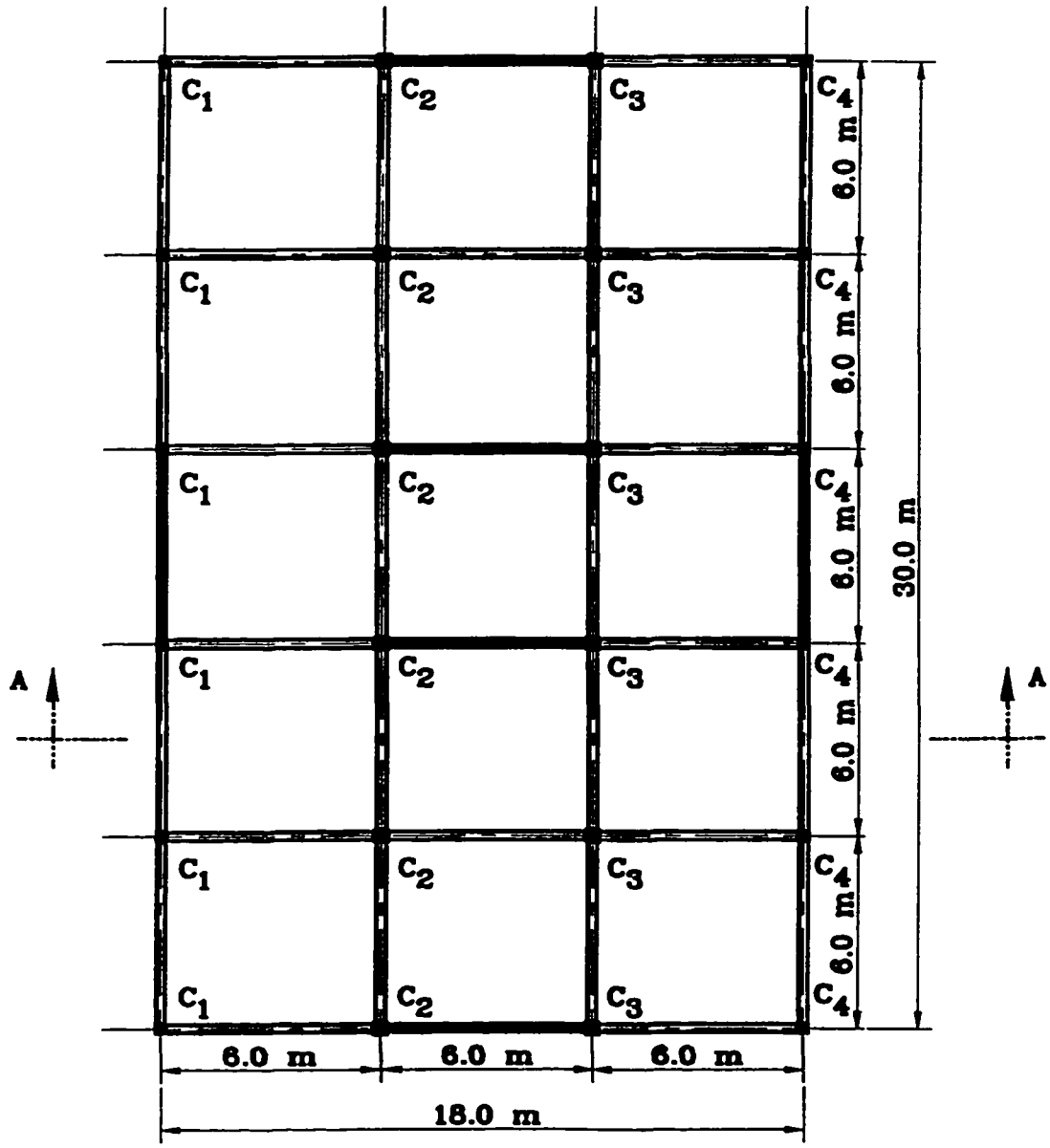

All beams are 250 x 600 mm.
Floor slab thickness is 150 mm.
C_1 and C_4 are 300 x 300 mm.
C_2 and C_3 are 400 x 400 mm.

Figure 7.17 Typical floor plan for the three storey building after rehabilitation.

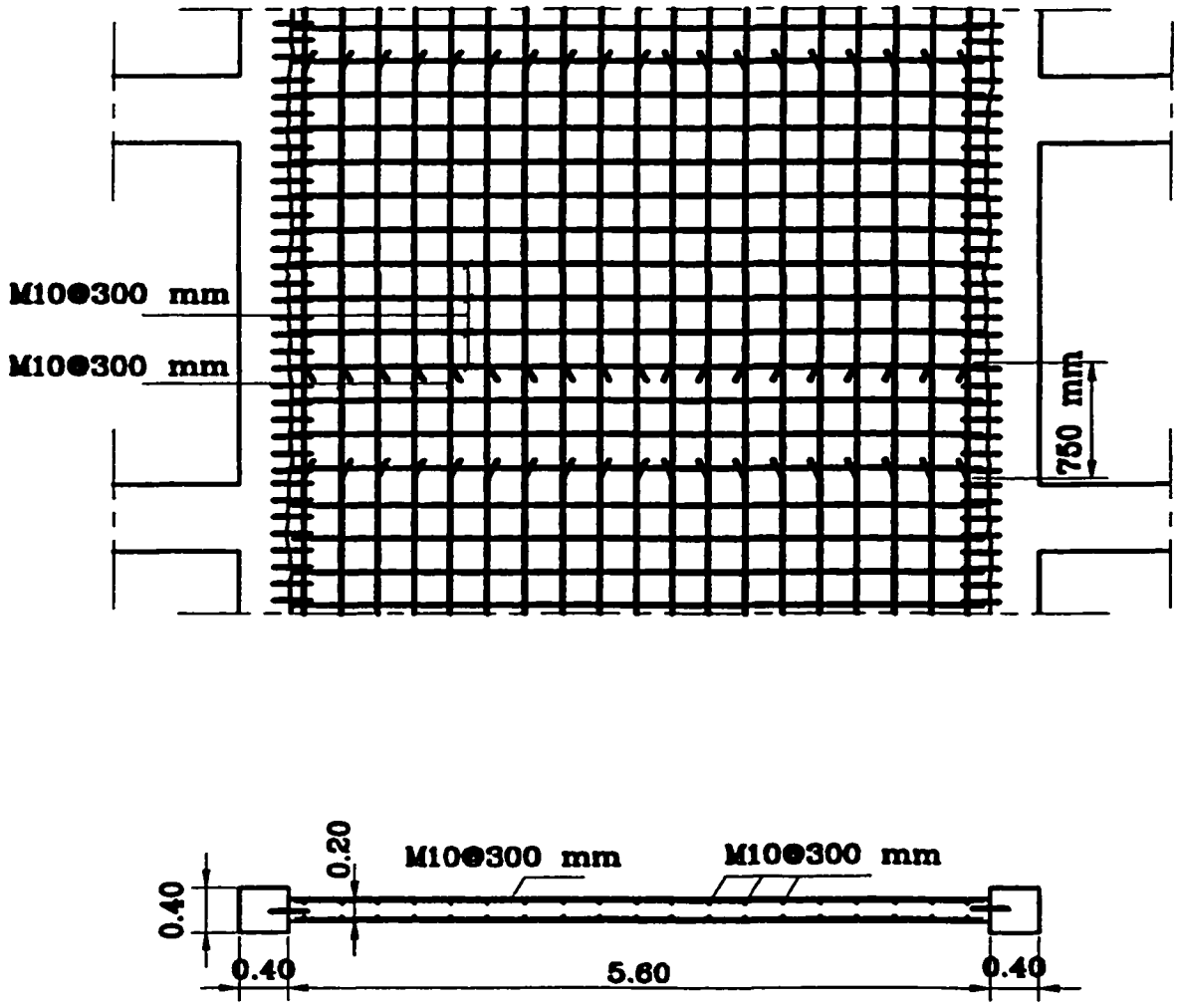

Figure 7.18 Details of RC walls used for building rehabilitation

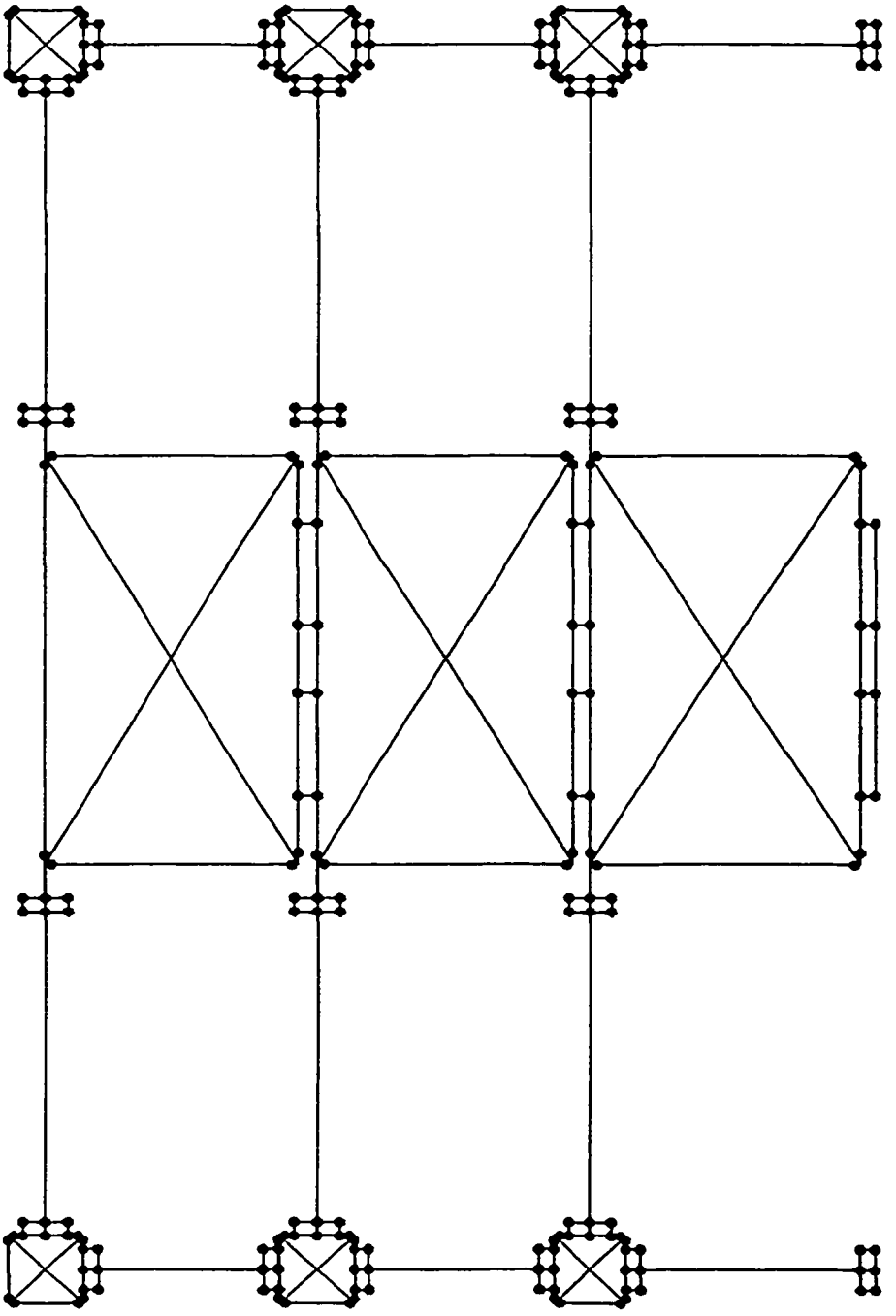

Figure 7.19 Computer model for the three-storey frame after rehabilitation

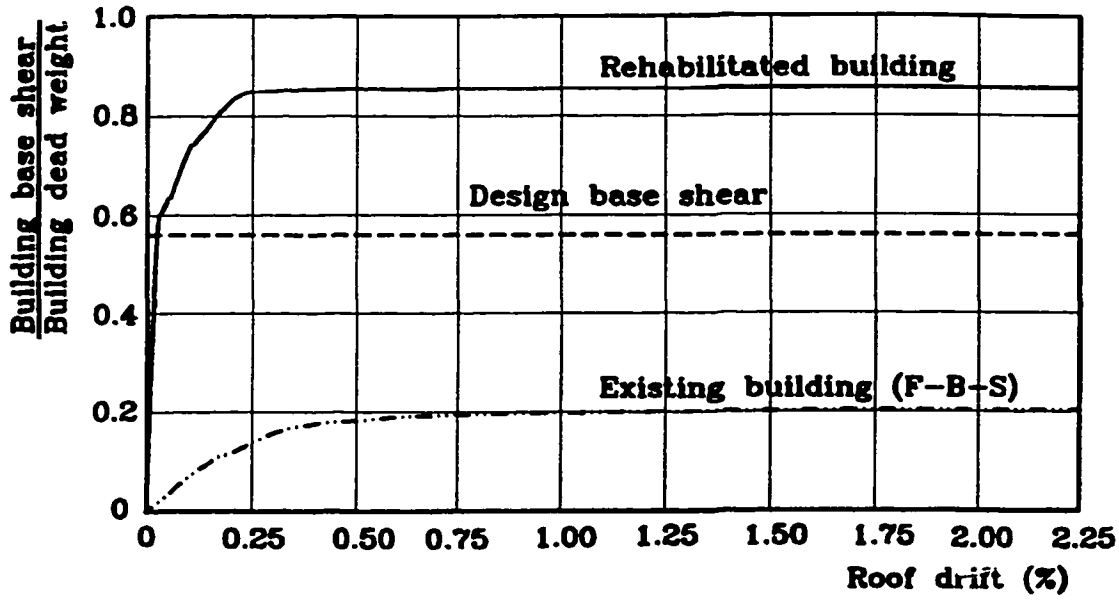

Figure 7.20 Base shear–roof drift relationship from pushover analysis.

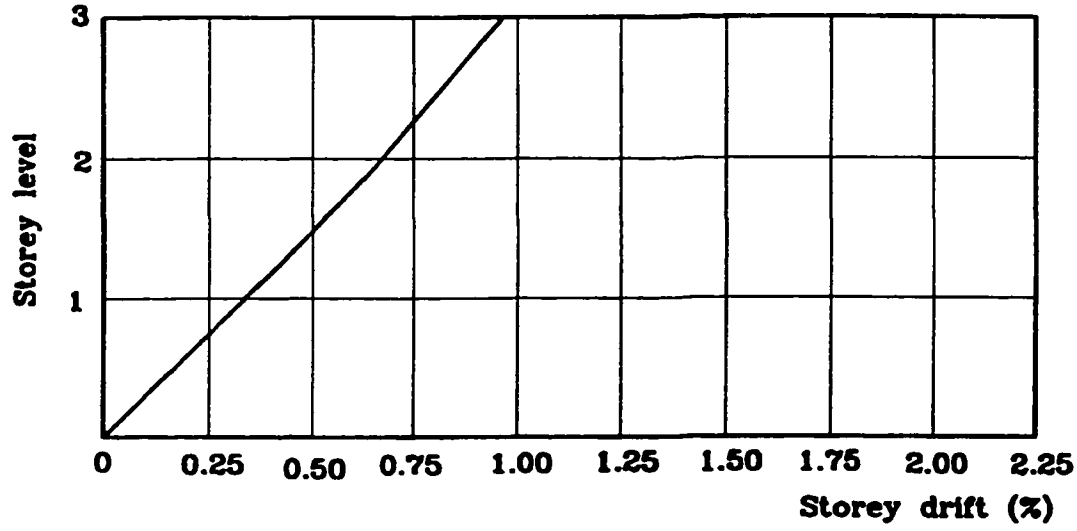

Figure 7.21 Storey drift at load level 1495 kN of the pushover analysis.

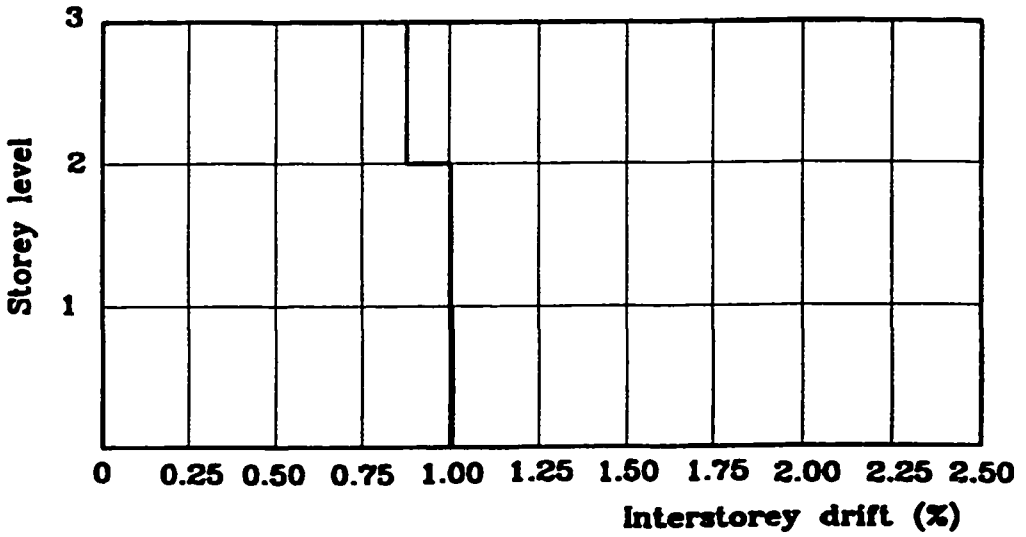

Figure 7.22 Interstorey drift at load level 1495 kN due to the pushover analysis.

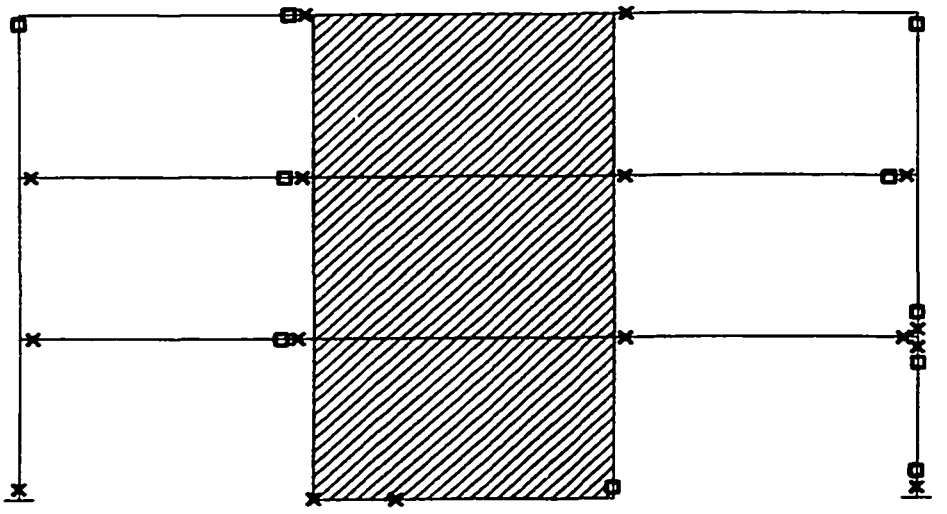

□ Concrete softening. × Bond slip softening.

Figure 7.23 Failure mechanism from the pushover analysis

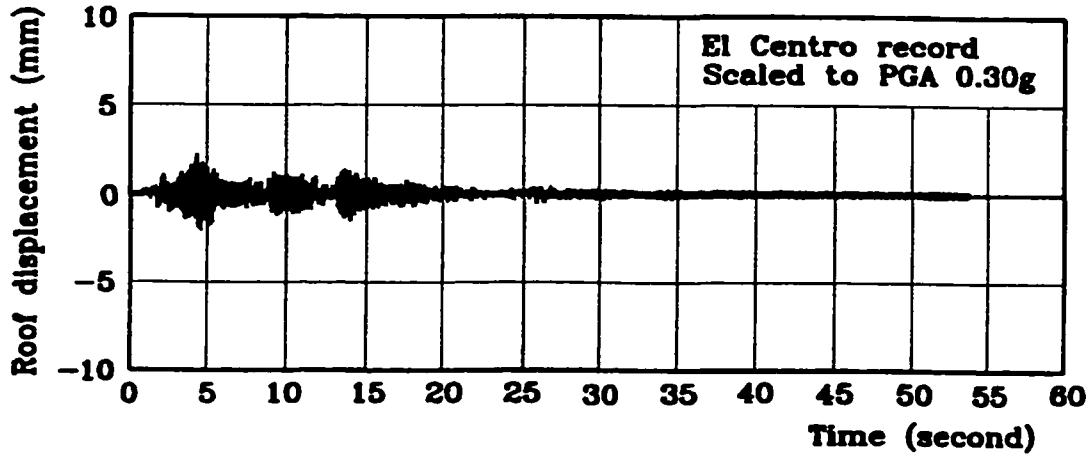

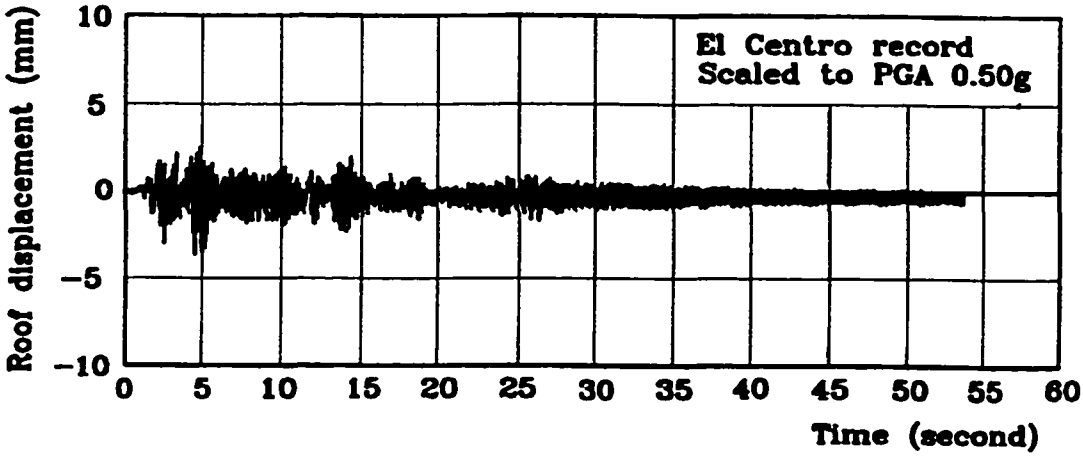

Figure 7.24 Roof displacement time histories for the 3-storey frame due to El Centro record.

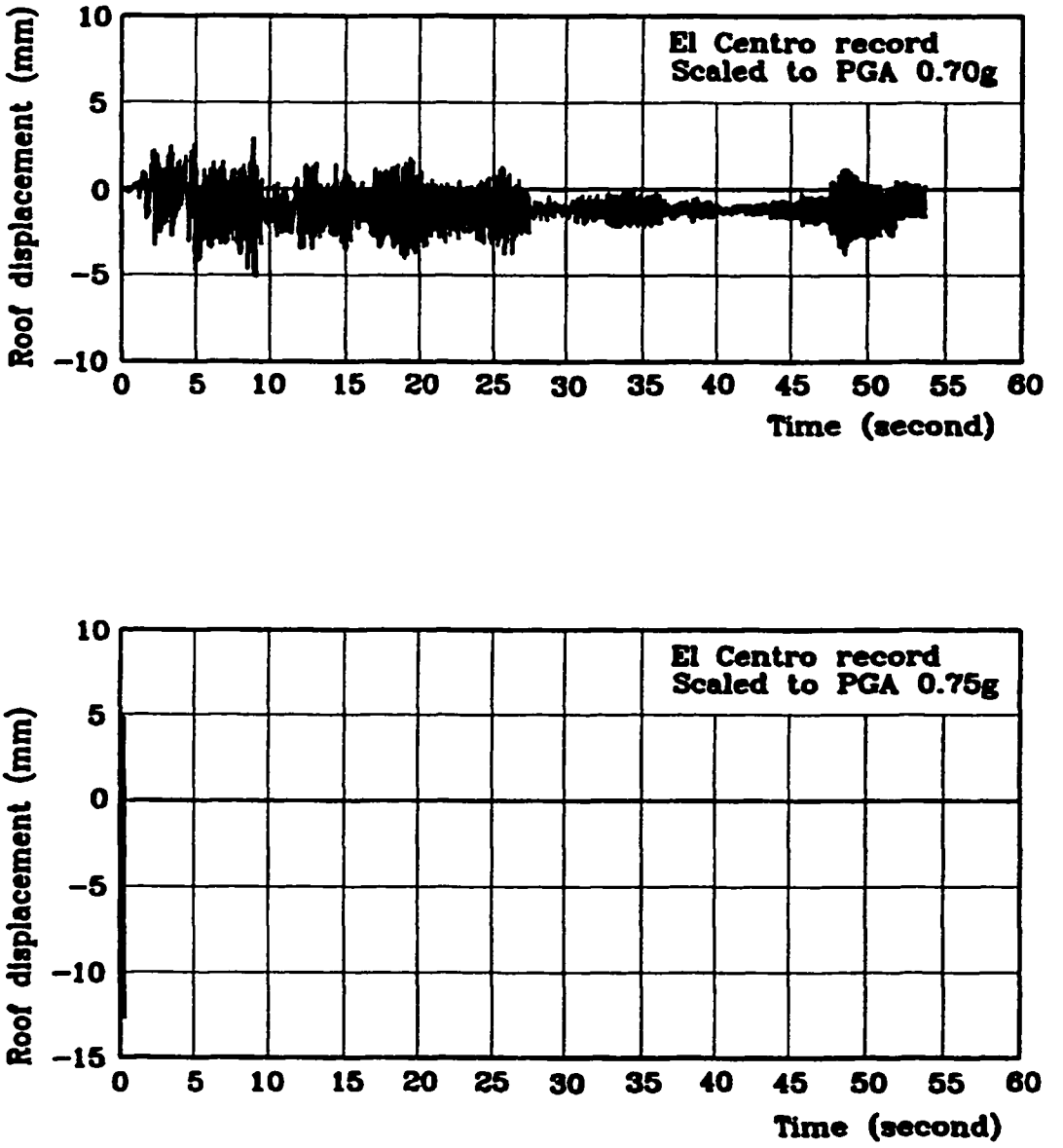

Figure 7.25 Roof displacement time histories for the 3-storey frame due to El Centro record.

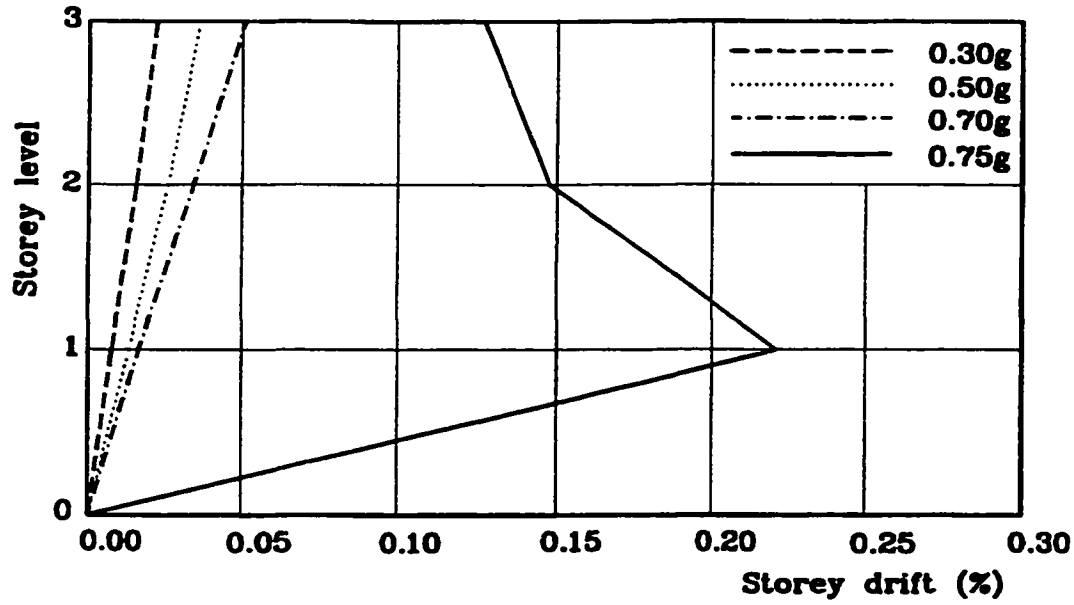

Figure 7.26 Maximum storey drift due to El Centro record

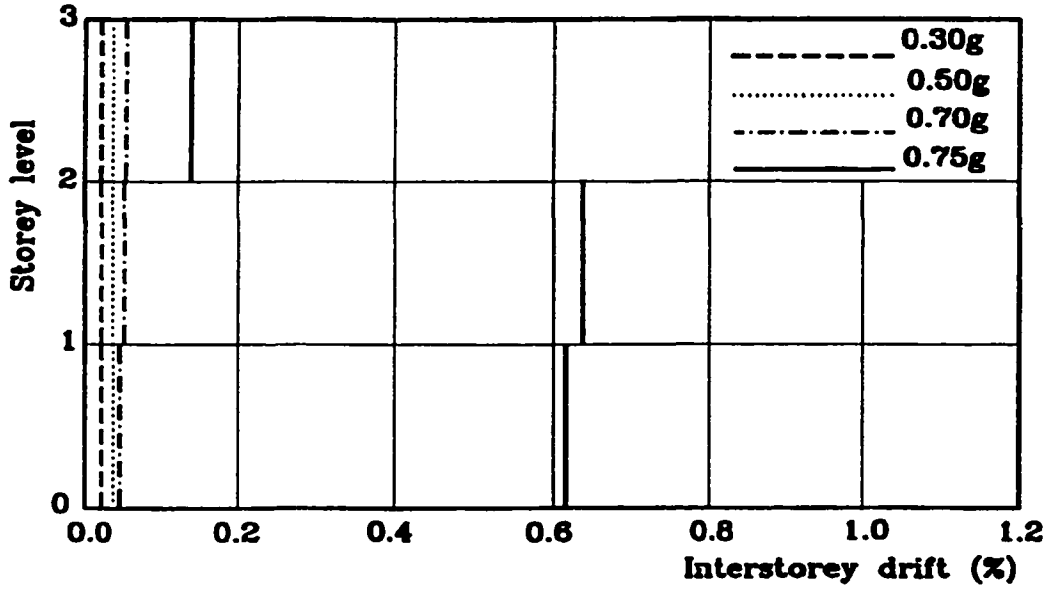

Figure 7.27 Maximum interstorey drift due to El Centro record

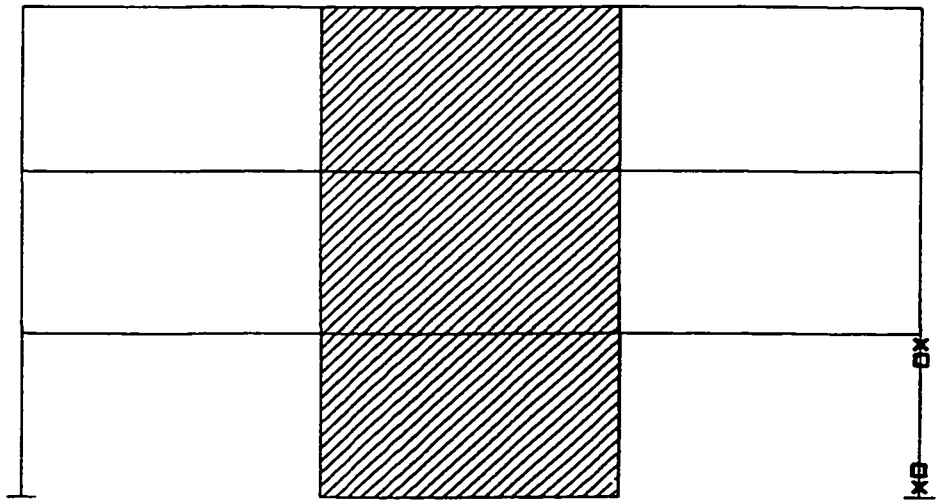

0.70 g

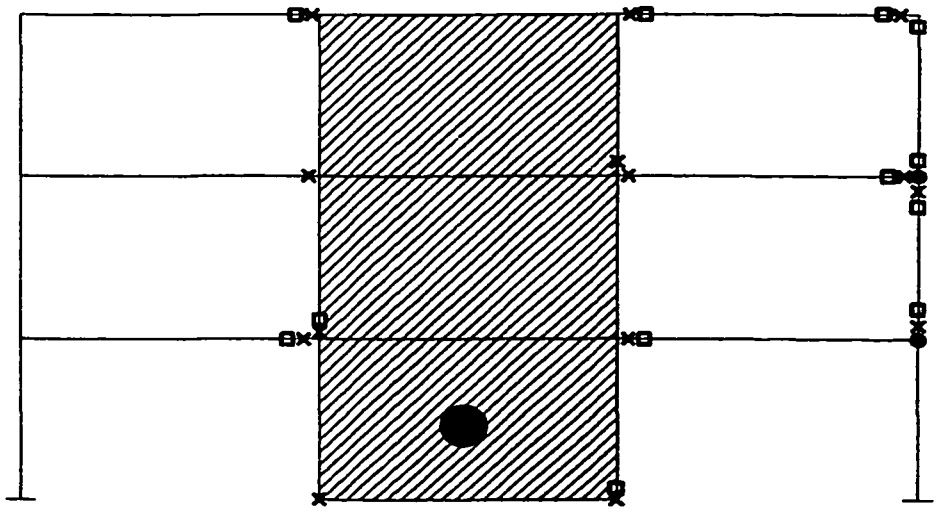

0.75 g

□ Concrete softening. × Bond slip softening.

● Beam–column joint shear failure

⬤ RC wall shear failure

Figure 7.28 Damage to the 3–storey building due to El Centro record scaled to the shown PGA values

CHAPTER 8

CONCLUSIONS AND RECOMMENDATIONS

8.1 SUMMARY AND CONCLUSIONS

The principal objective of this study is to develop an analytical model for the analysis of existing reinforced concrete buildings before and after rehabilitation using RC structural walls.

A macro-element is developed to model the flexural behaviour of RC beams and columns. The element consists of a series of four steel and five concrete springs connected by rigid plates. New hysteretic models for the steel and the concrete springs are proposed. The element model includes strength deterioration and softening parameters. These parameters are calculated based on the bond slip in the steel springs and the confining ratios. The element developed is limited to flexural behaviour and cases with small variations in the axial forces as in developing the element and calculating the element parameters, they were based on a given axial load. The shear behaviour was ignored.

Two macro-elements are developed to model the behaviour of RC beam-column joints and RC structural walls. The elements consist of a number of steel, concrete and shear springs connected by rigid members. The elements are tested using experimental results and are shown to be sufficiently accurate in predicting the behaviour of the specimens up to the failure

load. Moreover, the models are capable of accurately predicting the failure mechanism. The models are particularly effective in representing brittle modes of failure which are characteristic of existing nonductile RC frame structures. The developed models were used to determine the lateral load carrying capacity of a three-storey reinforced concrete building before and after rehabilitation.

Based on the development, validation and application of the presented new elements, the following conclusions are derived:

1. The developed hysteretic models for concrete, steel and shear are accurate and effective. Appropriate combination of these models was achieved in the developed macro elements for beams, columns, beam-column joints and structural walls. These elements are validated using experimental results and showed sufficient accuracy in predicting the specimens response and failure mechanism.
2. An equation to represent bond slip failure in the behaviour of the steel elements is introduced and tested. Design tables are developed to calculate the parameters involved in the equation depending on the bond slip characteristics. The methodology is found to be powerful and accurate in representing bond slip failure.
3. The results demonstrate the importance of including all potential modes of failure due to concrete crushing, bond slip and beam-column joint shear in the seismic assessment of structures. This is particularly important in the analysis of existing buildings with recognized inadequate lateral load resistance and poor detailing.
4. The lateral load carrying capacity of the building can be obtained using the pushover analysis. However, the pushover analysis cannot be used to estimate the building

ductility or its failure mechanism. This is mainly due to the cyclic stiffness deterioration that occurs when using nonlinear time-history analysis as it will accelerate the failure. The results showed that the building failure mechanism obtained from the pushover analysis is different from that obtained using earthquake excitation. The pushover analysis failed to predict the beam-column joints failure which is the main reason for building failure due to earthquake excitation as obtained from the dynamic analysis.

5. Due to the fact that anchorage properties (confinement, developed length, bars distribution) are inadequate in existing structures, representation of bond slip failure while analyzing existing structures is necessary. The results showed that ignoring bond slip failure will overestimate the building lateral strength.
6. Considering concrete softening in the analysis is expected to have a major effect in the case of concrete sections that are over-reinforced, or subjected to high axial loads. But most importantly, considering concrete softening is necessary to define the failure mechanism which will help in defining a suitable rehabilitation technique.
7. Rehabilitation using RC walls is effective in increasing the building lateral strength but it does not improve its ductility.
8. The percentage increase in the building lateral strength predicted using pushover analysis is nearly equivalent to the percentage increase in the PGA that will cause failure to the building predicted using time history analysis.

Finally, it should be mentioned that the presented results are based on a limited number of analyses of a specific frame. To establish general conclusions on the behaviour of

gravity load designed frames, a more comprehensive study is needed.

8.2 RECOMMENDATIONS FOR FUTURE RESEARCH

The following recommendations may be considered in future research involving modeling and analysis of existing RC buildings:

1. The developed macro element can be extended to take into account the effect of axial load variation.
2. Shear deformations should be included in the developed macro element for beams and columns.
3. A comprehensive analytical study on existing buildings of different heights and subjected to different earthquakes can be carried out to identify their response under seismic loading and to propose simplified methods to predict the seismic capacity of existing buildings.
4. A comprehensive analytical study on rehabilitation of existing buildings using RC walls to reach rehabilitation guidelines that are economical to use.
5. A comprehensive analytical/experimental study on different structural rehabilitation schemes.

REFERENCES

- Abouelfath, H., 1998, "Rehabilitation of Nonductile Reinforced Concrete Buildings Using Steel Systems", Ph.D. thesis, McMaster University, Hamilton, Ontario, Canada.

- ACI, 1963, "Building Code Requirements for Reinforced Concrete", American Concrete Institute Standard 318-63, Detroit, Michigan.

- Alath, S. and Kunnath, S., 1995, "Modeling Inelastic Shear Deformation in RC Beam-Column Joints", Proceedings of 10th Conference on Engineering Mechanics, University of Colorado at Boulder, Boulder, Colorado, pp. 822-825.

- Allen, D.E. and Rainer, J.H., 1995, "Guidelines for the Seismic Evaluation of Existing Buildings", Canadian Journal of Civil Engineering, Vol. 22, pp. 500-505.

- Aoyama, H., 1981, "A Method for the Evaluation of the Seismic Capacity of Existing Reinforced Concrete Buildings in Japan", Bulletin of the New Zealand National Society for Earthquake Engineering, Vol. 14, No. 3, pp. 105-130.

- Aoyama, H., 1986, "Seismic Strengthening of Existing Reinforced Concrete Buildings in Japan", Department of Architecture, Faculty of Engineering, University of Tokyo, Japan.

- Applied Technology Council, 1978, "A Handbook for Seismic Evaluation of Existing Building", Report ATC-22/FEMA-178, Washington, D.C.

- Applied Technology Council, 1987, "Evaluating the Seismic Resistance of Existing Buildings", Report ATC-14, Redwood City, California.

- Applied Technology Council, 1988, "Rapid Visual Screening of Buildings for Potential Seismic Hazards", Report ATC-21, FEMA-154, Federal Emergency Management Agency, Washington, D.C.

- Bhide, S.B. and Collins, M..P., 1989, "Influence of Axial Tension on the Shear Capacity of Reinforced Concrete Members", ACI Structural Journal, Vol. 86, No. 5, 570-581.

- Biddah, A., 1997, "Seismic Behaviour of Existing and Rehabilitated Reinforced

Concrete Frame Connections", Ph.D. thesis, McMaster University, Hamilton, Ontario, Canada.

- Chung, Y.S., Meyer, C. and Massanobu, S., 1989, "Modeling of Concrete damage", ACI Structural Journal, Vol. 86, pp. 259-271.

- Collins, M.P. and Mitchell, D., 1987, "Prestressed Concrete Basics", Canadian Prestressed Concrete Institute, Ottawa, Ontario, Canada.

- Collins, M.P., Mitchell, D., Adebar, P. and Vecchio, F.J., 1996, "A General Shear Design Method", ACI Structural Journal, Vol. 93, No. 1, 36-47.

- CSA CAN3-A23.3, 1994, "Design of Concrete Structures for Buildings", Canadian Standards Association, Rexdale, Ontario.

- Darwin, D., Zuo, J., Tholen, M. and Idun, E., 1996, "Development Length Criteria for Conventional and High Relative Rib Area Reinforcing Bars", ACI Structural Journal, Vol. 93, No. 3, pp. 347-359.

- Elmorsi, 1998, "Analytical Modeling of Reinforced Concrete Beam-Column Connections for Seismic Loading", Ph.D. Thesis, McMaster University, Hamilton, Ontario, Canada

- Endo, T., Okifuji, A., Sugano, S., Ayashi, T., Shimizu, T., Takahara, K., Saito, H. and Yoneyama, Y., 1984, "Practices of Seismic Retrofit of Existing Concrete Structures in Japan", Proceedings of the Eighth World Conference on Earthquake Engineering, San Francisco, California, Vol. I, pp. 469-476.

- Filippou, A.M., 1986, "A Simple Model for Reinforcing Bar Anchorages Under Cyclic Excitations", Journal of Structural Engineering, ASCE, Vol. 112, No. 7, pp. 1639-1659.

- Filippou, F.C., Popov, E.P. and Bertero, V.V., 1983, "Effect of Bond Deterioration on Hysteretic Behaviour of Reinforced Concrete Joints", UCB/EERC 83/19, University of California, Berkeley, CA.

- Ghobarah, A., 1998, "Seismic Assessment of Existing RC Structures", Progress in Structural Engineering and Materials, Vol. 2, No. 1.

- Ghobarah, A., Biddah, A. and Mahgoub, M., 1997a, "Rehabilitation of Reinforced Concrete Columns Using Corrugated Steel Jacketing", Journal of Earthquake Engineering, Vol. 1, No. 4, pp. 651-673.

- Ghobarah, A., Aziz, T.S. and Biddah, A., 1997b, "Rehabilitation of Reinforced Concrete Frame Connections Using Corrugated Steel Jacketing", ACI Structural Journal, Vol. 94, No. 3, pp. 283-294.

- Ghobarah, A. and Youssef, M., 1999, "Modeling of Reinforced Concrete Structural Walls", Engineering Structures, Vol. 21, No. 10, pp. 912-923.

- Ghusn, G.E. and Saiidi, M., 1986, "A Simple Hysteretic Element For Biaxial Bending of R/C Columns and Implementation in NEABS-86", Report No. NCEER-86-1, Civil Engineering Department, University of Nevada, Reno, Nevada.

- Giuriani, E., Plizzari, G. and Schumm, C., 1991, "Role of Stirrups and Residual Tensile Strength of Cracked Concrete on Bond", Journal of Structural Engineering, ASCE, Vol. 117, No. 1, pp. 1-18.

- Harajli, M., 1994, "Development/Splice Strength of Reinforcing Bars Embedded in Plain and Fiber Reinforced Concrete", ACI Structural Journal, Vol. 91, No. 5, pp. 511-520.

- Higashi, Y., Endo, T. and Shimizu, Y., 1981, "Experimental Studies on Retrofitting of Reinforced Concrete Structural Members", Proceedings of the Second Seminar on Repair and Retrofit of Structures, The University of Michigan, ANN ARBOR, Michigan, pp. 126-155.

- Hirosawa, M., 1981, "Criterion on the Evaluation of Seismic Safety of Existing Reinforced Concrete Buildings", Proceedings of the Second Seminar on Repair and Retrofit of Structures, The University of Michigan, An Arbor, Michigan, pp. 49-108.

- Hoffmann, G.W., Kunnath, S.K., Reinhorn, A.M., and Mander, J.B. 1992. "Gravity-Load-Designed Reinforced Concrete Buildings: Seismic Evaluation of Existing Construction and Detailing Strategies for Improved Seismic Resistance", Technical Report NCEER-92-0016, National Center for Earthquake Engineering Research, SUNY/Buffalo.

- Jiang, Y. and Saiidi, M., 1990, "Four Spring Element for Cyclic Response of R/C Columns", Journal of Structural Engineering, ASCE, Vol. 116, No. 4, pp. 1018-1029.

- Kent, D.C. and Park, R., 1971, "Flexural Members with Confined Concrete", Journal of the Structural Division, ASCE, Vol. 97, No. ST7, pp. 1969-1990.

- Lai, S.S., 1984, "Inelastic Analysis of Reinforced Concrete Space Frame Under Biaxial Earthquake Motions", Ph.D. Thesis, University of Toronto, Toronto, Ontario.

- Lai, S.S., Will, G.T. and Otani, S., 1984, "Model For Inelastic Biaxial Bending of Concrete Members", Journal of Structural Engineering, ASCE, Vol. 110, No. 11, pp. 2563-2584.

- Li, K.N., Aoyama, H. and Otani, S., 1988, "Reinforced Concrete Columns Under Varying Axial Load and Bi-Directional Lateral Load Reversals", Proceedings of Ninth World Conference on Earthquake Engineering, Vol. VIII, Tokyo-Kyoto, Japan, pp. 537-542.

- Linde, P. and Bachmann, H., 1994, "Dynamic Modeling and Design of Earthquake-Resistant Walls", Earthquake Engineering and Structural Dynamics, Vol. 23, No. 12, 1331-1350.

- Maison, B.F., 1992, "PC-ANSR A Computer Program for Nonlinear Structural Analysis", University of California, Berkeley, California.

- Mattock, A.H., 1979, "Flexural Strength of Prestressed Concrete Sections by programmable calculator", Journal Prestressed Concrete Institute, V. 24, No. 1, pp. 32-54.

- Miramontes, D., Merabet, O. and Reynouard, J.M., 1996, "Beam Global Model for the Seismic Analysis of RC Frames", Earthquake Engineering and Structural Dynamics, Vol. 25, pp. 671-688.

- Miranda, E., 1991, "Seismic Evaluation and Upgrading of Existing Buildings", Thesis Submitted for Partial Satisfaction of the Requirements for the Degree of Doctor of Philosophy, University of California at Berkeley, California.

- Monti, G., Fillippou, F.C. and Spacone, E., 1997, "Finite Element for Anchored Bars under Cyclic Load Reversals", Journal of Structural Engineering, ASCE, Vol. 123, No. 5, pp. 614-623.

- Mukaddam, M., Kasti, M., 1986, "Reinforced Concrete Joints under Cyclic Loading", Journal of Structural Engineering, ASCE, Vol. 112, No. 4, pp. 937-942.

- Orangun, C.O., Jirsa, J.O. and Breen, J.E., 1977, "A Reevaluation of Test Data on Development Length and Splices", American Concrete Institute Journal, ACI, Proceedings Vol. 74, No. 3, pp. 114-122.

- Otani, S., Kabeyasawa, T., Shiohara, H. and Aoyama, H., 1985, "Analysis of the Full Scale Seven Story Reinforced Concrete Test Structure", ACI SP-84, 203-239.

- Ozcebe, G. and Saatcioglu, M., 1989, "Hysteretic Shear Model for Reinforced

Concrete Members", Journal of Structural Engineering, ASCE, Vol. 115, No. 1, pp. 132-148.

- Pantazopoulou, S.J. and Bonacci, J.F., 1994, "On Earthquake-Resistant Reinforced Concrete Frame Connections", Canadian Journal of Civil Engineering, Vol. 21, pp. 307-328.

- Prakash, V. and Powell, G.H., 1992, "DRAIN-2DX Version 1.0: A Computer Program Distributed by NISEE/Computer Applications", Department of Civil Engineering, University of California, Berkeley, Califonia.

- Park, Y.J., Reinhorn, A.M. and Kunnath, S.K., 1987, "IDARC: Inelastic Damage Analysis of Reinforced Concrete Frame - Shear - Wall Structures", Technical Report NCEER-87-0008, State University of New York at Buffalo, Buffalo, NY.

- Pessiki, S.P., Conley, C.H., Gergely, P. and White, R.N., 1990, "Seismic Behavior of Lightly Reinforced Concrete Column and Beam-Column Joint Details", Technical Report NCEER-90-0014. National Center for Earthquake Engineering Research, Buffalo.

- Roufaiel, M.S.L. and Meyer, C., 1987, "Analytical Modeling of Hysteretic Behavior of R/C Frames", Journal of Structural Engineering, ASCE, Vol. 113, 429-444.

- Saiidi, M., 1982, "Hysteretic Models for Reinforced Concrete", Journal of the Structural Division, ASCE, Vol. 108, pp. 1077-1087.

- Scott, B.D., Park, R. and Priestley, M.J.N., 1982, "Stress-Strain Behavior of Concrete Confined by Overlapping Hoops at Low and High Strain Rates", ACI Journal, Vol. 79, No. 1, pp. 13-27.

- Sittipunt, C. and Wood, S.L., 1993, "Finite Element Analysis of Reinforced Concrete Shear Walls", Report No. UILU-ENG-93-2015, Department of Civil Engineering, University of Illinois at Urbana, Illinois.

- Stevens, N.J., Uzumeri, S.M. and Collins, M.P., 1987, "Analytical Modeling of Reinforced Concrete Subjected to Monotonic and Reversed Loading", Publication No. 87-1, University of Toronto, Toronto, Ontario, Canada.

- Takeda, T., Sozen, M.A. and Nielson, N.N., 1970, "Reinforced Concrete Response to Simulated Earthquakes", Journal of the Structural Division, ASCE, Vol. 96, 2557-2573.

- Taucer, F.T., Spacone, E. and Filippou, F.C., 1991, "A Fiber Beam-Column Element

for Seismic Response Analysis of Reinforced Concrete Structures", Report No. UCB/EERC-91/17, University of California, Berkeley, California.

- Ustuner, H., 1992, "An Analytical Study of the Mechanics of Bond Deterioration Caused by Yield Penetration", Thesis submitted in Conformity with the Requirements for the degree of Master of Applied Science, Department of Civil Engineering, University of Toronto, Toronto, Ontario.

- Vallenas, J.M., Bertero, V.V. and Popov, E.P., 1979, "Hysteretic Behavior of Reinforced Concrete Structural Walls", Report No. UCB/EERC-79/20, University of California, Berkeley, California.

- Vecchio, F.J. and Collins, M.P., 1986, "The Modified Compression Field Theory for Reinforced Concrete Elements Subjected to Shear", ACI Structural Journal, Vol. 83, No. 2, 219-231.

- Vulcano, A. and Bertero, V.V., 1987, "Analytical Models for Predicting The Lateral Response of RC Shear Walls: Evaluation of Their Reliability", Report No. UCB/EERC-87/19, University of California, Berkeley, California.

- Yankelevsky, D.Z. and Reinhardt, H.W., 1989, "Uniaxial Behavior of Concrete in Cyclic Tension", ASCE, Journal of Structural Engineering, Vol. 115, No. 1, pp. 166-182.

- Youssef, M. and Ghobarah, A., 1999, "Strength Deterioration due to Bond Slip and Concrete Crushing in Modeling of RC Members", ACI Structural Journal, Vol. 96, No. 6, pp. 956-966.